UNIVERSIDADE DO PORTO

FACULDADE DE ENGENHARIA

Master's Thesis

The Use of 'Double-Double' Laminates for Aeroelastic Tailoring

João Pedro Moreira Lima de Sousa

Supervisors:
Dr. Carolina Furtado
Dr. Federico Danzi

Thesis submitted to Universidade do Porto – Faculdade de Engenharia
in partial fulfilment of the requirements for the degree of
Master in Mechanical Engineering - Aeronautical and Vehicle Structures

MEM

U. PORTO
FEUP FACULDADE DE ENGENHARIA
UNIVERSIDADE DO PORTO
DEPARTAMENTO DE ENGENHARIA MECÂNICA
Faculdade de Engenharia

July 2024

Study hard what interests you the most in the most undisciplined, irreverent and original manner possible
Richard P. Feynman

Acknowledgements

First, I would like to express my sincere gratitude to Dr. Carolina Furtado and Dr. Federico Danzi, my advisors, for giving me the opportunity to develop this topic, and for the support, guidance and availability during this thesis and master's course. The collaboration in this work, all our meetings and the advice you provided me were truly rewarding. I have no doubt the expertise you shared with me will be invaluable throughout my professional career.

A very special thank you to my parents for their unconditional support and for always believing me and encouraging me to follow my ambitions. A sincere thank you for all your care, patience, support and guidance throughout my whole life.

Finally, to my friends for your encouragement and the shared memories during these five years at Faculdade de Engenharia da Universidade do Porto.

Abstract

Composite materials have been increasingly used in aircraft structures as they allow for significant weight savings, leading to higher efficiency. The design of composite structures has been guided by a set of rules which have made the design and manufacturing processes complex. Double-Double (DD) laminates present a new approach to composite laminates. Through a continuous field based approach based on laminate homogenisation, DD seek to enable simpler composite design, optimisation and manufacture. As a new concept, Double-Double still requires significant research to be fully understood and applied to aircraft structural design. Modern commercial aircraft have lightweight flexible structures which can deform significantly in flight. The field of aeroelasticity studies the interaction of aircraft flexibility and inertia with the aerodynamic forces and plays a significant role in aircraft design and certification. Aeroelastically tailored aircraft structures are achieved through optimisation the stiffness distribution of the structure to enable increased aircraft efficiency.

The current work seeks to explore the effect of Double-Double laminates on the aeroelastic behaviour of composite structures and provide insights on their potential use in aeroelastic tailoring. An aeroelastic model of a cantilevered plate is developed and used to evaluate Double-Double laminates with respect to a static aeroelastic condition and aeroelastic instabilities. This model is then introduced in a multi-objective optimisation framework, that considers both aeroelastic metrics, using a genetic algorithm. First, the aeroelastic objective space and the effect of homogenisation on aeroelastic behaviour are explored for a unidirectional DD laminate with constant thickness. Two configurations with thickness tapering are evaluated to understand their impact on the objective space. Several single and multi-objective optimisation studies considering both the static aeroelastic condition and the aeroelastic instability are performed, comparing Double-Double laminates to typical laminates used for aeroelastic tailoring. In the context of these optimisation studies, tow-steered DD laminates are also explored. Finally, a baseline aeroelastic model of a wingbox is developed to allow for the extension of the current work to more realistic aircraft structures.

The aeroelastic behaviour of Double-Double laminates is independent of laminate homogenisation. The drawbacks of unidirectional Double-Double laminates are easily addressed by thickness tapering and the introduction of tow steering. Through easier design and optimisation, Double-Double laminates are promising for aeroelastic tailoring of composite structures. Ultimately, the present work constitutes a valuable contribution to the understanding of aeroelastic behaviour of Double-Double laminates.

Keywords: Double-Double, Composite materials, Aircraft structures, Aeroelasticitity, Aeroelastic tailoring

Resumo

Os materiais compósitos têm sido cada vez mais utilizados em estruturas aeronáuticas, uma vez que permitem poupanças de peso significativas, conduzindo a uma maior eficiência. A conceção de estruturas em materiais compósitos tem sido orientada por um conjunto de regras que tornaram complexos os processos de conceção e fabrico. Os laminados 'Double-Double' (DD) apresentam uma nova perspetiva de laminados compósitos. Através de uma abordagem de campo contínuo baseada na homogeneização de laminados, os DD procuram permitir uma conceção, otimização e fabrico de compósitos mais simples. Sendo um novo conceito, Double-Double ainda requer uma investigação significativa para ser compreendido e aplicado ao projeto estrutural de aeronaves. As aeronaves comerciais modernas têm estruturas leves e flexíveis capazes de suster deformações significativas em voo. O campo da aeroelasticidade estuda a interação da flexibilidade e inércia da aeronave com as forças aerodinâmicas e desempenha um papel importante nos processos de conceção e certificação. As estruturas de aeronaves aeroelasticamente adaptadas são obtidas através da otimização da distribuição da rigidez da estrutura para permitir um aumento da eficiência da aeronave.

O presente trabalho procura explorar o efeito dos laminados Double-Double no comportamento aeroelástico de estruturas em materiais compósitos e fornecer informações sobre a sua potencial utilização na adaptação aeroelástica. Um modelo aeroelástico de uma placa encastrada é desenvolvido e utilizado para avaliar os laminados Double-Double em relação a uma condição aeroelástica estática e instabilidades aeroelásticas. Este modelo é depois introduzido numa estrutura de otimização multi-objetivo, que considera ambas as métricas aeroelásticas, utilizando um algoritmo genético. Em primeiro lugar, o espaço objetivo aeroelástico e o efeito da homogeneização no comportamento aeroelástico são explorados para um laminado DD unidirecional com espessura constante. Duas configurações com variação de espessura são avaliadas para compreender o seu impacto no espaço objetivo. Vários estudos de otimização simples e multi-objetivo são realizados, considerando tanto a condição aeroelástica estática como a instabilidade aeroelástica, comparando os laminados Double-Double com laminados tipicamente utilizados para a adaptação aeroelástica. No contexto destes estudos de otimização, são também explorados os laminados DD com fibras curvilíneas. Finalmente, é desenvolvido um modelo aeroelástico de uma estrutura de uma asa representativa de uma configuração atual de aeronave para permitir a extensão do trabalho atual a estruturas aeronáuticas mais realistas.

O comportamento aeroelástico dos laminados Double-Double é independente da homogeneização do laminado. As desvantagens encontradas para laminados Double-Double unidirecionais são facilmente ultrapassadas através da variação de espessura e da introdução de fibras curvilíneas. Através de uma conceção e otimização simples, os laminados Double-Doubles são promissores para a adaptação aeroelástica de estruturas compósitas. Em última análise, o presente trabalho constitui uma contribuição valiosa para a compreensão do comportamento aeroelástico dos laminados Double-Double.

Palavras-chave: Double-Double, Materiais compósitos, Estruturas aeronáuticas, Aeroelasticidade, Adaptação aeroelástica

Contents

List of Figures

List of Tables

Acronyms

AIC Aerodynamic Influence Coefficient.

CFRP Carbon Fibre-Reinforced Plastic.

CLT Classical Lamination Theory.

CRM Common Research Model.

DD Double-Double.

DLM Doublet-Lattice Method.

FPS Finite Plate Spline.

GA Genetic Algorithm.

HTP Horizontal Tailplane.

MAC Mean Aerodynamic Chord.

NSGA-II Non-dominated Sorting Genetic Algorithm II.

SBX Simulated Binary Crossover.

uCRM undeflected Common Research Model.

1
Introduction

1.1. Background and Motivation

Composite materials, in particular carbon fibre-reinforced polymers, have occupied an increasingly significant role in the aerospace and aeronautical industries, with some modern aircraft having over 50% of their structural weight in composite components. Compared to traditional aircraft materials like aluminium, composites allow for lighter structures leading to significant benefits in terms of fuel burn or aircraft range. However, while composite usage has developed, the way in which composites are designed has not changed significantly. Composite laminates are still bound by a set of rules developed decades ago that complicate their design and integration in complex structures. Current composite laminates are still limited by these guidelines for two main reasons: most experimental data available is of these laminates, and they are currently certified for aircraft structures.

The Double-Double family of laminates provides a new outlook on composite design that makes these rules unnecessary. It uses a novel continuous field based approach, grounded on laminate homogenisation through sublaminate repetition, to enable simplified laminate design, optimisation and manufacture. Being a new approach to composite design, Double-Double cannot be immediately implemented in structural design as they are not yet certified and still require significant research.

Modern aircraft structures are flexible, with wings capable of withstanding wingtip displacements of several metres. The effect of aircraft flexibility on aircraft behaviour has repercussions in terms of in-flight loads and structural failure and instability. These issues are studied by the field of aeroelasticity, which considers the interaction of aerodynamic, inertial and elastic forces. Aeroelastic behaviour is dominated by the stiffness of the structure, which in turn is highly influenced by the materials used. Given its significance in aircraft behaviour and the flexibility of modern aircraft, aeroelasticity and aeroelastic phenomena have now become mandatory points of evaluation for aircraft certification.

Composite materials have widely been studied to find optimal structural stiffness distribution with aeroelastic considerations, in what is known as aeroelastic tailoring. Aeroelastically tailored aircraft structures have been shown to provide significant benefits, allowing for lower weight, increased aerodynamic and fuel consumption efficiency as well as load reduction.

1.2. Research Question and Contributions

This thesis is driven by the need to understand the aeroelastic behaviour of composite structures using Double-Double laminates. Therefore, this work seeks to answer the following questions:

What effects do Double-Double laminates have on the aeroelastic response of composite structures?
How can Double-Double laminates be used for aeroelastic tailoring?

The main contributions of the thesis are the following:

- Integration of the finite element solver MSC Nastran in an automated optimisation framework based on the Python programming language
- Assessment of the impact of Double-Double laminates on static aeroelasticity and aeroelastic instability phenomena
- Establishment of a baseline aeroelastic model of a representative wingbox structure for aeroelastic tailoring studies

1.3. Thesis Outline

The thesis is structured as follows. In chapter 2 the relevant topics to the work developed are reviewed. Essential composite laminate mechanics are introduced and the design rules for conventional aerospace composites are explained. Double-Double laminates are presented, discussing their biggest differences to traditional laminates and their potential. Aircraft aeroelasticity and aeroelastic tailoring are also explored.

Chapter 3 presents the fundamental problem of the work developed: aeroelastic analysis of a cantilevered composite plate. An aeroelastic model, based on the finite element method with linearised potential flow aerodynamics, that allows for both static aeroelastic and flutter analysis is developed in the MSC Nastran solver and validated with available literature. The model is integrated in a multi-objective optimisation framework with a genetic algorithm in the python programming language and this framework is also validated.

Chapter 4 discusses the effects of Double-Double laminates on the aeroelastic behaviour of the plate. Static aeroelasticity and aeroelastic instabilities (divergence and flutter) are considered both individually and simultaneously. Both unidirectional and tow steered Double-Double laminates are explored.

In chapter 5, an aeroelastic model of a wingbox structure representative of a modern, long range commercial aircraft is developed to allow for the extension of the current work to more realistic aircraft structures.

Chapter 6 summarises the conclusions drawn throughout the thesis and provides recommendations for future work on this topic.

2
Literature Review

In this chapter, literature relevant to the subject areas of the work conducted in this thesis is reviewed. First, the mechanics of composite laminates are introduced through Classical Lamination Theory, lamination parameters and Tsai's modulus. This is followed by a brief review of design guidelines for aerospace composites. Double-Double laminates are then presented, highlighting their potential advantages in terms of laminate design and optimisation. Aircraft aeroelasticity, the most significant phenomena and its importance in current aircraft design and certification are discussed. Finally, the concept of aeroelastic tailoring is presented and several studies in this field are reviewed.

2.1. Composite Materials

Since their first introduction into primary structures of commercial aircraft in the 1980s, composite materials have been increasingly used in aircraft structures. Modern aircraft designs such as the Boeing 787 and Airbus A-350 have over 50% of their structural weight in composite materials [1]. The increased popularity of composite materials is mostly due to their attractive stiffness- and strength-to-weight ratios when compared to more traditional aircraft structural materials like aluminium [2]. Furthermore, by taking advantage of the anisotropy of composites, structural components can be tailored with more directional strength and stiffness.

A composite material can be defined as any material that consists of a combination of two or more materials/constituents. The focus of this work is on laminated fibre-reinforced composite materials. The basic building block of this type of composite is a ply (or lamina), where fibres, the reinforcement, are embedded in a polymer matrix. These plies are then stacked together in different orientations to form a laminate. It should be noted that laminates are not restricted to having plies with the same combination of fibre and matrix, or even to have all plies of composite material. An example of such laminated composite is GLARE, a composite laminate with aluminium plies interspersed with glass fibre plies, used in the upper fuselage of the Airbus A-380 aircraft [1, 2]. In aircraft primary structures, Carbon Fibre-Reinforced Plastics (CFRPs) with an epoxy matrix are widely used.

2.1.1. Classical Lamination Theory

The relation between the stresses and strains for a generally anisotropic linear elastic material is given by generalised Hooke's law as [1–3]:

$$\sigma_i = C_{ij}\varepsilon_j \qquad i, j \in [1, 6] \tag{2.1}$$

where σ_i are the stress components, C_{ij} is the stiffness matrix and ε_j are the strain components. In fibre-reinforced composite plies there are three mutually perpendicular symmetry planes and therefore they are orthotropic. For orthotropic materials, the stiffness matrix is defined by 9 independent terms and the stress-strain relation is expressed by Equation 2.2:

$$\begin{Bmatrix} \sigma_1 \\ \sigma_2 \\ \sigma_3 \\ \tau_{23} \\ \tau_{13} \\ \tau_{12} \end{Bmatrix} = \begin{bmatrix} C_{11} & C_{12} & C_{13} & 0 & 0 & 0 \\ C_{12} & C_{22} & C_{23} & 0 & 0 & 0 \\ C_{13} & C_{23} & C_{33} & 0 & 0 & 0 \\ 0 & 0 & 0 & C_{44} & 0 & 0 \\ 0 & 0 & 0 & 0 & C_{55} & 0 \\ 0 & 0 & 0 & 0 & 0 & C_{66} \end{bmatrix} \begin{Bmatrix} \varepsilon_1 \\ \varepsilon_2 \\ \varepsilon_3 \\ \gamma_{23} \\ \gamma_{13} \\ \gamma_{12} \end{Bmatrix} \tag{2.2}$$

Under a plane stress assumption ($\sigma_3 = \tau_{13} = \tau_{23} = 0$), Equation 2.2 can be further reduced to

$$\begin{Bmatrix} \sigma_1 \\ \sigma_2 \\ \tau_{12} \end{Bmatrix} = \begin{bmatrix} Q_{11} & Q_{12} & 0 \\ Q_{12} & Q_{22} & 0 \\ 0 & 0 & Q_{66} \end{bmatrix} \begin{Bmatrix} \varepsilon_1 \\ \varepsilon_2 \\ \gamma_{12} \end{Bmatrix} \tag{2.3}$$

where Q_{ij} are the plane stress reduced stiffness terms given by:

$$Q_{ij} = C_{ij} - \frac{C_{i3}C_{j3}}{C_{33}} \qquad i,j = 1,2,6 \tag{2.4}$$

The plane stress stiffness terms can also be expressed in terms of the longitudinal Young's modulus E_1, the transverse Young's modulus E_2, the shear modulus G_{12} and the Poisson's ratios ν_{12}, ν_{21} as:

$$\begin{aligned} Q_{11} &= \frac{E_1}{1-\nu_{12}\nu_{21}} & Q_{22} &= \frac{E_2}{1-\nu_{12}\nu_{21}} \\ Q_{12} &= \frac{\nu_{12}E_2}{1-\nu_{12}\nu_{21}} = \frac{\nu_{21}E_1}{1-\nu_{12}\nu_{21}} & Q_{66} &= G_{12} \end{aligned} \tag{2.5}$$

It should be noted that ν_{12} and ν_{21} are related by:

$$\frac{\nu_{12}}{E_1} = \frac{\nu_{21}}{E_2} \tag{2.6}$$

The previous equations have all been expressed in terms of the principal coordinate axis of a ply. However, in most laminates there are rotated plies whose axis do not coincide with the laminate axis. The in-plane stresses and strains in the global laminate axis system (xy) are related to the stresses and strains in the local ply coordinated system ($1-2$) by Equations 2.7 and 2.8, respectively.

$$\begin{Bmatrix} \sigma_1 \\ \sigma_2 \\ \tau_{12} \end{Bmatrix} = [\mathbf{T}] \begin{Bmatrix} \sigma_x \\ \sigma_y \\ \tau_{xy} \end{Bmatrix} \tag{2.7}$$

$$\begin{Bmatrix} \varepsilon_1 \\ \varepsilon_2 \\ \gamma_{12} \end{Bmatrix} = [\mathbf{R}]\,[\mathbf{T}]\,[\mathbf{R}]^{-1} \begin{Bmatrix} \varepsilon_x \\ \varepsilon_y \\ \gamma_{xy} \end{Bmatrix} \tag{2.8}$$

where the transformation matrix $[\mathbf{T}]$ is given by:

$$\mathbf{T} = \begin{bmatrix} \cos^2\theta & \sin^2\theta & 2\sin\theta\cos\theta \\ \sin^2\theta & \cos^2\theta & -2\sin\theta\cos\theta \\ -\sin\theta\cos\theta & \sin\theta\cos\theta & \cos^2\theta - \sin^2\theta \end{bmatrix} \tag{2.9}$$

where θ is the angle between the 1-axis and the x-axis, *i.e.* the ply angle. The matrix $[\mathbf{R}]$ is used since engineering strain is being considered and is defined as:

$$\mathbf{R} = \begin{bmatrix} 1 & 0 & 0 \\ 0 & 1 & 0 \\ 0 & 0 & 2 \end{bmatrix} \tag{2.10}$$

It is then possible to show that the transformed stiffness matrix, $\left[\overline{\mathbf{Q}}\right]$, is given by Equation 2.11.

$$\left[\overline{\mathbf{Q}}\right] = [\mathbf{T}]^{-1} [\mathbf{Q}] [\mathbf{T}]^{-T} \tag{2.11}$$

A laminate is composed of several plies, each with its own individual orientation, stacked on top of each other. Under Classical Lamination Theory (CLT) several assumptions are made [1–3]:

- the laminate is made up of perfectly bonded plies and the bonds are assumed infinitesimally thin and non-shear-deformable, *i.e.* the displacements are continuous across ply boundaries;
- sections normal to the middle surface remain straight and normal under deformation ($\gamma_{xz} = \gamma_{yz} = 0$);
- sections normal to the middle surface maintain a constant length ($\varepsilon_z = 0$);
- the thickness of the laminate is small compared to the other dimensions.

With these hypotheses, the stress of a given k layer can be related with the laminate middle surface strains and curvatures as:

$$\begin{Bmatrix} \sigma_x \\ \sigma_y \\ \tau_{xy} \end{Bmatrix}_k = \begin{bmatrix} \overline{Q}_{11} & \overline{Q}_{12} & \overline{Q}_{16} \\ \overline{Q}_{12} & \overline{Q}_{22} & \overline{Q}_{26} \\ \overline{Q}_{16} & \overline{Q}_{26} & \overline{Q}_{66} \end{bmatrix}_k \left\{ \begin{Bmatrix} \varepsilon_x^0 \\ \varepsilon_y^0 \\ \gamma_{xy}^0 \end{Bmatrix} + z \begin{Bmatrix} \kappa_x \\ \kappa_y \\ \kappa_{xy} \end{Bmatrix} \right\} \tag{2.12}$$

where $\varepsilon_x^0, \varepsilon_y^0, \gamma_{xy}^0$ are the laminate mid-surface strains and $\kappa_x, \kappa_y, \kappa_{xy}$ are the mid-surface curvatures. The force and moment resultants, $\boldsymbol{N}$ and $\boldsymbol{M}$ respectively, are defined by integrating the stresses over laminate thickness h as:

$$N_x = \int_{-\frac{h}{2}}^{\frac{h}{2}} \sigma_x \, dz \qquad N_y = \int_{-\frac{h}{2}}^{\frac{h}{2}} \sigma_y \, dz \qquad N_{xy} = \int_{-\frac{h}{2}}^{\frac{h}{2}} \tau_{xy} \, dz \tag{2.13}$$

$$M_x = \int_{-\frac{h}{2}}^{\frac{h}{2}} \sigma_x z \, dz \qquad M_y = \int_{-\frac{h}{2}}^{\frac{h}{2}} \sigma_y z \, dz \qquad M_{xy} = \int_{-\frac{h}{2}}^{\frac{h}{2}} \tau_{xy} z \, dz \tag{2.14}$$

Given that each ply can have its own orientation, the ply stiffnesses, although constant within each ply, are not necessarily the same from one ply to another. Therefore, the integrals of Equations 2.13 and 2.14 become summations over all N laminate plies. The force and moment resultants are then expressed as:

$$\begin{Bmatrix} N_x \\ N_y \\ N_{xy} \end{Bmatrix} = \begin{bmatrix} A_{11} & A_{12} & A_{16} \\ A_{12} & A_{22} & A_{26} \\ A_{16} & A_{26} & A_{66} \end{bmatrix} \begin{Bmatrix} \varepsilon_x^0 \\ \varepsilon_y^0 \\ \gamma_{xy}^0 \end{Bmatrix} + \begin{bmatrix} B_{11} & B_{12} & B_{16} \\ B_{12} & B_{22} & B_{26} \\ B_{16} & B_{26} & B_{66} \end{bmatrix} \begin{Bmatrix} \kappa_x \\ \kappa_y \\ \kappa_{xy} \end{Bmatrix} \tag{2.15}$$

$$\begin{Bmatrix} M_x \\ M_y \\ M_{xy} \end{Bmatrix} = \begin{bmatrix} B_{11} & B_{12} & B_{16} \\ B_{12} & B_{22} & B_{26} \\ B_{16} & B_{26} & B_{66} \end{bmatrix} \begin{Bmatrix} \varepsilon_x^0 \\ \varepsilon_y^0 \\ \gamma_{xy}^0 \end{Bmatrix} + \begin{bmatrix} D_{11} & D_{12} & D_{16} \\ d_{12} & D_{22} & D_{26} \\ D_{16} & D_{26} & D_{66} \end{bmatrix} \begin{Bmatrix} \kappa_x \\ \kappa_y \\ \kappa_{xy} \end{Bmatrix} \tag{2.16}$$

where

$$A_{ij} = \sum_{k=1}^{N} \left(\overline{Q}_{ij}\right)_k (z_k - z_{k-1}) \tag{2.17}$$

$$B_{ij} = \frac{1}{2}\sum_{k=1}^{N} \left(\overline{Q}_{ij}\right)_k \left(z_k^2 - z_{k-1}^2\right) \tag{2.18}$$

$$D_{ij} = \frac{1}{3}\sum_{k=1}^{N} \left(\overline{Q}_{ij}\right)_k \left(z_k^3 - z_{k-1}^3\right) \tag{2.19}$$

where $i, j = 1, 2, 6$ and z_k, z_{k-1} are the upper and lower coordinates of ply k as shown in Figure 2.1. Equations 2.15 and 2.16 can be expressed in a condensed form as:

$$\begin{Bmatrix} \boldsymbol{N} \\ \boldsymbol{M} \end{Bmatrix} = \begin{bmatrix} [\boldsymbol{A}] & [\boldsymbol{B}] \\ [\boldsymbol{B}] & [\boldsymbol{D}] \end{bmatrix} \begin{Bmatrix} \boldsymbol{\varepsilon^0} \\ \boldsymbol{\kappa} \end{Bmatrix} \tag{2.20}$$

In the previous equation, $\boldsymbol{A}$ is the in-plane (or membrane or extension) stiffness matrix, $\boldsymbol{D}$ is the bending (or flexural) stiffness matrix and $\boldsymbol{B}$ is the bending-extension coupling stiffness matrix. It is useful and convenient to normalise these stiffness matrices with respect to the laminate thickness h as:

$$[\boldsymbol{A}^*] = \frac{[\boldsymbol{A}]}{h} \qquad [\boldsymbol{B}^*] = \frac{2[\boldsymbol{B}]}{h^2} \qquad [\boldsymbol{D}^*] = \frac{12[\boldsymbol{D}]}{h^3} \tag{2.21}$$

These normalised stiffness matrices are expressed in consistent units, such as GPa, allowing for a better comparison between the elements of the different matrices. Furthermore, as they are normalised with respect to the thickness they also facilitate the comparison between different laminates.

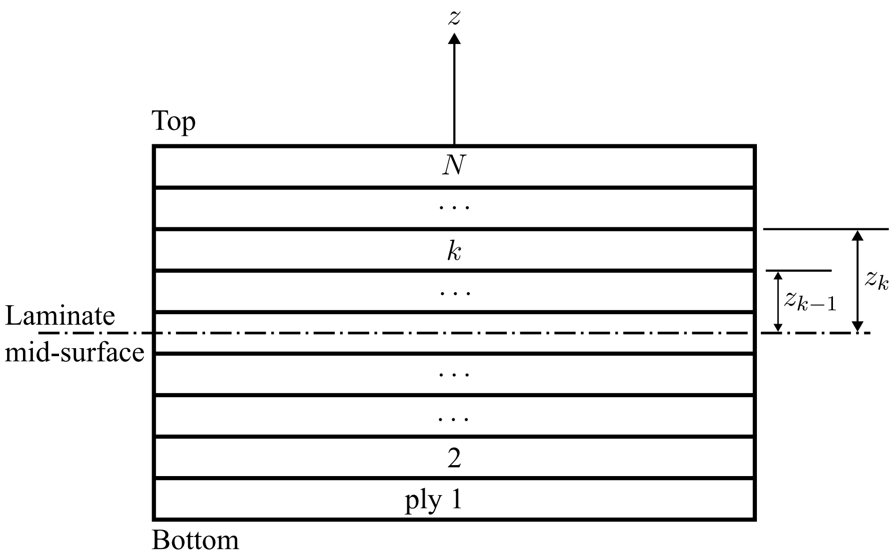

Figure 2.1: Generic N ply laminate and ply numbering system for Classical Lamination Theory

2.1.1.1. Lamination Parameters

Tsai and Pagano [4] proposed an alternative formulation for the laminate stiffness matrices where the stiffness matrix terms are functions of five material parameters, $\{U\}$, and twelve lamination parameters ($\xi_i^A, \xi_i^B, \xi_i^D$ where $i = 1, \ldots, 4$), given by:

$$\begin{Bmatrix} A_{11} \\ A_{22} \\ A_{12} \\ A_{66} \\ A_{16} \\ A_{26} \end{Bmatrix} = h \begin{bmatrix} 1 & \xi_1^A & \xi_2^A & 0 & 0 \\ 1 & -\xi_1^A & \xi_2^A & 0 & 0 \\ 0 & 0 & -\xi_2^A & 1 & 0 \\ 0 & 0 & -\xi_2^A & 0 & 1 \\ 0 & \xi_3^A/2 & \xi_4^A & 0 & 0 \\ 0 & \xi_3^A/2 & -\xi_4^A & 0 & 0 \end{bmatrix} \begin{Bmatrix} U_1 \\ U_2 \\ U_3 \\ U_4 \\ U_5 \end{Bmatrix} \tag{2.22}$$

$$\begin{Bmatrix} B_{11} \\ B_{22} \\ B_{12} \\ B_{66} \\ B_{16} \\ B_{26} \end{Bmatrix} = \frac{h^2}{2} \begin{bmatrix} 1 & \xi_1^B & \xi_2^B & 0 & 0 \\ 1 & -\xi_1^B & \xi_2^B & 0 & 0 \\ 0 & 0 & -\xi_2^B & 1 & 0 \\ 0 & 0 & -\xi_2^B & 0 & 1 \\ 0 & \xi_3^B/2 & \xi_4^B & 0 & 0 \\ 0 & \xi_3^B/2 & -\xi_4^B & 0 & 0 \end{bmatrix} \begin{Bmatrix} U_1 \\ U_2 \\ U_3 \\ U_4 \\ U_5 \end{Bmatrix} \tag{2.23}$$

$$\begin{Bmatrix} D_{11} \\ D_{22} \\ D_{12} \\ D_{66} \\ D_{16} \\ D_{26} \end{Bmatrix} = \frac{h^3}{12} \begin{bmatrix} 1 & \xi_1^D & \xi_2^D & 0 & 0 \\ 1 & -\xi_1^D & \xi_2^D & 0 & 0 \\ 0 & 0 & -\xi_2^D & 1 & 0 \\ 0 & 0 & -\xi_2^D & 0 & 1 \\ 0 & \xi_3^D/2 & \xi_4^D & 0 & 0 \\ 0 & \xi_3^D/2 & -\xi_4^D & 0 & 0 \end{bmatrix} \begin{Bmatrix} U_1 \\ U_2 \\ U_3 \\ U_4 \\ U_5 \end{Bmatrix} \tag{2.24}$$

The material parameters are functions of the reduced stiffness matrix terms, previously defined in Equations 2.3, 2.4, 2.5, and are given by:

$$\begin{aligned} U_1 &= (3Q_{11} + 3Q_{22} + 2Q_{12} + 4Q_{66})/8 \\ U_2 &= (Q_{11} - Q_{22})/2 \\ U_3 &= (Q_{11} + Q_{22} - 2Q_{12} - 4Q_{66})/8 \\ U_4 &= (Q_{11} + Q_{22} + 6Q_{12} - 4Q_{66})/8 \\ U_3 &= (Q_{11} + Q_{22} - 2Q_{12} + 4Q_{66})/8 \end{aligned} \tag{2.25}$$

The in-plane, $\xi^A_{[1,2,3,4]}$, coupling, $\xi^B_{[1,2,3,4]}$, and out-of-plane, $\xi^D_{[1,2,3,4]}$, lamination parameters are calculated as:

$$\xi^A_{[1,2,3,4]} = \frac{1}{h}\int_{-\frac{h}{2}}^{\frac{h}{2}} [\cos 2\theta, \sin 2\theta, \cos 4\theta, \sin 4\theta]\, dz \tag{2.26}$$

$$\xi^B_{[1,2,3,4]} = \frac{4}{h^2}\int_{-\frac{h}{2}}^{\frac{h}{2}} [\cos 2\theta, \sin 2\theta, \cos 4\theta, \sin 4\theta]\, z\, dz \tag{2.27}$$

$$\xi^D_{[1,2,3,4]} = \frac{12}{h^3}\int_{-\frac{h}{2}}^{\frac{h}{2}} [\cos 2\theta, \sin 2\theta, \cos 4\theta, \sin 4\theta]\, z^2\, dz \tag{2.28}$$

where h is the laminate thickness.

2.1.1.2. Tsai's Modulus

Tsai and Melo [5] proposed a new approach to characterise the stiffness of composite plies and laminates based on invariants, taking the trace of the in-plane stiffness matrix ($\mathrm{tr}(\boldsymbol{Q})$) as a material property. If tensorial strains are considered instead of engineering strains, then Equation 2.3 is rewritten as:

$$\begin{Bmatrix} \sigma_1 \\ \sigma_2 \\ \tau_{12} \end{Bmatrix} = \begin{bmatrix} Q_{11} & Q_{12} & 0 \\ Q_{12} & Q_{22} & 0 \\ 0 & 0 & 2Q_{66} \end{bmatrix} \begin{Bmatrix} \varepsilon_1 \\ \varepsilon_2 \\ \varepsilon_{12} \end{Bmatrix} \tag{2.29}$$

where $\varepsilon_{12} = \gamma_{12}/2$ is the tensorial shear strain and the in-plane stiffness matrix is:

$$[\boldsymbol{Q}] = \begin{bmatrix} Q_{11} & Q_{12} & 0 \\ Q_{12} & Q_{22} & 0 \\ 0 & 0 & 2Q_{66} \end{bmatrix} \tag{2.30}$$

The trace of $\boldsymbol{Q}$ is then defined by:

$$\mathrm{tr}(\boldsymbol{Q}) = Q_{11} + Q_{22} + 2Q_{66} \tag{2.31}$$

As trace is an invariant, it is independent of coordinate system and $\mathrm{tr}(\boldsymbol{Q})$ will always be the same independently of ply orientation. In fact, the trace of the normalised in-plane and flexural matrices of a laminate is the same as the trace of the in-plane stiffness matrix of a ply, as shown in Equation 2.32. Therefore, trace becomes a relevant property of the material being independent of coordinate system, material symmetry, loading condition (in-plane or flexural) and stacking sequence. Trace then represents the maximum stiffness of a composite. It has been proposed to name $\mathrm{tr}(\boldsymbol{Q})$ as *Tsai's Modulus* to recognise prof. Stephen W. Tsai's work in composite materials and on the discovery of this property [6].

$$\mathrm{tr}(\boldsymbol{Q}) = \mathrm{tr}(\boldsymbol{A}^*) = \mathrm{tr}(\boldsymbol{D}^*) \tag{2.32}$$

In Refs. [5, 6] the potential of Tsai's modulus as a scaling property in composite analysis, testing and design is explored. Furthermore, the concept of a 'Master Ply' for CFRP laminates using Tsai's modulus is presented.

2.1.2. Traditional Aerospace Composites

Conventional laminates used in aerospace and aeronautical industries follow a set of design rules. These guidelines were established to provided confidence in composite design for aircraft structures. These 'traditional' laminates, which have their ply angles restricted to $0°$, $\pm 45°$ and $90°$, will be referred to as Legacy Quad laminates. Legacy Quad laminates are still widely used mostly for two reasons: the majority of available experimental data is restricted to these laminates and these laminates are certified for use in aircraft structures. The most important design guidelines, which are available in literature such as Refs. [1, 7], are provided below:

1. **Laminates should be symmetric**. This uncouples the membrane and bending behaviour ($[B] = 0$) and reduces warping under thermal loads.

2. **Laminates should be balanced**, that is for every $+\theta$ ply in the laminate there should be a $-\theta$ ply. This removes the extension-shear coupling ($A_{16} = A_{26} = 0$).

3. **10% rule**. At least 10% of the plies in a laminate should be aligned with each of the four ply angle directions (0°, ±45° and 90°) to account for secondary load conditions. Although 10% is a common value, other values are also used (7%, 12%, 15%).

4. **Maximum ply grouping of 4 plies**. No more than 4 plies with the same orientation should be placed together in the laminate to prevent rapid growth of matrix cracks.

5. **Maximum inter-ply angle of 45°**. The difference in the angle between two adjacent plies should be less than or equal to 45° to minimise interlaminar shear stresses.

2.1.3. Double-Double

Double-Double (DD) is a new family of laminates recently proposed by Tsai [8] as an alternative to Legacy Quad laminates. DD laminates are based on the repetition of a 4-ply building block and are characterised by two angles, Φ and Ψ, which can vary between 0° and 90° and where the building block has two plies of each angle (one with positive angle and one with the negative). They can be defined in a condensed notation as $[\pm\Phi/\pm\Psi]_{rT}$ or by explicitly defining the building block stacking sequence with the rT subscript, where r is the number of building block repetitions and T stands for total number of plies. From this small definition already a significant difference can be found between Legacy Quad and DD laminates: while quads are discrete as they consist of permutations of 0°, ±45° and 90° plies, Double-Double are continuous. As DD laminates are made of ± pairs of ply angles, they are naturally balanced and therefore do not have extension-shear coupling ($A^*_{16} = A^*_{26} = 0$).

Homogenisation is a key concept for Double-Double. A laminate is considered homogenised if it has equal and uncoupled normalised in-plane and flexural stiffness as shown in Equation 2.33. Homogenisation removes the need for some of the design rules of Quad laminates. The in-plane and flexural stiffness behaviours are naturally uncoupled, meaning mid-plane symmetry does not need to be enforced. Sub-laminate repetition increases laminate homogenisation. DD laminates have thin 4-ply building blocks, making it easier to achieve laminate homogenisation [9].

$$\begin{aligned}[\boldsymbol{A}^*] &= [\boldsymbol{D}^*] \\ [\boldsymbol{B}^*] &= 0\end{aligned} \tag{2.33}$$

Homogenisation also facilitates ply drop-offs, enabling easier laminate tapering and potential weight savings. In Legacy Quad laminates, when plies are dropped, they need to be removed in symmetric pairs to maintain mid-plane symmetry. However, by dropping plies the percentage of each Quad ply angle change and this results in a discrete change of the in-plane and bending stiffnesses between the zones of the tapered laminate. With Double-Double tapering can easily be achieved by removal or addition of building blocks, modifying the overall stiffness by changing the thickness, similarly to metals, but the laminate stiffness matrices do not change between zones with different thicknesses [9]. Additional benefits of homogenisation in DD, particularly concerning manufacturing, exist and are explored more in depth in Refs. [8, 9]. True homogenisation is, nevertheless, difficult to achieve when manufacturing is considered. Therefore, a more practical homogenisation criterion using Tsai's modulus has been proposed by Zhao *et al.* [10] as:

$$\begin{aligned}\left|\left[A^*_{ij}\right] - \left[D^*_{ij}\right]\right| &< 2\% \text{ Tsai's modulus} \\ \left|\left[B^*_{ij}\right]\right| &< 2\% \text{ Tsai's modulus}\end{aligned} \tag{2.34}$$

Double-Double laminates allow only six possible building block stacking sequences [9]:

- Staggered 1: $[\Phi/-\Psi/-\Phi/\Psi]_{rT}$
- Staggered 2: $[\Phi/\Psi/-\Phi/-\Psi]_{rT}$
- Staggered 3: $[\Phi/-\Psi/\Psi/-\Phi]_{rT}$
- Staggered 4: $[\Phi/\Psi/-\Psi/-\Phi]_{rT}$
- Paired 1: $[\Phi/-\Phi/\Psi/-\Psi]_{rT}$
- Paired 2: $[\Phi/-\Phi/-\Phi/\Psi]_{rT}$

Recalling the definition of lamination parameters in Equations 2.26, 2.27 and 2.28, it can be seen that the lamination parameters of the in-plane stiffness matrix are independent of the stacking sequence as there is no z in the integral. In fact, the ξ_i^A lamination parameters depend only on the percentage of each unique ply angle inside a laminate, which for DD laminates is the same regardless of building block stacking sequence and repetitions. These parameters can then be calculated for any DD laminate from a building block stacking sequence, for instance Staggered 1, as:

$$\xi_1^A = \frac{\cos 2\Phi + \cos(-2\Phi) + \cos(-2\Psi) + \cos 2\Psi}{4} = \frac{\cos 2\Phi + \cos 2\Psi}{2} \tag{2.35}$$

$$\xi_2^A = \frac{\cos 4\Phi + \cos(-4\Phi) + \cos(-4\Psi) + \cos 4\Psi}{4} = \frac{\cos 4\Phi + \cos 4\Psi}{2} \tag{2.36}$$

$$\xi_3^A = \frac{\sin 2\Phi + \sin(-2\Phi) + \sin(-2\Psi) + \sin 2\Psi}{4} = 0 \tag{2.37}$$

$$\xi_4^A = \frac{\sin 4\Phi + \sin(-4\Phi) + \sin(-4\Psi) + \sin 4\Psi}{4} = 0 \tag{2.38}$$

If we combine the four previous equations with the definition for laminate homogenisation and how the laminate stiffness matrices can be obtained from lamination parameters, it becomes clear that for Double-Double only the two lamination parameters $\xi_1^A = \xi_1^D$ and $\xi_2^A = \xi_2^D$ are necessary to describe a laminate. The expressions for the calculation of these parameters as a function of the DD angles are repeated below for completeness.

$$\xi_1^A = (\cos 2\Phi + \cos 2\Psi)/2 \tag{2.39}$$

$$\xi_2^A = (\cos 4\Phi + \cos 4\Psi)/2 \tag{2.40}$$

The reciprocal relations establishing the angles from the lamination parameters can be obtained from the previous equations as:

$$\cos 2\Psi = \xi_1^A + \sqrt{-\xi_1^{A^2} + \xi_2^A/2 + 0.5} \tag{2.41}$$

$$\cos 2\Phi = 2\xi_1^A - \cos 2\Psi \tag{2.42}$$

Zhao *et al.* [10] derived, based on Lagrange multipliers, the feasible space of DD in terms of these lamination parameters, as shown in Figure 2.2, and further confirmed that $\xi_1^A = \xi_1^D$ and $\xi_2^A = \xi_2^D$. Selecting a Double-Double stacking sequence from the six ones shown above is simple: as long as the number of repeats is sufficient to ensure homogenisation any of the stacking sequences can be used. As lightweight structures are an ever present need in aerospace and aircraft structures and efficient laminate tapering can lead to significant weight savings, it is of interest to know which stacking sequences allow for homogenisation with the lowest number of repeats. Zhao *et al.* [10] found that through a combination of Staggered 1 and Staggered 3 the homogenisation criterion of Equation 2.34 can be met in the entire Double-Double domain. The choice between these two stacking sequences is done based on lamination parameters and is explained in further detail in section 4.1.

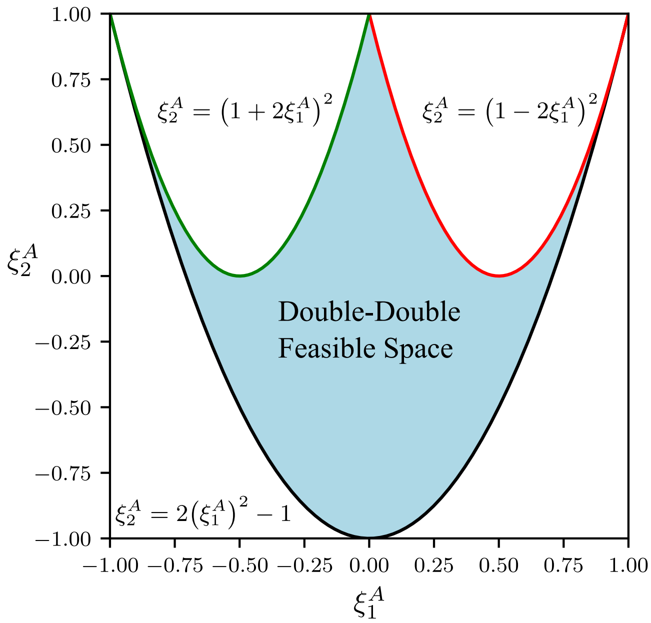

Figure 2.2: Double-Double feasible domain in lamination parameter space

Overall, Double-Double laminates offer the following advantages [8, 9]:

- Simpler laminate design due to a continuous field without unnecessary design rules;
- Simpler laminate characterisation: laminates are described only with two parameters (angles or lamination parameters) and the number of building block repeats
- Homogenisation:
  - Only one laminate stiffness matrix ($[\boldsymbol{A}^*]$) needs to be calculated;
  - Easier thickness tapering, leading to higher weight savings;
- Low number of possible stacking sequences: maximum of 6, with 2 preferable for faster homogenisation.

2.1.3.1. Simplified Laminate Optimisation

The optimisation of composite structures is inherently connected with obtaining the ideal laminate stacking sequence. The complexity of a composite optimisation problem is related to the scale of the problem and the chosen design variables, with the latter usually determining the type of optimisation performed. A review of optimisation strategies for composite laminates can be found in Refs. [11, 12]. In laminate optimisation, the stacking sequence can be obtained by considering the individual ply angles or lamination parameters as design variables.

In the first approach, by considering ply angles as discrete design variables the laminate stacking sequence can be directly obtained from the optimisation process. Heuristic optimisation approaches, such as Genetic Algorithms (GAs), are particularly well suited for these discrete optimisation problems. However, if the optimisation problems are of a large scale, such as typical aircraft structures, these optimisers become computationally expensive as they require a high number of function evaluations and laminates have a high number of plies leading to high dimensional problems [13].

On the other hand, lamination parameters are continuous and convex [14] making them ideal for gradient based optimisers. Furthermore, a given laminate is always described by a fixed number of variables: the 12 lamination parameters and the laminate thickness, meaning the problem dimension can be easily controlled and is defined by the number of regions or individual laminates to optimise. Gradient based optimisers are better suited for large scale applications where function evaluations are more computationally expensive, as they require fewer iterations for convergence. However, these solutions do not obtain final stacking sequences. Therefore, an additional discrete optimisation process needs to be performed to recover stacking sequences from the set of lamination parameters and laminate thickness [13]. The process of obtaining stacking sequences from lamination parameters is complex since with Quad laminates there are multiple laminates that can have the same lamination parameters [9]. Additional manufacturing constraints such as laminate blending between adjacent zones of the same component add to this complexity [13].

It is then possible to conclude that optimisation of large structures with Legacy Quad laminates is a complex task. With Double-Double, however, these problems are simplified. First, DD is continuous so efficient gradient based optimisers can be used. As was shown in the previous section, the DD angles and lamination parameters are directly related, so there is little difference between choosing one or the other as optimisation design variables. In fact, there is only a small advantage in choosing the angles as design variables, since, besides lower and upper bounds, lamination parameters require the imposition of the feasible region of Figure 2.2 as a design constraint. Finally, if stacking sequence is selected between Staggered 1 and Staggered 3 based on lamination parameters as proposed by Zhao *et al.* [10], it can be obtained directly as a consequence of the optimisation process.

2.2. Aeroelastic Tailoring

2.2.1. Aircraft Aeroelasticity

The field of aeroelasticity studies the interaction between aerodynamic, inertial, and elastic forces for a flexible structure and the phenomena it can lead to [15, 16]. It is applied in the design of several structures such as helicopters, wind turbine blades, bridges, etc., playing a significant role in modern aircraft structures. The field of aeroelasticity is famously summarised in Collar's aeroelastic triangle [15–17], shown in Figure 2.3, showing how different branches of aeroelastic study result from the interaction of the three types of forces. Static aeroelasticity, stability and control, and mechanical vibrations result from the two of the three forces interacting. Dynamic aeroelasticity, on the other hand, requires the interaction of all three forces.

Static aeroelasticity addresses the interaction of the flexible structure with aerodynamic loads in a steady state condition, *i.e.* with forces and movements being time independent. Aerodynamic load distribution in steady/equilibrium manoeuvres and the deformed wing shape are directly affected by the flexibility of the wing structure. Inadequate structural stiffness can lead to penalties in drag, control surface effectiveness, and aircraft trim and stability behaviour. The two critical phenomena in static aeroelasticity are **divergence** and **control reversal**. **Divergence** happens when the moments resulting from the aerodynamic loads overcome the restoring moments due to structural stiffness, resulting in

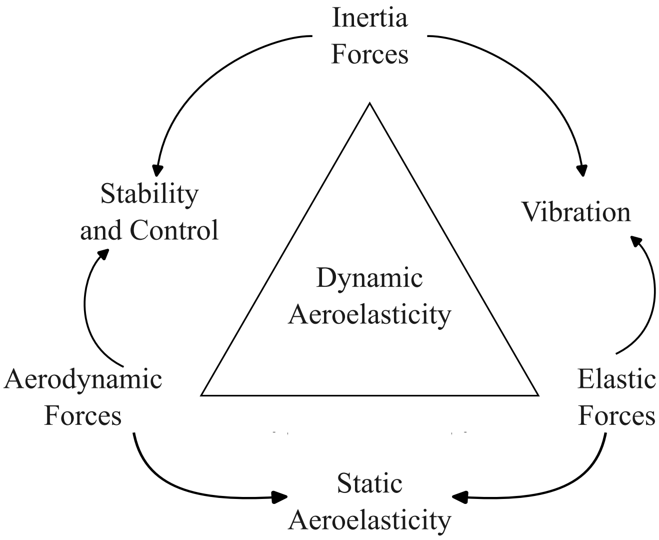

Figure 2.3: Collar's aeroelastic triangle (adapted from [15])

structural failure. The most common type is wing torsional divergence [15, 16]. One of the earliest known failures attributed to divergence was that of Langley's monoplane flying machine a few days before the Wright brothers' flight [16, 17]. The failure was due to insufficient torsional stiffness. When the machine was rebuilt a few years later with different wing trussing, significantly increasing the stiffness, it flew successfully. **Control reversal** happens when the aircraft velocity is higher than a critical velocity. As the aircraft speed increases, control effectiveness decreases until a critical speed, the *control reversal speed*, where the application of control surface has no effect. Beyond this speed, applying control surface has the opposite effect of what is intended [15, 16]. Even though control reversal may not result in failure, it is not acceptable to have very slow or no response near the reversal velocity, and the reverse effect beyond it. Some military aircraft use an active control system to take advantage of control reversal and achieve high manoeuvrability [15].

Dynamic aeroelasticity deals with the oscillatory effects of the interaction between the elastic, aerodynamic, and inertia forces. The main phenomenon of interest is **flutter**, a dynamic instability that results from the unfavourable coupling of the three forces and involves multiple modes of vibration. **Flutter** is a self-excited unstable vibration, where the structure effectively extracts energy from the airflow, and can often lead to structural failure. The unsteady nature of the aerodynamic forces and moments created by the oscillatory motion of the structure is the biggest difficulty in flutter analysis, particularly in the transonic regime [15, 16].

Aeroelastic considerations play a vital role in the design and certification process of modern aircraft. Regulatory agencies require that aircraft be free of any aeroelastic instability (flutter, divergence, control reversal) and are fully stable and controllable within the design flight envelope. For the accurate calculation of aircraft loads, both static and dynamic, it is also necessary to include relevant aeroelastic effects [15, 18, 19]. The relation between the three force types considered in aeroelasticity and the loads an aircraft experiences can be summarised by modifying Collar's triangle into a loads triangle, shown in Figure 2.4 [15].

Equilibrium (or **trimmed/steady**) **manoeuvres** consider the aircraft under longitudinal or lateral manoeuvres, experiencing accelerations normal to the flight path and pitching at a steady pitch rate. For example, steady banked turn and a pull-up from a dive are considered equilibrium manoeuvres. **Dynamic**

manoeuvres are the time-varying (dynamic) responses an aircraft experiences as the results of failure conditions or transient pilot control inputs. **Ground manoeuvre loads** consider all the conditions an aircraft is in contact with the ground through the landing gear. The load conditions can be both steady and dynamic, e.g. turning, taxiing, landing, braking. **Gust and turbulence** deal with the aircraft passing through moving air, responding to continuous turbulence or discrete gusts [15].

It is then clear that new structural designs (with new materials in a significant part of the structure, different aircraft layout/configuration, etc.) and new control configurations need to be studied for their impact on aeroelastic effects. The purpose of this thesis is to analyse the impact of using Double-Double laminates on aeroelastic behaviour.

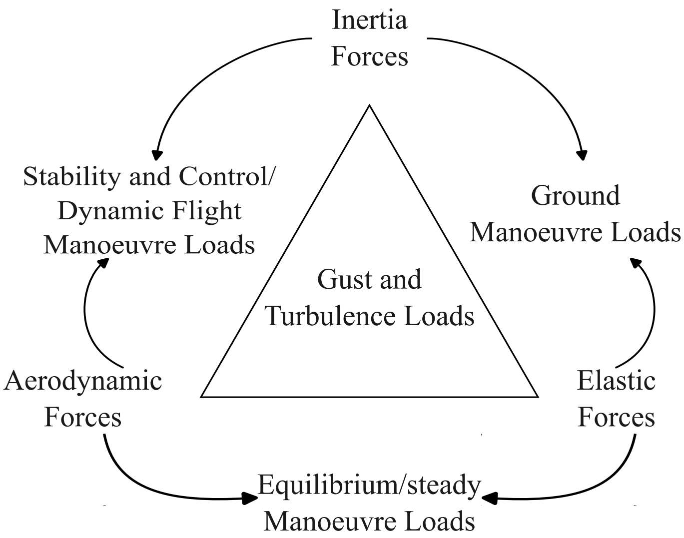

Figure 2.4: Loads triangle (adapted from [15])

2.2.2. Aeroelastic Tailoring: Concept and Studies

The structural design of modern aircraft is driven by a need for minimum weight to achieve higher performance and efficiency. Shirk *et al.* [20] defined aeroelastic tailoring as "the embodiment of directional stiffness into an aircraft structural design to control aeroelastic deformation, static or dynamic, in such a fashion as to affect the aerodynamic and structural performance of that aircraft in a beneficial way". Typical performance metrics considered in aeroelastic tailoring research include: lower weight airframes through manoeuvre and gust load alleviation, increase of critical aeroelastic velocity, lower fuel consumption, improved aerodynamic performance, etc. Composite materials have been prominently used in aeroelastic tailoring as their anisotropic nature allows for a higher control of the stiffness distribution and overall bending-twist coupling.

Note that aeroelastic tailoring can be achieved in a passive way, that is by modifying the stiffness distribution of the structure, or with an active approach combining the stiffness distribution modification with control surface augmentation and/or morphing structures [21–23]. This dissertation will focus on passive aeroelastic tailoring.

Aeroelastic tailoring effectively results in a modification of the structure's primary stiffness direction, as shown in Figure 2.5, changing the bending and torsional stiffness of the structure as well as the coupling between the two [21, 22]. The wing's primary stiffness direction is defined as "the locus of points where the structure exhibits the most resistance to bending deformation", whereas the structural reference axis is “the conventional wing structure elastic axis” [21]. When the primary stiffness direction is forward of the reference axis, the upwards bending of the wing results in a leading edge down twist, or wash-out behaviour. An aft primary stiffness direction results in a bending-twist coupling that causes a leading edge upwards twist with an upwards bending, or wash-in behaviour [20, 21]. Although both wash-out and wash-in cause improvements on wing performance, as shown in Figure 2.5, there is a clear compromise with one another. While wash-out results in higher divergence velocity is it accompanied by a lower flutter velocity, with the opposite being true for wash-in [22, 24].

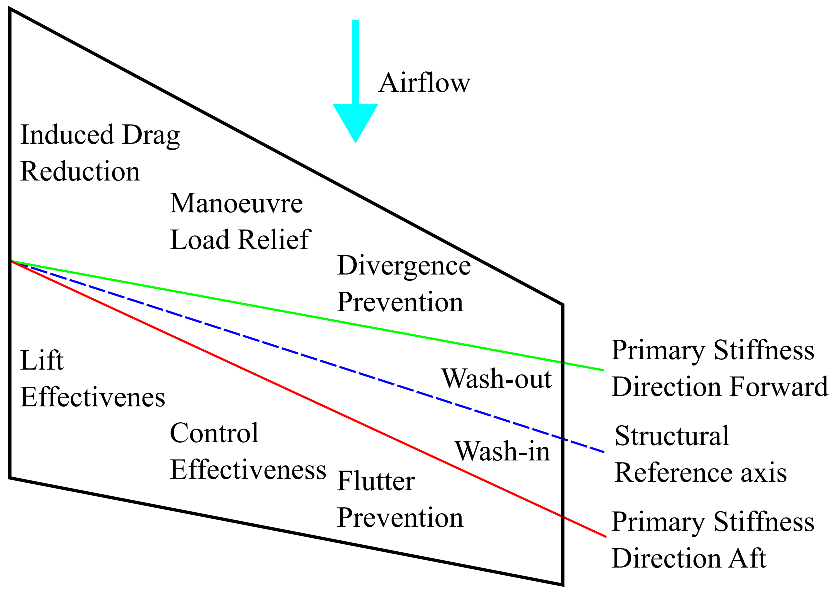

Figure 2.5: Benefits of aeroelastic tailoring based on the location of the primary stiffness direction (adapted from [20, 21])

Given its definition, aeroelastic tailoring is intrinsically a multidisciplinary problem involving the structural, control and aerodynamic behaviour of the aircraft. One of the best known applications of aeroelastic tailoring is the Grumman X-29 forward-swept wing demonstrator, where tailored composite materials were used to produce a bending-twist coupling that would limit the wing twist and prevent divergence [20].

The studies of Weisshaar [25, 26] and Shirk *et al.* [20] are among the first works on aeroelastic tailoring. Weisshaar [25] studied the effect of modifying fibre orientation of swept wings on the static aeroelastic metrics of divergence velocity, spanwise centre of pressure location, lift effectiveness, and lateral control effectiveness. Shirk *et al.* [20] formally defined aeroelastic tailoring and performed an historical review of its use, identifying relevant design trends. In Ref. [26], Weisshaar also performed a review of the work conducted about aeroelastic tailoring both for static and dynamic aeroelasticity with a focus on composite laminates. Weisshaar presented conceptual models used in some aeroelastic studies along with relevant equations and highlighted design trade-offs that might require consideration.

Hollowell and Dugundji [27] investigated the effect of bending-twist coupling on divergence and flutter behaviour of unswept rectangular wings idealised by cantilevered plates of graphite/epoxy laminates. Experimental and analytical studies with a Rayleigh-Ritz approach and unsteady, two-dimensional aerodynamics were performed on laminate plates with several amounts of bending-twist coupling and ply angles limited to 0°, ±30°, ±45° and 90°. At low angles of attack, plates with negative stiffness coupling, that is with a positive bending also resulting in upward leading edge twist, experienced divergence.

Plates with positive bending-twist coupling exhibited flutter, with high positive coupling values allowing for the delay of stall flutter at higher angles of attack.

Kameyama and Fukunaga [28] studied the effect of laminate configuration and sweep angle on the flutter and divergence behaviour of composite plates. The impact of laminate configuration was analysed through a representation of the flutter and divergence velocities in the lamination parameter space. It was found that there is a discontinuity of the critical velocity due to a switch in the critical flutter mode. A minimum weight aeroelastic tailoring optimisation of a composite plate subjected to flutter and divergence constraints was performed using a genetic algorithm with the lamination parameters as the design variables.

A recent trend on aeroelastic tailoring studies has been on the use of tow steered laminates. Stodieck *et al.* [29, 30] examined the effect of tow steered laminates on the vibration behaviour, flexural axis position, flutter and divergence velocities, and gust loads of a cantilevered plate wing. It was found that tow steered laminates increase the design space and allowed for higher flutter velocities and significant load reduction. Stanford *et al.* [31] performed studies on similar cantilevered composite plate considering a static aeroelastic condition, and flutter and divergence behaviour. They reached similar conclusions in terms of potential for load reduction with tow steered laminates. Furthermore, it was also found that even when a more limited steering concept was used, where instead of allowing individual ply steering a fixed core laminated was rotated along a given path, it was still possible to obtain improvements in terms of load response.

Regarding more realistic wingbox structures, the NASA Common Research Model (CRM) configuration has been used in several aeroelastic tailoring studies. Stodieck *et al.* [32] explored mass minimisation aeroelastic tailoring with one and two-dimensional tow steered laminates considering manoeuvre (strains and buckling), flutter, gust and control effectiveness constraints. Compared with unidirectional laminates it was found that 2D steering allowed for a 10.5% mass reduction. Stanford *et al.* [33] performed mass optimisation studies of the CRM wingbox with different tailoring approaches using metallic materials, functionally graded materials, balanced and unbalanced composites (both unidirectional and tow steered), and trailing edge control surfaces. Stress and panel buckling under trimmed manoeuvres and a transonic flutter constraint were considered. Tow steered laminates allowed for a mass reduction of 6% when compared to the design with balanced unidirectional laminates. Jutte *et al.* [34] also performed mass minimisation tailoring considering tow steered composites, functionally graded materials and curvilinear structural elements (spars, ribs, stringers).

Kenway *et al.* [35] performed aerostructural optimisation of the CRM configuration with higher fidelity aerodynamics with the objective of minimising fuel burn. The optimisation procedure was limited to metallic wingbox structures but allowed for changes in the wing planform and airfoils while maintaining the same initial wing area. The optimal design found an increased aspect ratio from 9 to 12.6 and achieved an 8.8% fuel burn reduction. More recently, Brooks *et al.* [36] carried out an optimisation study on this higher aspect ratio version of the CRM with respect to fuel burn considering aluminium, conventional composite and tow steered composite designs. The optimal conventional composite design achieved an 8.7% improvement of fuel burn and a structural mass reduction of 39% in relation to the optimal aluminium structure. Compared to conventional composites, the tow steered design achieved a reduction of 10% in mass and 0.4% in fuel burn.

3 Aeroelastic Model of a Cantilevered Plate

In this thesis we aim to evaluate the effect of Double-Double laminates on the aeroelastic behaviour of composite structures. With this objective in mind, and given that Double-Double were only recently proposed, first, the aeroelastic analysis of a simple structure is performed. This chapter presents the problem of aeroelastic analysis of a cantilevered composite plate wing. An aeroelastic model based on the finite element method and linearised potential flow aerodynamics that evaluates a static aeroelastic condition and the instability (flutter or divergence) behaviour of the structure is developed and validated against available literature. For the evaluation of the plate in the static aeroelastic condition, a theory for the mechanical failure of composite laminates is explained and used. Furthermore, an optimisation framework to determine and evaluate the optimal Double-Double laminates considering both aeroelastic metrics is also implemented and validated.

3.1. Problem Statement

The problem was adapted from Refs. [27, 31] and consists of the analysis of a cantilevered (fully clamped at the root) composite plate of chord $c = 76.2\,\mathrm{mm}$ and span $s = 305\,\mathrm{mm}$, as shown in Figure 3.1, under subsonic airflow. This geometrical configuration is well-known and has been used for the study of aeroelastic behaviour with composites and other materials [27–31, 37]. First, the model will be described and validated and will then be used to compare the aeroelastic behaviour of Double-Double laminates with those from literature. The composite ply properties of the plate are listed in Table 3.1, where E_1 and E_2 are the longitudinal and transverse Young's Modulus, respectively, ν_{12} is the Poisson's ratio, G_{12} is the shear modulus and ρ is the density. The previously mentioned works with composite materials have mostly used 6-ply symmetric laminates with a ply thickness of $0.134\,\mathrm{mm}$ since that was the original configuration given in Ref. [27]. As Double-Double laminates are based on the repetition of a 4-ply building block, the number of plies and the ply thickness were adjusted to maintain the same total mass. For a plate with constant thickness, this translates to adjusting the number of plies and ply thickness so that the total laminate thickness of $0.804\,\mathrm{mm}$ is maintained. The exact values used in the different analyses conducted are detailed in the relevant sections.

The aeroelastic behaviour is assessed through a **static aeroelastic condition** and the **critical aeroelastic velocity**, *i.e.* the lowest velocity at which either flutter or divergence occurs. For the **static aeroelastic load case**, the plate is considered with a 5° angle of attack and an airflow velocity of $20\,\mathrm{m/s}$ as in Ref. [31]. As the air flows around the plate, aerodynamic loads are generated, causing the plate to deform.

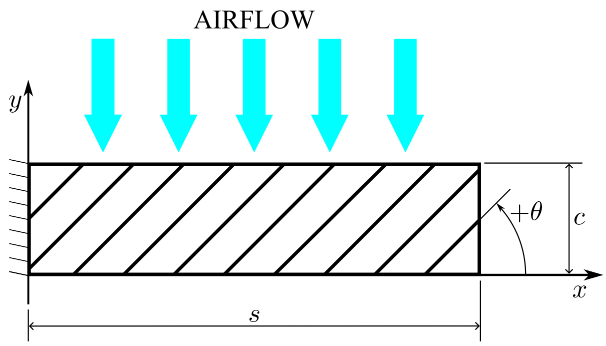

Figure 3.1: Plate problem

Table 3.1: Ply properties for composite plate problem

Property	Value	Property	Value
E_1	98.0 GPa	X_T	1314 MPa
E_2	7.9 GPa	X_C	1220 MPa
ν_{12}	0.28	Y_T	43 MPa
G_{12}	5.6 GPa	Y_C	168 MPa
ρ	1520 kg/m^3	S_{12}	48 MPa

The deformation of the plate leads to a change in the aerodynamic loads. This is an iterative process until a final deformed configuration of the plate is found, at which the aerodynamic loads are balanced by internal elastic loads. The failure condition of the laminate is evaluated with the Tsai-Wu failure criterion. This criterion is a non-phenomenological ply-by-ply failure analysis implemented for composite materials with unidirectional plies which describes the plane stress failure envelope by the following scalar valued tensorial quadratic function [38, 39]:

$$f(\sigma) = F_1\sigma_1 + F_2\sigma_2 + F_{11}\sigma_1^2 + F_{22}\sigma_2^2 + F_{66}\tau_{12}^2 + 2F_{12}\sigma_1\sigma_2 = 1 \tag{3.1}$$

where

$$F_1 = \left(\frac{1}{X_T} - \frac{1}{X_C}\right) \qquad F_2 = \left(\frac{1}{Y_T} - \frac{1}{Y_C}\right) \qquad F_{11} = -\frac{1}{X_T X_C}$$

$$F_{22} = -\frac{1}{Y_T Y_C} \qquad F_{66} = \frac{1}{S_{12}^2} \qquad F_{12} = \frac{F_{12}^*}{\sqrt{X_T X_C Y_T Y_C}}$$

with

- X_T, X_C - allowable stress in the longitudinal (fibre) direction for tension and compression, respectively
- Y_T, Y_C - allowable stress in the transverse direction for tension and compression, respectively
- S_{12} - allowable stress in shear
- F_{12}^* (normalised interaction factor) can be determined from combined-stress tests. Typical values are generally between -1 and 0. If this term is equal to $-1/2$ the Tsai-Wu criterion can be reduced to the von Mises criterion for an isotropic material with equal tensile and compressive strengths.

A value of $f(\sigma) \geq 1$ indicates that a ply has failed. While $f(\sigma)$ allows the determination if a ply has failed, it provides no information regarding how close that ply is to failure. It is possible to define a strength ratio, R as the ratio between ultimate strength and the applied stresses. Noting that Equation 3.1 is the expanded form of:

$$F_{ij}\sigma_i\sigma_j + F_i\sigma_i = 1 \tag{3.2}$$

By allowing the stress components, σ_i, to reach their ultimate values, σ_i^{ult}, and replacing with the strength ratio as $\sigma_i^{ult} = R\sigma_i^{applied}$, the previous equation can be rewritten as [39]:

$$\left[F_{ij}\sigma_i\sigma_j\right] R^2 + \left[F_i\sigma_i\right] R - 1 = 0 \tag{3.3}$$

The strength ratio is then the positive root of this quadratic equation:

$$R = -\left(\frac{b}{2a}\right) + \sqrt{\left(\frac{b}{2a}\right)^2 + \frac{1}{a}} \tag{3.4}$$

with

$$a = F_{ij}\sigma_i\sigma_j \qquad b = F_i\sigma_i$$

This ratio can assume any positive value with the following interpretation:

- When $R = 1$, failure happens
- When $R > 1$, the applied stress can be increased by a factor equal to R to reach the failure condition
- When $R < 1$, the applied stress passed the strength by a factor equal to $1/R$

It is also possible to establish a failure index as the inverse of the strength ratio [39], $k = 1/R$, which can also take any positive value and has the inverse interpretation of R:

- When $k = 1$, failure happens
- When $k > 1$, the applied stress passed the strength by a factor equal to k
- When $k < 1$, the applied stress can be increased by a factor equal $1/k$ to reach the failure condition

The **critical aeroelastic velocity** was found through a flutter analysis. The airflow velocity was increased from $5\,\mathrm{m/s}$ to $100\,\mathrm{m/s}$ and the lowest velocity at which the plate became unstable, either dynamically (flutter) or statically (divergence), was determined.

To evaluate Double-Double laminates, the following analyses using the previously mentioned aeroelastic metrics (Tsai-Wu failure index for static aeroelastic load case and critical aeroelastic velocity) were performed:

- Sensitivity analysis of the effect of homogenisation and Double-Double angles on the objective space defined by the two metrics;
- Single-objective optimisation to minimise the Tsai-Wu failure index under the static aeroelastic load case;
- Single-objective optimisation to maximise the critical aeroelastic velocity;
- Multi-objective optimisation considering the objectives for the single-objective optimisation procedures, *i.e.* minimising Tsai-Wu failure index and maximising critical aeroelastic velocity.

3.2. Modelling Approach

To perform the aeroelastic analysis, the MSC Nastran finite element solver was used. The plate was discretised with 6 degree-of-freedom triangular shell elements (`CTRIAR`) with a mesh of 12x48 elements in the chordwise and spanwise direction, respectively, as shown in Figure 3.2a. The laminate stacking sequences were input with `PCOMP` cards and the coordinate system used for ply orientation is the one shown in Figure 3.1, with 0° plies spanwise and 90° plies chordwise.

Aerodynamics were modelled using the Doublet-Lattice Method (DLM) which is internally implemented in MSC Nastran. The DLM is based on linearised potential flow aerodynamics and is an extension of the steady Vortex-Lattice method to unsteady flow. It considers that the undisturbed flow is uniform and is either steady or varying harmonically [40]. The fundamentals of DLM and its modelling in MSC Nastran are presented in Appendix A.1. A mesh of 12x48 boxes (Figure 3.2b) in the chordwise and spanwise direction, respectively, was used. The connection between the structural and aerodynamic models was done with a Finite Plate Spline (FPS) mesh of 18x72 elements in the chordwise and spanwise direction, respectively, to transfer loads and displacements. The spline was specified with a `SPLINE1` card and the set of 7x25 nodes highlighted in Figure 3.2a was used for the interpolation. The theory behind the use of FPS is explained in Appendix A.2.

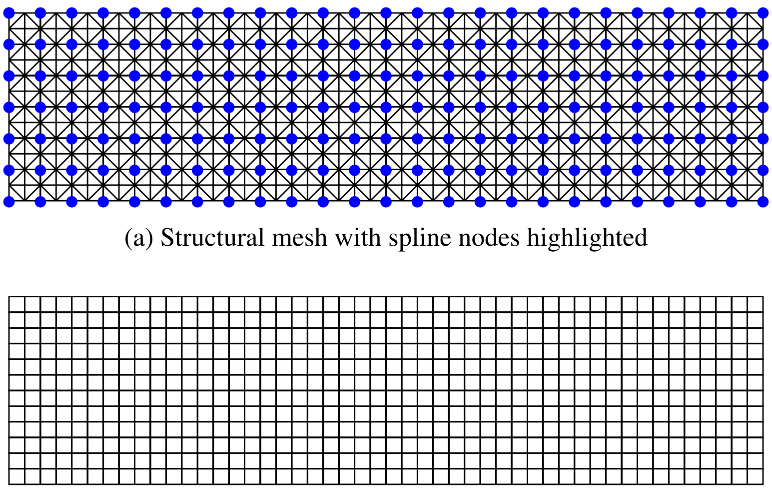

(a) Structural mesh with spline nodes highlighted

(b) Aerodynamic mesh

Figure 3.2: Plate mesh

3.2.1. Flutter Analysis

The equation of motion of an N degree-of-freedom aeroelastic system is given by [15]:

$$\mathbf{A}\ddot{q} + (\rho V \mathbf{B} + \mathbf{D})\,\dot{q} + \left(\rho V^2 \mathbf{C} + \mathbf{E}\right) q = \boldsymbol{0} \tag{3.5}$$

where

- $\mathbf{A}$ is the structural inertia (mass) matrix
- $\mathbf{B}$ is the aerodynamic damping matrix
- $\mathbf{D}$ is the structural damping matrix

- $\mathbf{C}$ is the aerodynamic stiffness matrix
- $\mathbf{E}$ is the structural stiffness matrix
- q are the generalised coordinates

The system frequencies and damping ratios at a given flight condition (air speed and altitude) can be found by an eigenvalue solution by combining the expression $\mathbf{I}\dot{q} - \mathbf{I}\dot{q} = \boldsymbol{0}$, where $\mathbf{I}$ is the $N \times N$ identity matrix, with the previous equation into:

$$\begin{bmatrix} \mathbf{I} & 0 \\ 0 & \mathbf{A} \end{bmatrix} \begin{Bmatrix} \dot{q} \\ \ddot{q} \end{Bmatrix} - \begin{bmatrix} 0 & \mathbf{I} \\ -\left(\rho V^2 \mathbf{C} + \mathbf{E}\right) & -\left(\rho V \mathbf{B} + \mathbf{D}\right) \end{bmatrix} \begin{Bmatrix} q \\ \dot{q} \end{Bmatrix} = \boldsymbol{0} \tag{3.6}$$

which can be rewritten as:

$$\begin{Bmatrix} \dot{q} \\ \ddot{q} \end{Bmatrix} - \begin{bmatrix} 0 & \mathbf{I} \\ -\mathbf{A}^{-1}\left(\rho V^2 \mathbf{C} + \mathbf{E}\right) & -\mathbf{A}^{-1}\left(\rho V \mathbf{B} + \mathbf{D}\right) \end{bmatrix} \begin{Bmatrix} q \\ \dot{q} \end{Bmatrix} = \boldsymbol{0} \tag{3.7}$$

The simplified form of this equation is given by:

$$\dot{\boldsymbol{x}} - \mathbf{Q}\boldsymbol{x} = \boldsymbol{0} \tag{3.8}$$

whose solution can be found by assuming $\boldsymbol{x} = \boldsymbol{x}_0 e^{\lambda t}$ with Equation 3.8 becoming:

$$\left(\mathbf{I}\lambda - \mathbf{Q}\right)\boldsymbol{x}_0 = \boldsymbol{0} \qquad \text{or} \qquad \left(\mathbf{Q} - \mathbf{I}\lambda\right)\boldsymbol{x}_0 = \boldsymbol{0} \tag{3.9}$$

which is in the classic eigenvalue problem form $\left(\mathbf{A} - \mathbf{I}\lambda\right)\boldsymbol{x} = \boldsymbol{0}$. The eigenvalues λ of the system are given in complex conjugate pairs as:

$$\lambda_j = -\xi_j \omega_j \pm i\omega_j \sqrt{1 - \xi_j^2}, \quad j = 1, 2, \ldots, N \tag{3.10}$$

where ω_j and ξ_j are the natural frequencies and the damping ratios, respectively.

Due to the unsteady nature of the aerodynamics, the aerodynamic matrices $\mathbf{B}$ and $\mathbf{C}$ depend on the reduced frequency:

$$k = \frac{\omega c}{2V} \tag{3.11}$$

where c is the chord. The eigenvalue problem of Equations 3.7 and 3.8 can be solved if the $\mathbf{B}$ and $\mathbf{C}$ matrices are known. However, to determine these matrices, the reduced frequency of interest is required, which can only be found if the eigenproblem is solved. Therefore, it is not possible to solve the flutter problem in a direct manner. To address this issue, frequency matching methods such as the '*k*' or '*p-k*' methods were developed [15].

In the '*p-k*' method, for each air speed of interest, an initial guess of the frequency of the mode is made and the corresponding reduced frequency is calculated. The aerodynamic matrices $\mathbf{B}$ and $\mathbf{C}$ are calculated for that reduced frequency. The frequencies for the system are determined from equation 3.8 and the frequency solution closest to the initial guess is taken as the next guess. This process is repeated until the frequencies converge and the corresponding damping is extracted. This process is repeated for all modes, for all air speeds (flight conditions) of interest. The set of frequency, damping and air speed values are assembled and typically plotted in the so-called Vg and $V\omega$ plots, and the aeroelastic instability speed is found when the damping is zero.

In MSC Nastran[1], flutter analysis is available in `SOL 145` and the fundamental flutter equation for the '*p*-*k*' method is given by [40]:

$$\left[M_{hh}p^2 + \left(B_{hh} - \frac{1}{4}\rho\bar{c}VQ^I_{hh}/k\right)p + \left(k_{hh} - \frac{1}{2}\rho V^2 Q^R_{hh}\right)\right]\{u_h\} = 0 \tag{3.12}$$

where

- M_{hh} is the modal mass matrix
- B_{hh} is the modal damping matrix
- K_{hh} is the modal stiffness matrix
- Q^I_{hh} is the modal aerodynamic damping matrix, a function of Mach number, m, and reduced frequency, k. Imaginary part of Q_{hh}.
- Q^R_{hh} is the modal aerodynamic stiffness matrix, function of Mach number, m, and reduced frequency, k. Real part of Q_{hh}.
- $Q_{hh} = Q^R_{hh} + iQ^I_{hh}$ = Aerodynamic Influence Coefficient (AIC) matrix
- $p = \omega(\gamma \pm i)$ is the eigenvalue
- γ is the transient decay rate coefficient
- $\omega = 2\pi f$ is the circular frequency
- $\bar{c}$ is the reference length
- ρ is the fluid density
- V is the velocity
- u_h is the modal amplitude vector

Note that the reduced frequency and the circular frequency are not independent, as:

$$k = \frac{\omega\bar{c}}{2V} = \frac{\bar{c}}{2V}\mathrm{Im}\,(p) \tag{3.13}$$

The eigenvalues p are either complex conjugate pairs or real. The damping g is given by:

$$g = \begin{cases} 2\gamma & \text{if } p \text{ is complex} \\ \gamma = \frac{p\bar{c}}{V\ln 2} & \text{if } p \text{ is real} \end{cases} \tag{3.14}$$

An instability is detected when the damping crosses from negative to positive, and the corresponding critical velocity for that instability is the velocity at which $g = 0$. Note that both the damping, g, and the damping ratio, ξ, can be used to analyse the occurrence of instability. However, they require different interpretation, particularly in the flutter plots. While the critical velocity for an instability is also found at $\xi = 0$, ξ and g have opposing signs, therefore when using the damping ratio an instability is found

[1] In this document whenever the methods implemented in MSC Nastran are presented the notation used in the corresponding documentation [40] is adopted to avoid introducing any source of conflict or confusion for the reader

when ξ crosses from positive to negative [15]. For the 'p-k' method the damping ratio can be calculated from the obtained eigenvalue as [41]:

$$\xi = \frac{-\text{Re}(p)}{\sqrt{\text{Re}(p)^2 + \text{Im}(p)^2}} \tag{3.15}$$

where Re and Im stand for the amplitude of the real and imaginary part, respectively. Unless explicitly stated otherwise, when damping is mentioned in the context of flutter in this work it refers to the damping g.

The type of instability is determined based on the nature of the eigenvalue: for complex eigenvalues, the instability is flutter and for real eigenvalues, which have a null complex component corresponding to zero frequency, *i.e.* non-oscillatory motion, the instability is divergence.

The Q_{hh} matrix is obtained as follows [40]. Two transformations need to be applied to the Aerodynamic Influence Coefficient (AIC) matrix Q_{kk}, defined in Equation A.7, so it can be used in the flutter analysis:

1. The matrix has to be applied to the structural model using a spline technique
2. A modal reduction has to be applied to obtain the matrices in generalised form

These transformations are expressed as:

$$[Q_{ii}] = [\phi_{ai}]^T [G_{ka}]^T [WTFACT] [Q_{kk}] [G_{ka}] [\phi_{ai}] \tag{3.16}$$

where

1. Q_{ii} is the generalised aerodynamic matrix
2. ϕ_{ai} is a matrix of i-set normal mode vectors in the physical a-set
3. G_{ka} is the spline matrix defined in Equation A.10 reduced to the a-set
4. $WTFACT$ is the same weighting matrix as W_{kk} defined in Equation A.9

If extra points used for the representation of control systems, required in aeroservoelastic analysis, are included in the flutter analysis and the deflections of the extra points result in displacements in the aerodynamic model, then the downwash information needs to be explicitly provided in two `DMI` entries:

$$\{w_j\} = [D1JE + ikD2JE] \{u_e\} \tag{3.17}$$

where $\{u_e\}$ is a vector of extra point displacements, $D1JE$ and $D2JE$ are the required entries, and $\{w_j\}$ is the resulting downwash. Generalised aerodynamics for the extra points are computed as:

$$[Q_{ie}] = [\phi_{ai}]^T [G_{ka}]^T [WTFACT] [Q_{ke}] \tag{3.18}$$

where Q_{ke} is defined similarly to Q_{kk} as:

$$[Q_{ke}] = [WTFACT] [S_{kj}] [A_{jj}]^{-1} [D1JE + ikD2JE] \tag{3.19}$$

The Q_{hh} matrix used in the flutter analysis is a merged matrix defined as:

$$[Q_{hh}] = \begin{bmatrix} Q_{ii} & Q_{ie} \\ 0 & 0 \end{bmatrix} \tag{3.20}$$

where the h-set is a combination of the i-set normal modes and the e-set extra points.

In flutter analysis, the calculation of the aerodynamic matrices and their transformation into generalised aerodynamic matrices are computationally expensive. To save resources, these matrices are computed for specific sets of reduced frequency and Mach number and are interpolated from the calculated values for all other combinations of reduced frequency and Mach number.

For the flutter analysis setup with the 'p-k' method in MSC Nastran, a total of 8 modes were specified, although only the results of the first 4 modes were output as from other works in identical plates the instability happened within these modes [27–31] and it allowed for faster post-processing of the results. The sea level air density of $\rho = 1.225\,\mathrm{kg/m^3}$ was used and the airflow velocity was varied from $5\,\mathrm{m/s}$ to $100\,\mathrm{m/s}$ with increments of $0.5\,\mathrm{m/s}$. The Mach number was kept constant at $M = 0$ as compressibility effects are negligible in this velocity range. The set of reduced frequencies used for the calculation of the aerodynamic matrices is shown in Table 3.2. This set was selected to allow sufficient accuracy in the interpolation of the aerodynamic matrices in a wide range of reduced frequencies. The critical aeroelastic velocity was determined by finding the lowest velocities at which the real part of the eigenvalue of a given mode crossed from negative to positive, and determining the corresponding velocity at which $\mathrm{Re}(p) = 0$ by linear interpolation. Note that $\mathrm{Re}(p) = 0 \implies g = 0$.

Table 3.2: Set of reduced frequencies for calculation of aerodynamic matrices

Reduced Frequency, k	
0.005	0.25
0.01	0.275
0.025	0.3
0.05	0.5
0.075	0.75
0.1	1
0.125	2
0.15	5
0.175	10
0.2	

3.2.2. Static Aeroelastic Analysis

Static aeroelastic analysis is available in MSC Nastran through `SOL 144` and it employs a quasi-steady trim approach, with the following set of equations [40]:

$$[K_{aa} - \overline{q}Q_{aa}]\{u_a\} + [M_{aa}]\left\{\ddot{U}_{aa}\right\} = \overline{q}\,[Q_{ax}]\{u_x\} + \{P_a\} \tag{3.21}$$

where

- $\overline{q}$ is the dynamic pressure
- K_{aa} is the structural stiffness matrix
- M_{aa} is the structural mass matrix
- $\{u_a\}$ is the vector of nodal deflections
- $\left\{\ddot{U}_{aa}\right\}$ is the vector of nodal accelerations

- $\{P_a\}$ is the vector of applied loads (for example, gravity) plus aerodynamic loads due to user input pressures and/or downwash velocities (e.g. jig-twist distribution, incidence)
- $\{u_x\}$ is the vector of extra aerodynamic points used to describe trim variables such as control surfaces rotation
- Q_{aa} is the aerodynamic influence coefficient matrix which provides the forces at the structural grid points due to structural deformations
- Q_{ax} is the aerodynamic influence coefficient matrix which provides the forces at the structural grid points due to unit deflections of the aerodynamic extra points

The aerodynamic influence coefficient matrices Q_{aa} and Q_{ax} are obtained as follows. The downwash equation A.4 for static aeroelasticity becomes:

$$\{w_j\} = [D_{jk}]\{u_k\} + [D_{jx}]\{u_x\} + \left\{w_j^g\right\} \tag{3.22}$$

where

- $\{w_j\}$ is the downwash vector (for example, angles of attack)
- u_k is the vector of aerodynamic displacements (deformations)
- w_j^g represents an initial static aerodynamic downwash. It includes, primarily, the static incidence distribution that may arise from an initial angle of attack, camber, or twist
- $[D_{jk}]$ is the substantial derivative matrix for the aerodynamic displacements. (This term is the D_{jk}^1 of Equation A.4. The D_{jk}^2 is not used for the quasi-steady analysis)
- $[D_{jx}]$ is the substantial derivative matrix for the extra aerodynamic points

The theoretical aerodynamic pressures are taken from Equation A.8 as:

$$\{f_j\} = \overline{q}\,[A_{jj}]^{-1}\{w_j\} \tag{3.23}$$

and the aerodynamic forces given by Equation A.9 can be rewritten as:

$$\{P_k\} = \overline{q}\,[W_{kk}]\,[S_{kj}]\,[A_{jj}]^{-1}\{w_j\} + \overline{q}\,[S_{kj}]\left\{f_j^e/\overline{q}\right\} \tag{3.24}$$

The vector of aerodynamic extra points $\{u_x\}$ specifies the values of aerodynamic trim variables. MSC Nastran has several predefined variables including incidence angles (angle of attack and sideslip angle), roll, pitch and yaw rates, two translational (vertical and lateral) and three rotational accelerations. There are also variables for control surface deflection. The $[D_{jx}]$ matrix provides the downwash velocities of unit values of the aerodynamic extra points. Under the quasi-steady assumption, accelerations do not result in any downwash.

The aerodynamic forces are transferred to the structure with the spline matrix of Equation A.10 reduced to the a-set, giving the Q_{aa} and Q_{ax} matrices, respectively, as:

$$[Q_{aa}] = [G_{ka}]^T\,[W_{kk}]\,[S_{kj}]\,[A_{jj}]^{-1}\,[D_{jk}]\,[G_{ka}] \tag{3.25}$$

$$[Q_{ax}] = [G_{ka}]^T\,[W_{kk}]\,[S_{kj}]\,[A_{jj}]^{-1}\,[D_{jx}] \tag{3.26}$$

MSC Nastran's static aeroelastic solution allows for free (unrestrained) rigid body motion degrees of freedom used to calculate adequate trim conditions, such as angle of attack, for a given flight condition. Stability and speed derivatives can also be determined from this solution. The implementation of the different analyses and the separation between the free body motion degrees of freedom and the restrained ones is done from Equation 3.21 and can be found in the relevant documentation [40].

From the static aeroelastic analysis, it is also possible to determine the divergence dynamic pressure for restrained components. Divergence is a static instability, therefore considering only the displacement terms, Equation 3.5 of the aeroelastic system becomes [15]:

$$\left(\rho V^2 \mathbf{C} + \mathbf{E}\right) q = 0 \tag{3.27}$$

and divergence happens at the non-trivial solution:

$$\left|\rho V^2 \mathbf{C} + \mathbf{E}\right| = 0 \tag{3.28}$$

which can also be expressed as an eigenvalue problem. MSC Nastran implements this solution with the eigenvalue approach, considering only the displacement terms of Equation 3.21 [40]:

$$[K_{ll} - \lambda Q_{ll}]\,\{u_l\} = 0 \tag{3.29}$$

where the l subscript denotes the restrained degrees of freedom. Only roots that are purely imaginary and positive are physically meaningful, and the divergence dynamic pressure is given by:

$$\overline{q}_d = -\lambda^2 \tag{3.30}$$

While this is not used to evaluate the divergence behaviour of the plate directly, it is used as a constraint in the optimisation process, as will be explained further in the document.

The Mach number, dynamic pressure and trim parameters of the condition of interest are provided to the solver as a `TRIM` entry. The Mach number was set to $M = 0$ as in the flutter analysis and the dynamic pressure corresponding to $20\,\mathrm{m/s}$ with a sea level air density of $1.225\,\mathrm{kg/m^3}$ is $\overline{q} = \rho V^2/2 = 245\,\mathrm{Pa}$. The $5°$ angle of attack was input in the trim parameter `ANGLEA` as $0.0872665\,\mathrm{rad}$. A zero pitch rate also needs to be specified in the trim parameter `PITCH` which is defined as $q\overline{c}/2V$ where q is the pitch rate (not to be confused with dynamic pressure) in $\mathrm{rad/s}$. From the deformed shape of the plate, MSC Nastran computes the strength ratios for each ply of each element of the structural mesh, which were then post-processed externally to calculate the corresponding failure index.

3.2.3. Validation

To validate the flutter analysis, flutter and divergence velocities were determined for the layups in the experimental and computational results reported in Refs. [27, 28]. All the laminates are 6-ply symmetric laminates with a ply thickness of $0.134\,\mathrm{mm}$. The comparison of the obtained flutter and divergence velocities is done in Tables 3.3 and 3.4, respectively. The tables show that the obtained results have a good agreement with the experimental values of Ref. [27] and the computational results of Ref. [28]. The observed differences with respect to the computational results are to be attributed to the different numerical method used for evaluating unsteady aerodynamics in Ref. [27] and by different mesh densities used in Ref. [28]. Nevertheless, there is a good agreement of the aeroelastic behaviour of the plate.

A comparison was also made in Table 3.5 with the optimal laminates found in Ref. [31] for the static aeroelastic case and the instability velocity. The laminates have the same ply thickness as the one previously described. It should be noted that in Ref. [31] a different coordinate system for ply

Table 3.3: Flutter velocities for model validation with Refs. [27] and [28]

Laminate	Flutter Speed $\mathrm{m/s}$			
	Current Work	Ref. [27] Exp.	Ref. [27] Comp.	Ref. [28]
$[0_2/90]_S$	25.21	25	21.0	23.0
$[+45/-45/0]_S$	40.75	> 32	39.0	40.1
$[+45_2/90]_S$	28.24	28	27.8	27.5
$[-45_2/90]_S$	28.81	Divergence	27.8	27.8
$[+30_2/90]_S$	27.88	27	27.8	27.1
$[-30_2/90]_S$	30.98	Divergence	30.0	37.3

Table 3.4: Divergence velocities for model validation with Refs. [27] and [28]

Laminate	Divergence Speed $\mathrm{m/s}$			
	Current Work	Ref. [27] Exp.	Ref. [27] Comp.	Ref. [28]
$[0_2/90]_S$	30.36	Flutter	25.0	30.6
$[+45/-45/0]_S{}^*$	82.10	> 32	No divergence	No divergence
$[+45_2/90]_S{}^*$	67.16	Flutter	No divergence	No divergence
$[-45_2/90]_S$	12.47	12.5	11.1	13.7
$[+30_2/90]_S{}^*$	74.66	Flutter	No divergence	No divergence
$[-30_2/90]_S$	13.32	11.7	11.5	13.8

*The divergence velocity was calculated in Refs. [27, 28] with the eigenvalue approach described in the previous section. This method should give the same result as analysing the damping in the flutter analysis. It is unclear why this difference happened. Nevertheless, this did not affect the determination of the critical aeroelastic velocity for these laminates, which was due to flutter. This behaviour was not found to compromise the analyses conducted in this work.

orientation was used, therefore the ply angles were adjusted to the coordinate system used in this work. The obtained results are close to the ones reported in Ref. [31] with the highest difference of 3.7% in the Tsai-Wu failure index. The current work also does not overpredict the behaviour of the laminates as a higher failure index and a lower critical velocity were found. The small differences are possibly due to different nodes being used for the spline, as all the remaining mesh densities are identical. Furthermore, the eigenvalue migration in the flutter analysis of the corresponding optimal laminate shown in Figure 3.3a is similar to the one from Ref. [31], Figure 3.3b. Note that the frequency in Hz corresponds to the imaginary part of the eigenvalue, which is the frequency in $\mathrm{rad/s}$, divided by 2π. Therefore, it is possible to conclude that the implemented model is capable of predicting with a good level of accuracy the aeroelastic behaviour of the cantilevered plate.

Table 3.5: Validation of static aeroelastic and flutter analyses with Ref. [31]

Analysis	Laminate	Metric	Current Work	Ref. [31]
Static Aeroelastic	$[4.3/12.2/-7.6]_S$	Tsai-Wu failure index	0.0359	0.0346
Flutter	$[39.3/-46.8/-50.7]_S$	Instability velocity $\mathrm{m/s}$	45.17	45.98

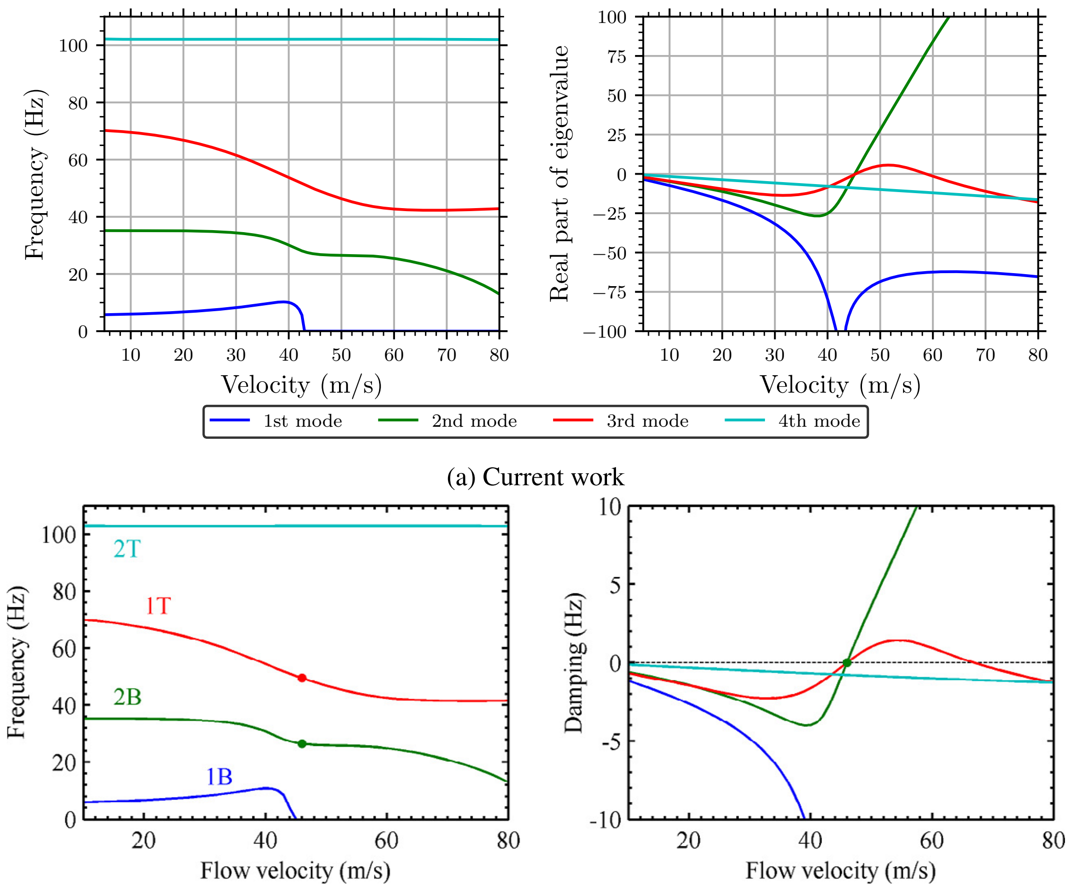

(a) Current work

(b) Reference [31]

Figure 3.3: Eigenvalue migration for laminate $[39.3/-46.8/-50.7]_S$

3.3. Optimisation Procedure

The optimisation procedures were conducted in the Python programming language. In particular, the *pymoo* framework was used [42]. A Genetic Algorithm (GA) was used for the optimisation as the MSC Nastran simulations were not computationally expensive, the number of variables was low, and there was a possibility of discontinuous objective space. The selected algorithm was the Non-dominated Sorting Genetic Algorithm II (NSGA-II), an elitist multi-objective optimisation algorithm, which has been used as a benchmark to evaluate other multi-objective evolutionary algorithms. Its biggest difference from a simple genetic algorithm lies in the survival and mating selection operators [43].

3.3.1. Basic Concepts of Multi-objective Optimisation

It is necessary to introduce some basic concepts of multi-objective optimisation before a more detailed description of the implementation. These concepts are widely available in optimisation literature and are typically presented considering a multi-objective optimisation problem that seeks to minimise all the objectives [44]. Specialising them to the current bi-objective optimisation study that seeks to minimise one objective while maximising a second one, the mathematical problem can be reformulated as follows:

$$min f_1(\boldsymbol{x}) \wedge max f_2(\boldsymbol{x}) \quad , \boldsymbol{x} \in \boldsymbol{S} \tag{3.31}$$

where $\boldsymbol{x} = (x_1, x_2)$ is the vector that represents the design variables and $\boldsymbol{S}$ is the space of admissible solutions, *i.e.* the design space. A vector of the objectives to optimise can also be defined as: $\boldsymbol{F}(\boldsymbol{x}) = (f_1(\boldsymbol{x}), f_2(\boldsymbol{x}))$. The set $\boldsymbol{Y} = \boldsymbol{F}(\boldsymbol{S})$ is the objective space.

In multi-objective optimisation, the objectives tend to conflict with each other, as improving one tends to worsen the others. The solution of multi-objective optimisation problems is not a single design but the set of designs with the best compromise between objectives. To compare the solutions taking into account this compromise, the concept of *Dominance* is of particular importance:

> An objective vector $\boldsymbol{u} = (u_1, u_2)$ dominates $\boldsymbol{v} = (v_1, v_2)$ (represented by $\boldsymbol{u} \prec \boldsymbol{v}$) if and only if
>
> $$u_1 \leq v_1 \wedge u_2 \geq v_2 \wedge (u_1 < v_1 \vee u_2 > v_2) \tag{3.32}$$

A Pareto optimum can then be defined as any solution where it is impossible to improve one objective without the other becoming worse, that is, a Pareto optimum is a non-dominated solution. This is formally defined as:

> A solution $\boldsymbol{x}^* \in \boldsymbol{S}$ is a Pareto optimum if
>
> $$\forall \boldsymbol{x} \in \boldsymbol{S} : \boldsymbol{F}(\boldsymbol{x}) \nprec \boldsymbol{F}(\boldsymbol{x}^*) \tag{3.33}$$

The set of Pareto optima is then given by:

$$\mathcal{P}^* = \{\boldsymbol{x} \in \boldsymbol{S} | \nexists \boldsymbol{x}' \in \boldsymbol{S}, \boldsymbol{F}(\boldsymbol{x}') \prec \boldsymbol{F}(\boldsymbol{x})\} \tag{3.34}$$

The Pareto front is then the image of the set of Pareto optima in the objective space, that is the Pareto front is composed of the corresponding objective values for each solution in the set of Pareto optima. It is the Pareto front that provides an idea of the compromise between the objectives, and obtaining it is the main task of a multi-objective optimisation and it is defined as:

$$\mathcal{P}\boldsymbol{F}^* = \{\boldsymbol{F}(\boldsymbol{x}), \boldsymbol{x} \in \mathcal{P}^*\} \tag{3.35}$$

It is also possible to introduce two points that provide information about the range of values in the Pareto Front: the ideal point and the *Nadir* point (or worst point). The ideal point is the point that optimises all objectives and is a utopian solution as it is infeasible in the design space. The *Nadir* is the point that has the worst value for all objectives over the Pareto set.
A point $\boldsymbol{y}^* = (y_1^*, y_2^*)$ is an ideal point if it minimises $f_1(\boldsymbol{x})$ and maximises $f_2(\boldsymbol{x})$:

$$\boldsymbol{y}^* = (min\,(f_1(\boldsymbol{x})), max\,(f_2(\boldsymbol{x}))), \boldsymbol{x} \in \boldsymbol{S} \tag{3.36}$$

A point $\boldsymbol{y}^* = (y_1^*, y_2^*)$ is the *Nadir* point if it maximises $f_1(\boldsymbol{x})$ and minimises $f_2(\boldsymbol{x})$ over the Pareto set:

$$\boldsymbol{y}^* = (max\,(f_1(\boldsymbol{x})), min\,(f_2(\boldsymbol{x}))), \boldsymbol{x} \in \mathcal{P}^* \tag{3.37}$$

Figure 3.4 shows a representation of these concepts for the presented problem.

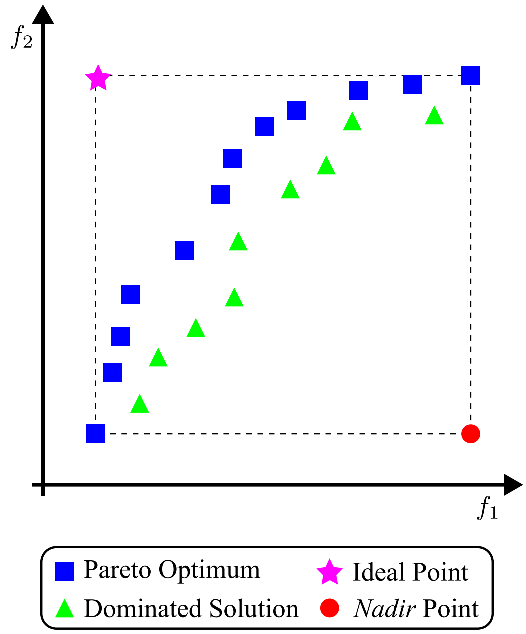

Figure 3.4: Multi-objective optimisation concepts

3.3.2. Implementation

In the present work, we seek to study the aeroelastic behaviour of composite plates. In particular, the use of Double-Double laminates is analysed. For that purpose, several optimisation studies will be performed. As previously mentioned, it was chosen to perform the optimisation using a genetic algorithm. In particular, the implementation of the NSGA-II in the *pymoo* framework was used.

Throughout the analyses the only variables used were angles, discretised by lower and upper bounds, θ_{min} and θ_{max}, respectively, and an angle step, θ_{step}. Treating the angles this way allowed for discrete angle problems, with larger θ_{step} such as $5°$ and $10°$ for example, and, by considering small values of θ_{step}, problems where the angles are close to continuous. The angles were mapped into integers which were used as variables in the algorithm. All the angles from θ_{min} to θ_{max} with the step θ_{step} were stored in a vector. The algorithm variable was the index of the vector element, ranging from 0 to $n-1$, where n is the number of elements in the vector determined by θ_{min}, θ_{max}, and θ_{step}.

The modification of the MSC Nastran input files (.bdf files) and the post-processing of simulation results were done with in-house built code using common Python packages as well as pyNastran [45], which allows for an easier interface with several of Nastran's input and output files. When evaluating the static aeroelastic load case, the highest Tsai-Wu failure index, considering all plies in all elements, was used as the objective value. The divergence dynamic pressure was also determined as explained in section 3.2.2. Since divergence can result in structural failure, if the divergence dynamic pressure was equal or lower than the one in the static aeroelastic load case (245 Pa) it was considered that the laminate had failed and a failure index of 10 was assigned to the objective. *pymoo*'s implementation considers the minimisation of all objectives, therefore the negative of the critical aeroelastic velocity was used as the objective in the algorithm, as minimising the negative results in the maximisation of the critical aeroelastic velocity.

The survival selection operator in NSGA-II is based on two parameters: non-domination and crowding distance. First, a combined population of parent and offspring solutions is ranked into non-dominated fronts, where all solutions within each front are dominated by the same number of solutions. Low rank fronts are preferred, with the first front having all non-dominated solutions. These fronts are added sequentially to the next generation's population, until a front is reached where adding all solutions from that front would surpass the allowed number of solutions in the population. The solutions to be kept are selected by sorting the solutions in that population by crowding distance. The crowding distance gives an estimate of the density of solutions surrounding a particular solution and is used to ensure diversity in the population. The solutions with the extreme values of each objective (maximum and minimum) are assigned a crowding distance of infinity as it is desired they are always kept. For all other solutions the crowding distance is the sum of the absolute normalised difference in function values for the two adjacent solutions in every objective. The solutions with higher crowding distance are chosen for the next population [43].

In NSGA-II mating selection is done with a modified tournament selection. Two solutions are randomly selected from the population and compared based on domination. If one solution dominates the other, it is selected for crossover. In case neither solution is dominant, the one with the higher crowding distance is selected. The crossover operator used was Simulated Binary Crossover (SBX) [46, 47] with a distribution index $\eta_c = 3$. The crossover probability was set to 100% so that every time two parents were selected crossover happened. For the mutation operator, polynomial mutation [48] with a distribution index $\eta_c = 20$ and a mutation probability of 15% was used. The populations had 20 individuals and the same number of offspring were generated.

The algorithm terminated when one of two criteria was verified: a maximum number of generations was reached or the objective did not improve more than a specified tolerance over the last 20 generations. For the single-objective optimisation problems, the evolution of the objective value is simply done by comparing the objective value of the single best solution of the current generation with the ones from the previous generations. For multi-objective problems, *pymoo*'s implementation of the criterion proposed in Ref. [49] was used. This criterion considers the evolution of the ideal and *Nadir* points through the generations. Once they have stabilised, these points are used to normalise the objectives and an evaluation of the evolution of the solutions in the Pareto front is performed. A detailed explanation of the criterion can be found in Ref. [49]. Table 3.6 shows the maximum number of generations and objective tolerance considered for the different optimisation problems.

Table 3.6: Parameters for optimisation algorithm termination

Optimisation Problem	Objective Tolerance	Maximum No Generations
Static Aeroelastic	1×10^{-5}	120
Aeroelastic Instability	0.001	120
Multi-objective	0.025	200

3.3.3. Validation

To validate the implementation, the optimisation of 6-ply symmetric unidirectional laminates with a ply thickness of $0.134\,\mathrm{mm}$, as in Ref. [31], was performed. The optimisation variables were the angles for three plies, discretised between $-90°$ and $90°$ with a step of $0.1°$. For the single-objective optimisations, the algorithm was executed for five different seeds to verify proper convergence. Tables 3.7 and 3.8 show the results of the optimisation for the Tsai-Wu failure index in the static aeroelastic case and for the critical aeroelastic velocity, respectively. The results show that the algorithm converged consistently for similar values of the objectives, despite some differences in the optimal ply angles. The obtained optimal laminates and objective values are also consistent with the ones found in Ref. [31], previously shown in Table 3.5.

A multi-objective optimisation was also performed. The obtained Pareto front is shown in Figure 3.5a and the corresponding front from Ref. [31] is the red one in Figure 3.5b. The algorithm was able to find a similar front to Ref. [31] with well distributed solutions along the front. Overall, the implemented optimisation procedure is effective in finding optimal laminates for aeroelastic response both for single and multi-objective optimisation. The results obtained in this section will later be used for comparison with Double-Double laminates.

Table 3.7: Validation of static aeroelastic single-objective optimisation

	Algorithm Seed	Optimal Laminate	Tsai-Wu failure index
Current Work	1	$[4.4/13.0/13.1]_S$	0.03401
	73	$[3.9/15.0/12.2]_S$	0.03399
	163	$[4.0/14.4/12.6]_S$	0.03398
	387	$[4.6/12.9/12.9]_S$	0.03403
	500	$[3.5/16.9/11.4]_S$	0.03405
Reference [31]	—	$[4.3/12.2/-7.6]_S$	0.0359*

*Value found with current work simulations (see Table 3.5)

Table 3.8: Validation of critical aeroelastic velocity single-objective optimisation

	Algorithm Seed	Optimal Laminate	Critical Aeroelastic Velocity $(\mathrm{m/s})$
Current Work	1	$[36.6/-41.2/-37.7]_S$	45.60
	73	$[36.9/-40.7/-47.5]_S$	45.56
	163	$[37.4/-40.6/-9.6]_S$	45.17
	387	$[-46.1/25.9/48.8]_S$	43.35
	500	$[35.6/-36.0/-36.2]_S$	45.53
Reference [31]	—	$[39.3/-46.8/-50.7]_S$	45.17*

*Value found with current work simulations (see Table 3.5)

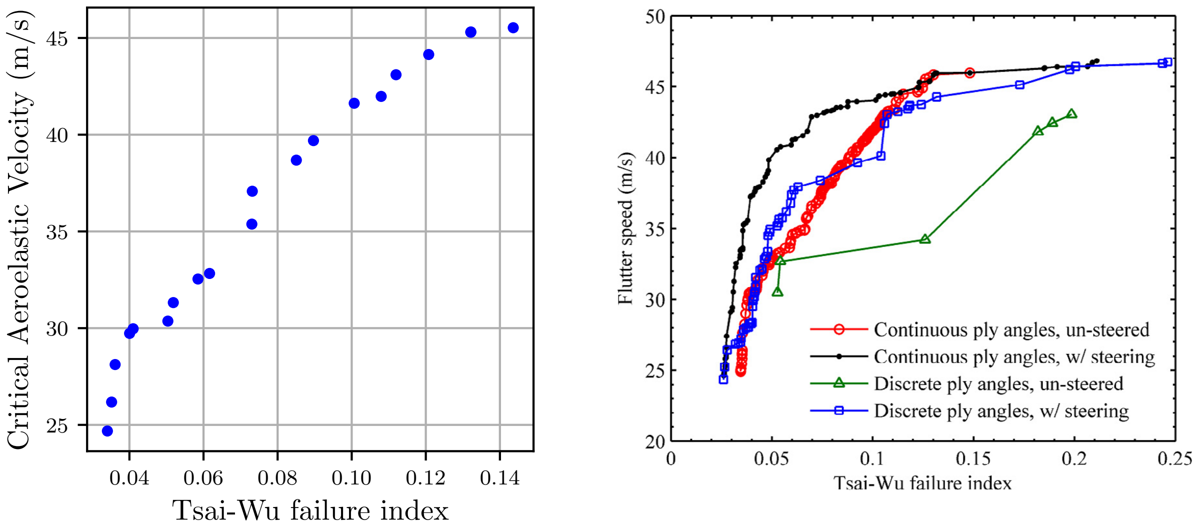

(a) Current work

(b) Reference [31]. (red front)

Figure 3.5: Pareto front for multi-objective optimisation validation

4 Double-Double Cantilevered Plate Results

This chapter explores the effect of Double-Double laminates on the aeroelastic behaviour of a cantilevered composite plate. First, a sensitivity analysis is performed on constant thickness plates. This analysis allows for an investigation of the objective space as a function of our design variables: the two Double-Double angles Φ and Ψ. Moreover, in this analysis the effect of homogenisation on the aeroelastic metrics is also studied. Secondly, a sensitivity analysis of two plates with thickness tapering is done to understand the effect of these configurations on the objective space of both aeroelastic metrics considered. Finally, several optimisation studies are conducted in order to compare unidirectional and tow steered Double-Double laminates with other laminates used in similar studies.

4.1. Sensitivity Analysis on Constant Thickness Plate

To understand the effect of the degree of homogenisation of Double-Double laminates on the aeroelastic behaviour, a sensitivity analysis was performed considering 4 different number of repeats of the Double-Double building block: 4, 6, 8 and 10 repeats. To maintain consistency and allow for a direct comparison between the different number of repeats and with available literature, the ply thicknesses were calculated to maintain the same mass as 6-ply laminates with ply thickness of $0.134\,\mathrm{mm}$, as mentioned in chapter 3. The laminates considered for this sensitivity analysis were chosen to have constant thickness. Therefore, the ply thickness for each number of repeats was determined to maintain the total laminate thickness of $0.804\,\mathrm{mm}$. The obtained ply thickness for each number of repeats is shown in Table 4.1. Note that this results in thin-ply laminates which are currently not used in commercial aircraft structures due to production difficulties. As the objective of this work was simply to explore the effect of Double-Double laminates on the aeroelastic behaviour, this aspect of manufacturability was not taken into account in this problem.

Table 4.1: Ply thicknesses for sensitivity analysis

Number of repeats	Ply thickness
$r = 4$	$t = 50.25\,\mu\mathrm{m}$
$r = 6$	$t = 33.5\,\mu\mathrm{m}$
$r = 8$	$t = 25.125\,\mu\mathrm{m}$
$r = 10$	$t = 20.1\,\mu\mathrm{m}$

The sensitivity analysis was performed with a 'brute force' approach, evaluating all possible combinations of the Double-Double angles Φ and Ψ, where $0° \leq \Phi, \Psi \leq 90°$, with an angle step of $5°$. Double-Double is intended to be used in a homogenised state. Homogenisation of a laminate is defined when the laminate has equal normalised membrane and bending stiffness matrices and a null normalised bending-extension coupling matrix:

$$\begin{aligned} [\boldsymbol{A}^*] &= [\boldsymbol{D}^*] \\ [\boldsymbol{B}^*] &= 0 \end{aligned} \tag{4.1}$$

In reality, achieving true homogenisation is not feasible taking manufacturing into account. Therefore, a laminate is considered homogenised when the terms of the normalised bending-extension coupling matrix and the difference between the terms of the normalised membrane and bending stiffness matrices are small. It has been proposed using 2% of Tsai's modulus as a threshold for homogenisation criterion, considering the largest absolute component of $[B^*]$ and $[A^*] - [D^*]$ [8]. The homogenisation criterion is then defined as:

$$\begin{aligned} \left| \left[A^*_{ij}\right] - \left[D^*_{ij}\right] \right| &< 2\% \text{ Tsai's modulus} \\ \left| \left[B^*_{ij}\right] \right| &< 2\% \text{ Tsai's modulus} \end{aligned} \tag{4.2}$$

Increasing the number of repeats of a sub-laminate increases how homogeneous a laminate is. Therefore, if the stacking sequence is chosen so that homogenisation is guaranteed for 4 repeats, the laminates with higher repeats will also be homogeneous. It has been shown in Ref. [10] that the homogenisation criterion of Equation 4.2 can be met by choosing between two stacking sequences: Staggered 1 - $[\Phi/-\Psi/-\Phi/\Psi]$ and Staggered 3 - $[\Phi/-\Psi/\Psi/-\Phi]$. The stacking sequence is based on the in-plane lamination parameters ξ_1^A and ξ_2^A as shown in Figure 4.1. The expression for the two coloured parabolas were taken from Ref. [50]. ξ_1^A and ξ_2^A are related to the Double-Double angles Φ and Ψ by Equations 4.3 and 4.4, previously shown in section 2.1.3, respectively.

$$\xi_1^A = \left(\cos 2\Phi + \cos 2\Psi\right)/2 \tag{4.3}$$

$$\xi_2^A = \left(\cos 4\Phi + \cos 4\Psi\right)/2 \tag{4.4}$$

It should be noted that for Staggered 3 it is important whether $\Phi \geq \Psi$ or $\Phi < \Psi$. For this stacking sequence the requirement related to the bending-extension coupling matrix is the most restrictive and the terms of $[B^*]$ vary depending on whether $\Phi \geq \Psi$ or $\Phi < \Psi$ [51].

It is known that in thin-ply laminates an *in situ* effect occurs, where some of the ply strengths increase with decreasing ply thickness [52]. The Tsai-Wu failure index is used in the static aeroelastic condition as a measure as the overall stress level on the plate. Therefore, as the objective is to obtain a notion of the stresses on the plate and the Tsai-Wu failure index depends on the ply strengths, the *in situ* effect was not considered as to not influence the failure index and allow for a direct comparison between the different Double-Double laminates and with available literature.

4.1.1. Static Aeroelastic Condition

The results of the sensitivity analysis for the static aeroelastic condition are shown in Figure 4.2. The objective space is well-defined without any discontinuities and seems insensitive to the number of repeats. The majority of laminates do not fail under the static aeroelastic condition, that is they have a failure index lower than 1. The region of lower failure index is where the Double-Double angles are closer to the spanwise direction (0°), which is consistent as the loading condition is of combined bending-torsion but dominated by bending and requires higher stiffness in this direction. Table 4.2 shows that the lowest failure index was found for the same Double-Double angles independently of the number of repeats.

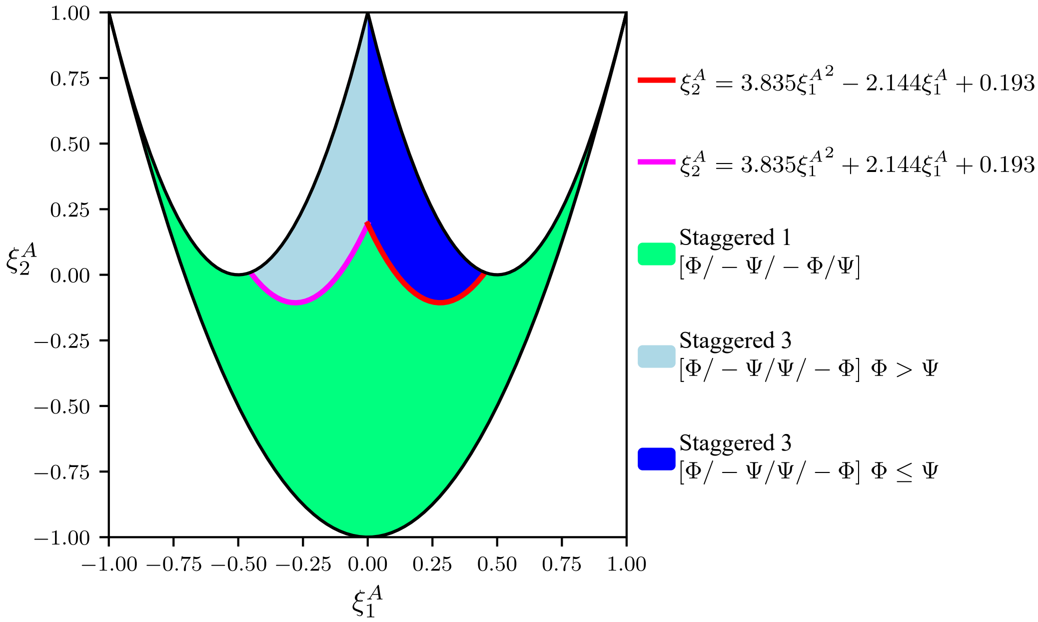

Figure 4.1: Double-Double stacking sequence selection based on lamination parameters to meet 2% Tsai's modulus homogenisation threshold with 4 repeats

The failure index of the best laminate increased with the number of repeats. This increase in the failure index is likely explained by the decrease of the bending-twist coupling terms with higher building block repeats.

Table 4.2: Double-Double laminates with lowest Tsai-Wu failure index in sensitivity analysis of untapered plate

Number of repeats	Double-Double angles	Stacking sequence	Tsai-Wu failure index
$r = 4$	$\Phi = 10°, \Psi = 5°$	$[10/-5/-10/5]_{4T}$	0.067578
$r = 6$	$\Phi = 10°, \Psi = 5°$	$[10/-5/-10/5]_{6T}$	0.071734
$r = 8$	$\Phi = 10°, \Psi = 5°$	$[10/-5/-10/5]_{8T}$	0.074462
$r = 10$	$\Phi = 10°, \Psi = 5°$	$[10/-5/-10/5]_{10T}$	0.076029

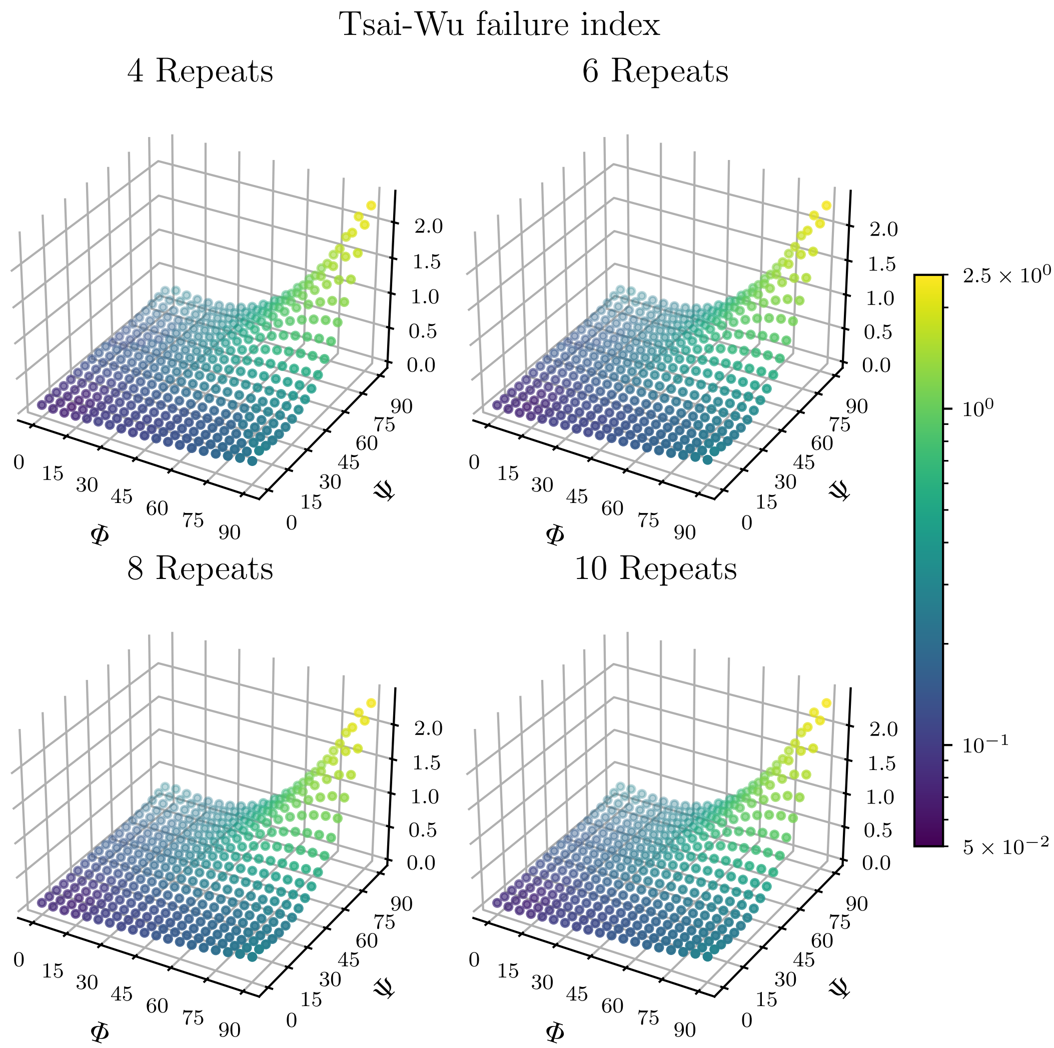

Figure 4.2: Sensitivity analysis results for static aeroelastic condition of untapered plate. Tsai-Wu failure index$\geq$ 1 means laminate failure

4.1.2. Critical Aeroelastic Velocity

The values obtained from the critical aeroelastic velocity sensitivity analysis are shown in Figure 4.3. There is a clear discontinuity in the objective space which becomes more similar as the number of repeats increases. This discontinuity is caused by a change in the critical aeroelastic mode between the 2nd and 3rd modes, as will be explained further below. Outside the discontinuity, the objective space shows no significant changes with the number of repeats. The highest instability velocity is always found near the discontinuity. The laminates with highest critical aeroelastic velocity for each number of repeats are shown in Table 4.3. Although there are some differences in the angles, they are small and the angles are close, therefore the laminate stiffness is similar. The changes in critical velocity are small as the difference between the highest and lowest velocity is of 2.73%.

The fact that the best laminates are found near the discontinuity poses a potential challenge in the aeroelastic tailoring of the plate. Small simulation errors or a slight change in Double-Double angles of the solutions in this region, caused for instance by manufacturing tolerances, can result in a significant drop of the critical velocity, which is undesirable in terms of structural stability.

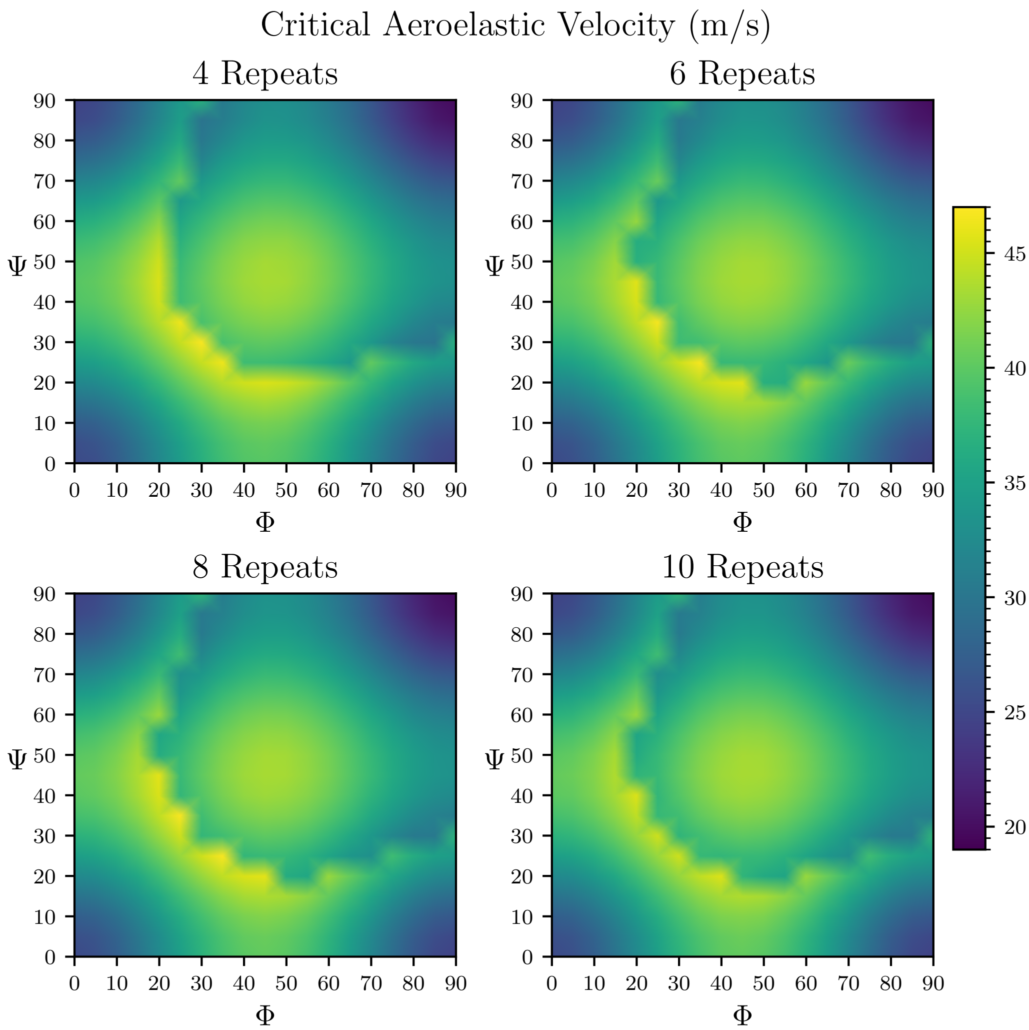

Figure 4.3: Sensitivity analysis for critical aeroelastic velocity of untapered plate

Table 4.3: Double-Double laminates with highest critical aeroelastic velocity in sensitivity analysis of untapered plate

Number of repeats	Double-Double angles	Stacking sequence	Critical Aeroelastic Velocity (m/s)
$r = 4$	$\Phi = 30°$, $\Psi = 30°$	$[30/-30/-30/30]_{4T}$	46.73
$r = 6$	$\Phi = 25°$, $\Psi = 35°$	$[25/-35/-25/35]_{6T}$	46.57
$r = 8$	$\Phi = 25°$, $\Psi = 35°$	$[25/-35/-25/35]_{8T}$	46.68
$r = 10$	$\Phi = 20°$, $\Psi = 40°$	$[20/-40/-20/40]_{10T}$	45.49

Since the critical aeroelastic velocity is insensitive to the number of repeats of the building block, the discontinuity in the objective space was further explored considering 8 repeats. For that purpose, the simulations were repeated for all Double-Double angles with an angle step of 2.5°. Figure 4.4

shows that the discontinuity became better defined by decreasing the angle step. The highest velocity is found near the discontinuity and it can be observed that on both sides of the discontinuity the objective space is smooth and well-defined. Analysing the instability frequency shown in Figure 4.5, a similar behaviour is found. There is a large discontinuity in frequency in the same region and the space on both sides of the discontinuity is smooth. This large change in frequency indicates that the critical mode changes. In Figure 4.6 it can be seen that the aeroelastic instability is dominated by the 2nd and 3rd modes, and the change in critical mode is the cause of the previously discussed discontinuity in the critical velocity and frequency spaces. It should be noted that no Double-Double laminate was found for which divergence was the critical aeroelastic instability, as can be seen in Figure 4.5, since there are no 0 frequency points. As Double-Double is used in a homogenised state, the bending-twisting coupling terms of the $[\boldsymbol{D}]$ are small compared to the remaining terms and therefore, there is no significant unfavourable bending-twisting coupling that could result in early torsional divergence.

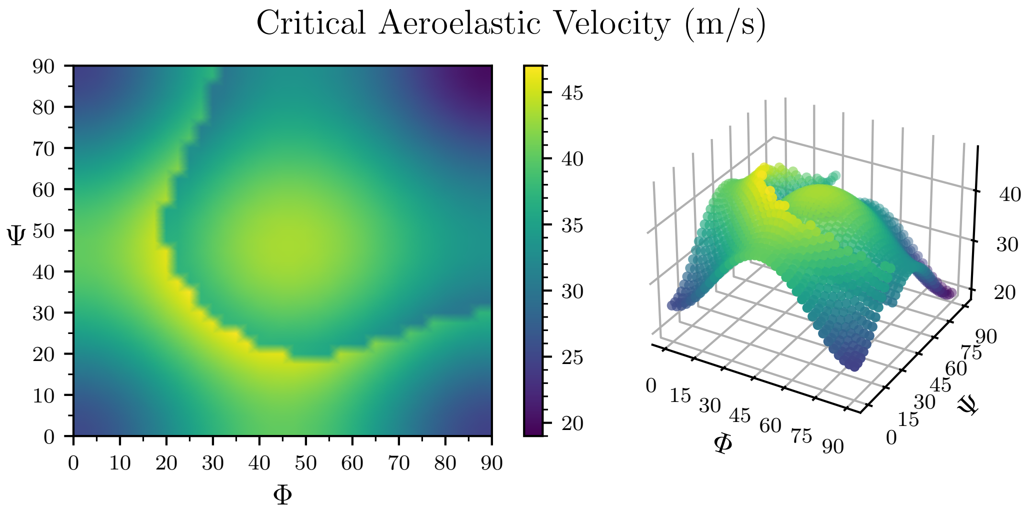

Figure 4.4: Critical aeroelastic velocity for 8 repeats with angle step of 2.5°

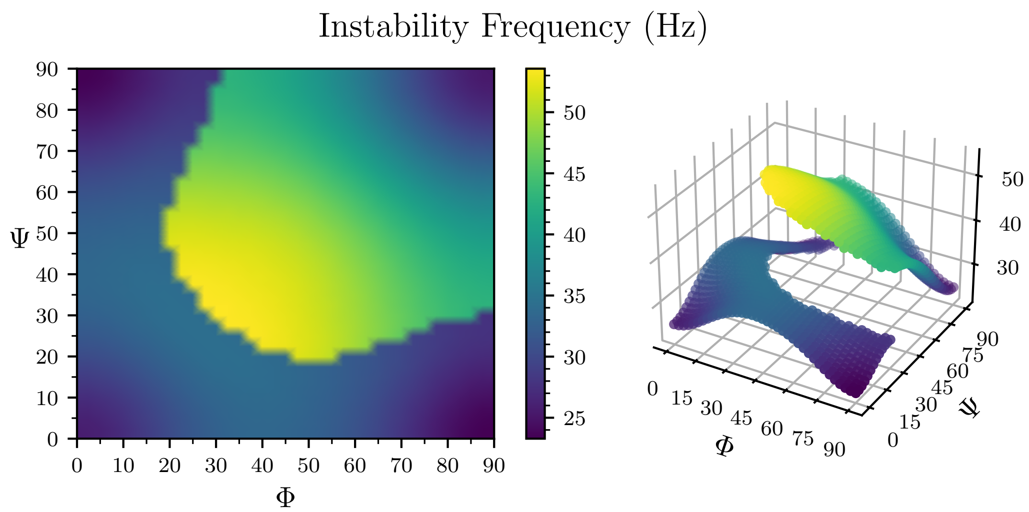

Figure 4.5: Instability frequency for 8 repeats with angle step of 2.5°

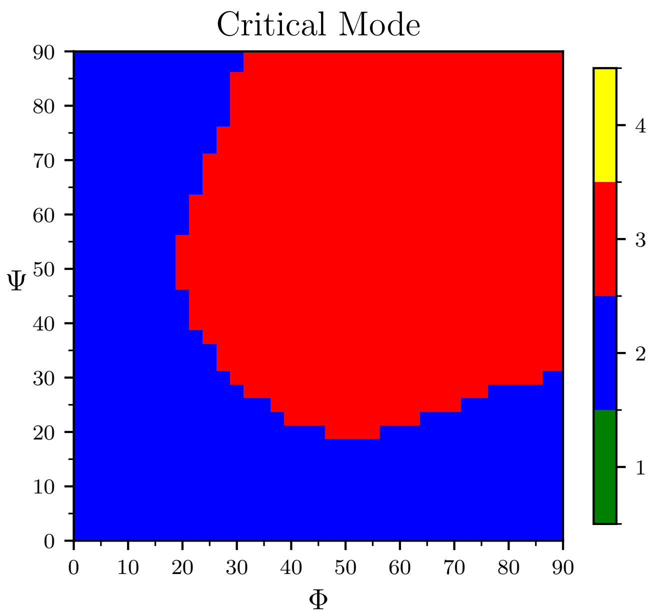

Figure 4.6: Critical mode for 8 repeats with angle step of 2.5°

4.2. Sensitivity Analysis on Thickness Tapered Plates

One of the main advantages proposed by Double-Double is higher weight savings by easier thickness tapering compared to traditional quad laminates. With this in mind, additional analyses were performed for two configurations with thickness variation: one configuration with thickness changing in the spanwise direction, decreasing from root to tip, and another with thickness tapering in the chordwise direction, decreasing from leading to trailing edge. These configurations were selected as each is expected to improve one of the aeroelastic behaviour metrics used in this work. In the static aeroelastic condition the loading is dominated by bending and, therefore, the higher stresses will be found at the root of the plate.

By having a higher thickness at the root in the spanwise tapered configuration, a lower stress level is expected which will translate in lower Tsai-Wu failure index. The chordwise tapered configuration seeks to take advantage of a known mass balancing effect, where moving the mass axis forward, accomplished here by having higher thickness near the leading edge, increases the flutter velocity [15, 16].

For the tapering, the plate was divided in 4 section spanwise and chordwise for each respective configuration. The number of Double-Double building block repeats for each section went from 10 to 4 in steps of 2, from higher to lower thickness respectively. A ply thickness of $28.71\,\mu\mathrm{m}$ was used for both configurations, in order to maintain the same mass as laminate with a constant thickness of $0.804\,\mathrm{mm}$, as in the previous studies. The Φ and Ψ angles are maintained for each section. The simulations were performed for all Double-Double angles with an angle step of $5°$.

4.2.1. Spanwise Thickness Tapering

Figure 4.7 shows the Tsai-Wu failure index for the spanwise tapered configuration. As expected, increasing the laminate thickness at the root allowed for a reduction of the stress level and the failure index decreased significantly. No laminate fails under the static aeroelastic condition as the highest failure index is of 0.7878. The lowest failure index was found for the same Double-Double laminate as in the sensitivity analysis of the plate with constant thickness: $[\pm 10°/\pm 5°]$ with a failure index of 0.033694, less than half of the lowest one found in Table 4.2 for the sensitivity analysis of the untapered plate. It can be seen, in Figure 4.8, that this configuration also resulted in an increase of the critical aeroelastic velocity, when compared to the untapered laminates of section 4.1.2. The highest critical velocity found was of $52.95\,\mathrm{m/s}$ for the Single-Double laminate $[\pm 45]$. The critical instability is also always flutter as there is no laminate with 0 instability frequency. Regarding the critical instability mode, it can be seen in Figure 4.9 that the instability is dominated by the 2nd, 3rd and 4th modes.

Figure 4.10 shows the eigenvalue evolution of 3 laminates of the spanwise tapered configuration, each with a different critical mode. It should be noted that for the Single-Double laminate with $\Phi = \Psi = 60°$ in Figure 4.10b, the 4th mode is the critical one and it is a hump mode that barely passes to the unstable region ($\mathrm{Re}(p) \geq 0$) and quickly restabilises.

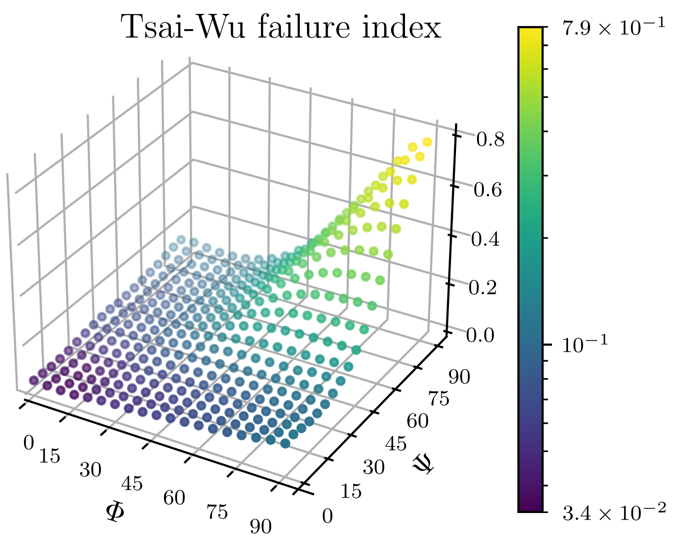

Figure 4.7: Tsai-Wu failure index for the spanwise tapered configuration. Tsai-Wu failure index≥ 1 means laminate failure

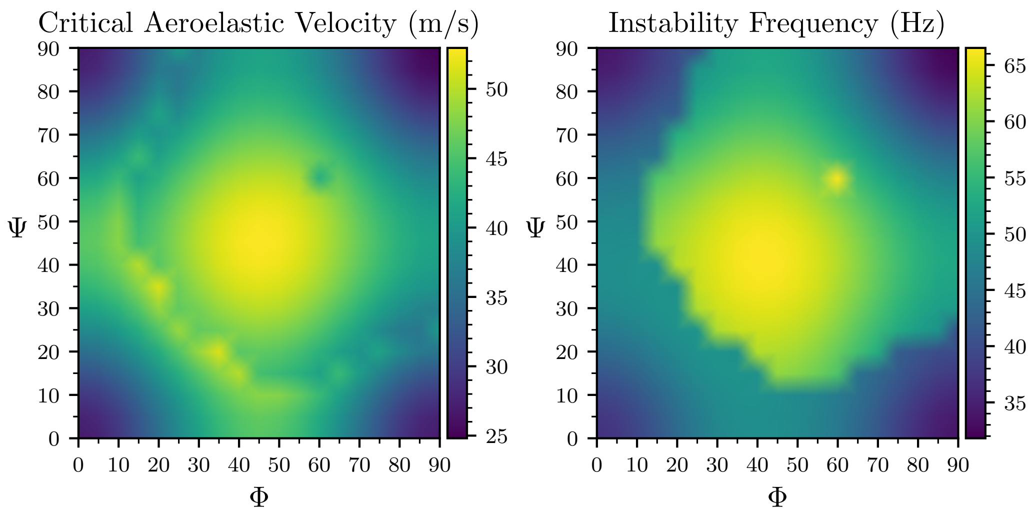

Figure 4.8: Aeroelastic instability for the spanwise tapered configuration

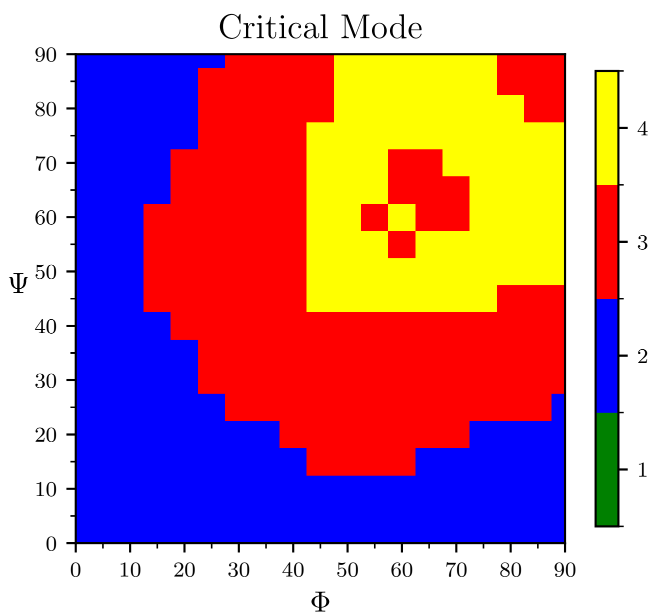

Figure 4.9: Critical mode for the spanwise tapered configuration

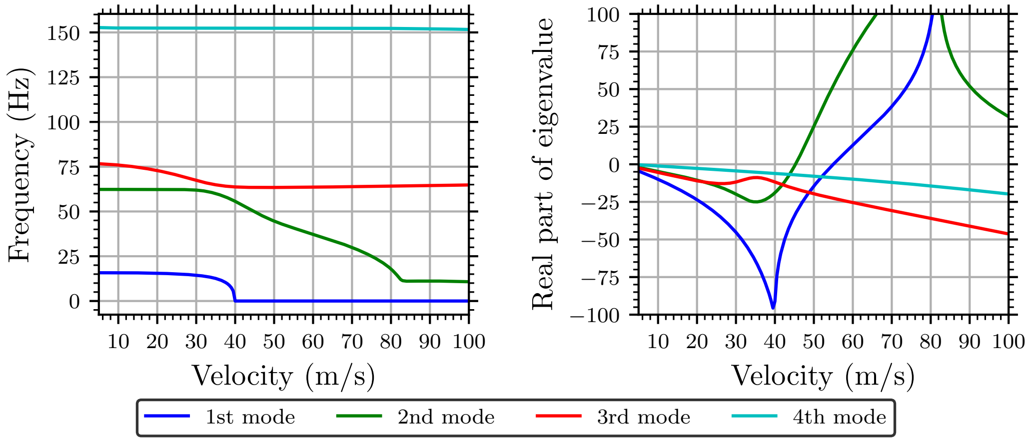

(a) $\Phi = 30°$ $\Psi = 15°$ - 2nd mode critical

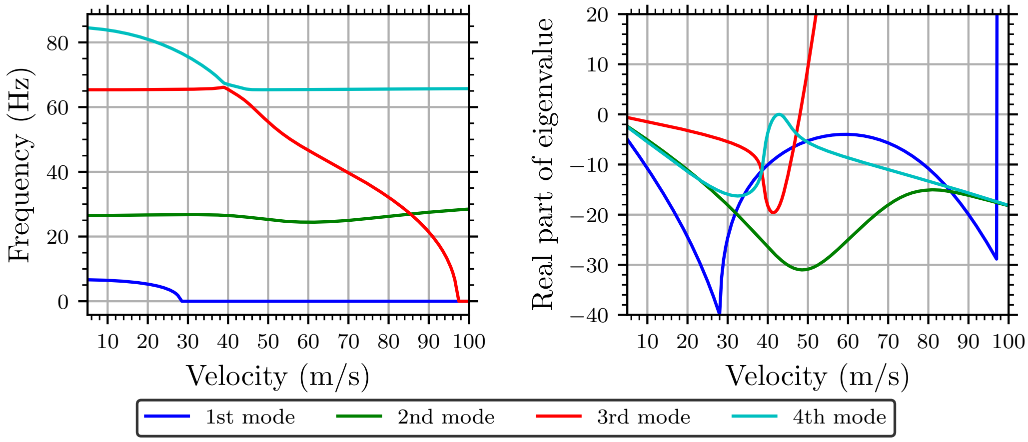

(b) $\Phi = 60°$ $\Psi = 60°$ - 4th mode critical

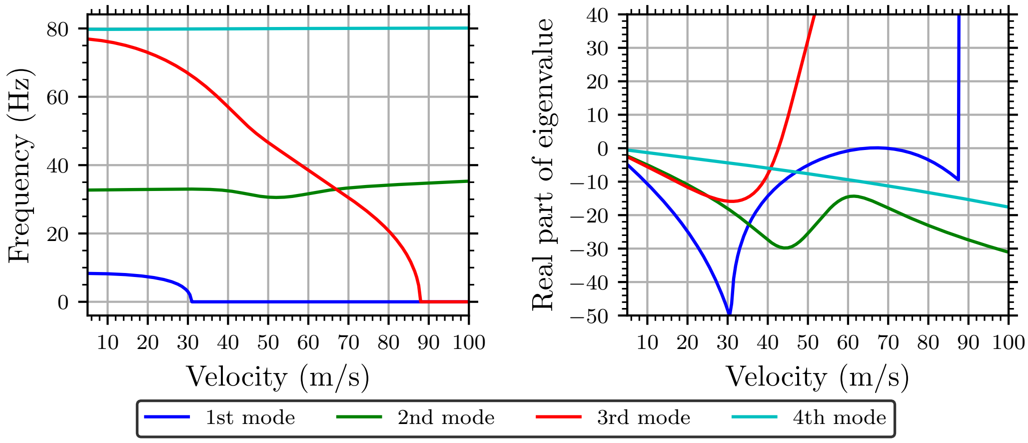

(c) $\Phi = 80°$ $\Psi = 45°$ - 3rd mode critical

Figure 4.10: Eigenvalue migration of 3 Double-Double laminates in the spanwise tapered configuration

4.2.2. Chordwise Thickness Tapering

The Tsai-Wu failure index for the chordwise tapered configuration is shown in Figure 4.11. Compared to the untapered laminates, the failure index decreased. All Double-Double laminates in the chordwise tapered configuration have a failure index below 1. The lowest failure index is found for fibres in the spanwise direction, that is for the Single-Double case with 0° plies, with a failure index of 0.042236. As anticipated, by shifting the mass axis forward with higher leading edge thickness, the chordwise tapered configuration increases the critical aeroelastic velocity, as can be seen in Figure 4.12. The Single-Double $[\pm 50]$ achieves the highest velocity of $59.05\,\mathrm{m/s}$. The discontinuity in the objective space is considerably different from the previous ones. The critical aeroelastic modes are the 2nd and 3rd modes, with the 3rd mode being the critical one for a larger region of the design space (see Figure 4.13).

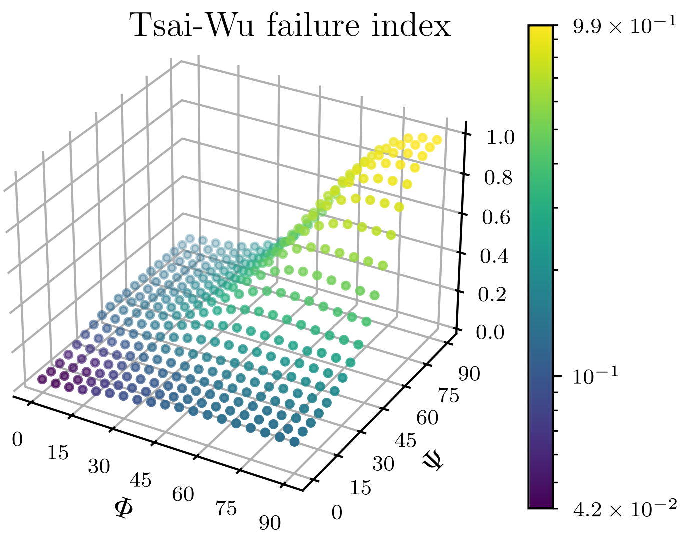

Figure 4.11: Tsai-Wu failure index for the chordwise tapered configuration. Tsai-Wu failure index≥ 1 means laminate failure

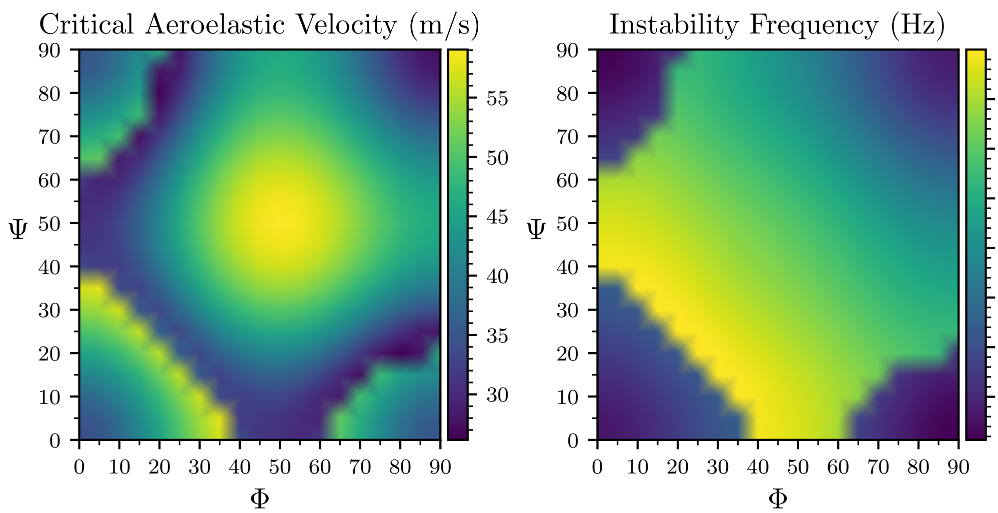

Figure 4.12: Aeroelastic instability for the chordwise tapered configuration

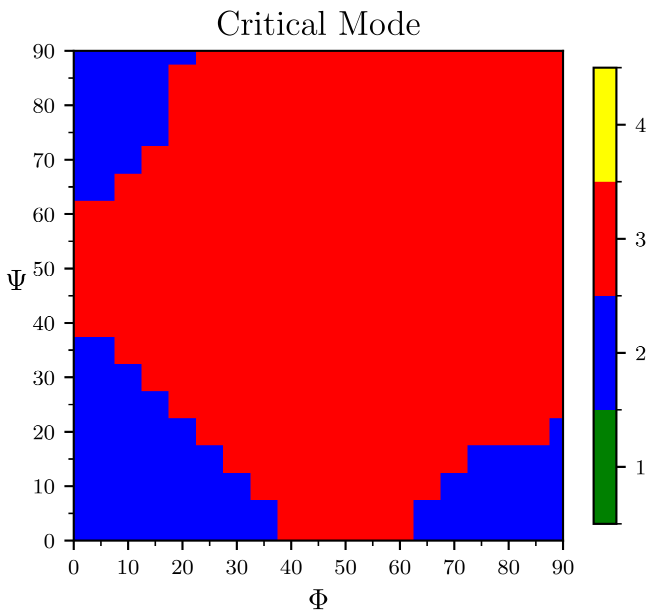

Figure 4.13: Critical mode for the chordwise tapered configuration

4.3. Optimisation Results

To further explore the aeroelastic behaviour of the composite plate using Double-Double laminates several optimisation studies were performed:

- Single-objective optimisation to minimise the Tsai-Wu failure index under the static aeroelastic load case
- Single-objective optimisation to maximise the critical aeroelastic velocity
- Multi-objective optimisation considering the objectives for the single-objective optimisation procedures, *i.e.* minimising Tsai-Wu failure index and maximising critical aeroelastic velocity.

The results of these studies are here presented and compared with the ones of 6-ply symmetric laminates shown in Section 3.3.3. Besides analysing unidirectional Double-Double laminates, the concept of tow steered Double-Double was also explored. Unlike conventional unidirectional laminates, in tow steered laminates the fibres in a ply can follow a curvilinear path. This way it is possible to obtain laminates with variable stiffness, opening up the design space. In this work, it was considered that the fibre angle could only change along the spanwise direction so that fibres are always parallel chordwise. In the current work, the fibre angle was taken as changing linearly and the fibre angle θ at a given spanwise position is determined as:

$$\theta = \frac{(\theta_{tip} - \theta_{root})\,x}{s} + \theta_{root} \tag{4.5}$$

where:

- x: position along the span
- s: plate span

- θ_{root}: fibre angle at the plate root
- θ_{tip}: fibre angle at the plate tip

This linear fibre angle variation results in a curvilinear fibre path defined by Equation 4.6, [53, 54]. Equations 4.5 and 4.6 are expressed according to the coordinate system presented in Figure 3.1, when the problem was presented.

$$y = \frac{s}{\theta_{tip} - \theta_{root}} \left\{ - \ln \left[\cos \left(\frac{(\theta_{tip} - \theta_{root})\, x}{s} + \theta_{root} \right) \right] + \ln \left[\cos \left(\theta_{root} \right) \right] \right\} \tag{4.6}$$

The introduction of tow steering in the finite element model requires the calculation of the fibre angle, for all plies, at the centre of each finite element. Given that the fibre angle variation in this work is only in the spanwise direction, with the angle being the same along the chord, this requires evaluating the fibre angle at the x coordinate of the centre of the element. Elements that are aligned chordwise, *i.e.* their centres share the same x coordinate, have equal fibre angle. Furthermore, the difference in x coordinate of the element centre of two adjacent triangular elements within the same chordwise column of elements is minimal and results in insignificant angle change. Therefore, to introduce tow steering in the finite element model, the angles were computed according to Equation 4.5 for each ply at the centre x coordinate of each of the 48 chordwise columns of elements. The individual columns of elements were then assigned their own stacking sequence (`PCOMP` entry).

For the tow steered laminates, the stacking sequence was not selected based on lamination parameters as there would be a possibility of having Staggered 1 in one part of the plate and Staggered 3 in another, which would cause a ply angle discontinuity and would not be manufacturable. To address this, stacking sequence and number of repeats were selected so that the homogenisation criterion was met with only one stacking sequence. It has been shown that with 8 repeats the 2% Tsai's modulus homogenisation criterion can be met in the entire Double-Double domain with Staggered 1 [10]. Therefore, for the optimisation studies, all Double-Double laminates (unidirectional and steered) were considered with 8 repeats of the building block and a ply thickness of $25.125\,\mu\text{m}$. The stacking sequence was chosen between Staggered 1 and Staggered 3, based on lamination parameters, for unidirectional laminates, and only Staggered 1 was used for steered laminates.

4.3.1. Static Aeroelastic Condition

The results of the single-objective optimisation of the Tsai-Wu failure index under the static aeroelastic condition are presented in Table 4.4. In can be seen that both Double-Double laminates (unidirectional and tow steered) have a higher failure index than the unbalanced 6-ply symmetric laminates. The failure index of the unidirectional Double-Double is over twice that of the 6-ply laminates. Comparing the normalised stiffness matrices of the optimal 6-ply symmetric and unidirectional Double-Double laminates in Figure 4.14, the largest differences are found in the coupling terms A^*_{16} and D^*_{16}. The bending-twist coupling term D^*_{16} is of particular interest. In our problem, if a laminate has a positive D^*_{16} then when the plate bends positively (upwards) it will also twist leading edge downwards. This results in a wash-out effect, countering the aerodynamic loads. For the 6-ply laminate D^*_{16} is over 60 times that of the Double-Double laminate, thus it achieves a higher load reduction and a lower failure index.

It should be noted that even though the failure index of both the 6-ply unbalanced laminates and unidirectional Double-Double laminates is low and far from failure, the most important factor is their relative magnitude. If the stress levels were increased 5 times, so would the failure index. Therefore, Double-Double laminates would fail for half the failure stresses of the 6-ply symmetric laminates, indicating a significant drawback in the use of Double-Double laminates for this type of loading condition due to the absence of bending-twist coupling.

Table 4.4: Static aeroelastic condition optimisation results

	Optimal Laminate	Tsai-Wu failure index
6-ply symmetric:	$[4.0/14.4/12.6]_S$	0.03398
Double-Double:	$\Phi = 11.8$ $\Psi = 7.4$	0.072642
Double-Double Tow Steering:	Root: $\Phi = 6.1$ $\Psi = 1.4$ Tip: $\Phi = 42.4$ $\Psi = 38.4$	0.056545

$$[\boldsymbol{A}^*] = \begin{bmatrix} 92.29 & 5.1 & 14.19 \\ & 8.52 & 1.63 \\ & & 8.47 \end{bmatrix} \text{GPa} \qquad [\boldsymbol{D}^*] = \begin{bmatrix} 95.09 & 3.83 & 9.81 \\ & 8.27 & 1.01 \\ & & 7.20 \end{bmatrix} \text{GPa}$$

$$[\boldsymbol{B}^*] = [0]\,\text{GPa}$$

(a) 6-ply symmetric: $[4.0/14.4/12.6]_S$

$$[\boldsymbol{A}^*] = \begin{bmatrix} 93.73 & 4.47 & 0 \\ & 8.35 & 0 \\ & & 7.85 \end{bmatrix} \text{GPa} \qquad [\boldsymbol{D}^*] = \begin{bmatrix} 93.73 & 4.47 & 0.16 \\ & 8.35 & 0.015 \\ & & 7.85 \end{bmatrix} \text{GPa}$$

$$[\boldsymbol{B}^*] = \begin{bmatrix} -0.065 & 0.030 & 0.18 \\ & 0.006 & 0.028 \\ & & 0.030 \end{bmatrix} \text{GPa}$$

(b) Double-Double: $\Phi = 11.8$ $\Psi = 7.4$

Figure 4.14: Comparison of normalised stiffness matrices of optimal DD and 6-ply symmetric laminates for static aeroelastic condition

The introduction of tow steering in the Double-Double laminate allowed a reduction of the failure index by 22.16%. In the tow steered solution, the Double-Double angles are closer to $0°$ at the root and open to near $40°$ at the tip. Figure 4.15 shows the spanwise evolution of the normalised stiffness terms of the tow steered Double-Double laminate. At the root the dominating stiffness terms are the ones related to the spanwise direction A^*_{11} and D^*_{11}. This is a result of the angles at the root being closer to $0°$, and is consistent with the loading condition which causes higher stresses at the root. The terms of the bending-extension matrix and the bending-twist coupling terms of the flexural matrix, D^*_{16} and D^*_{26}, are small along the span, which is expected as the laminate is homogenised.

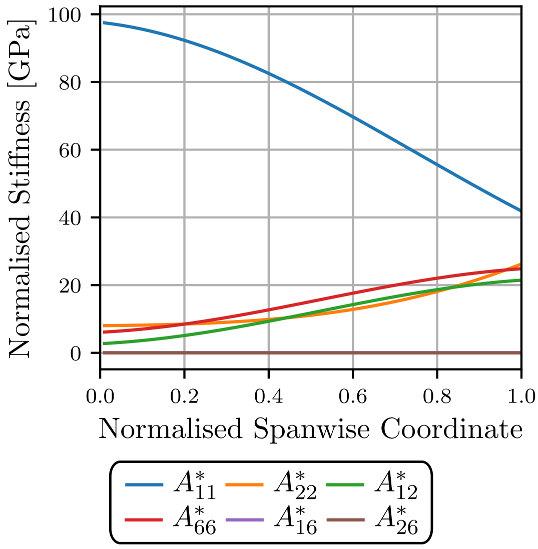

(a) $[A^*]$

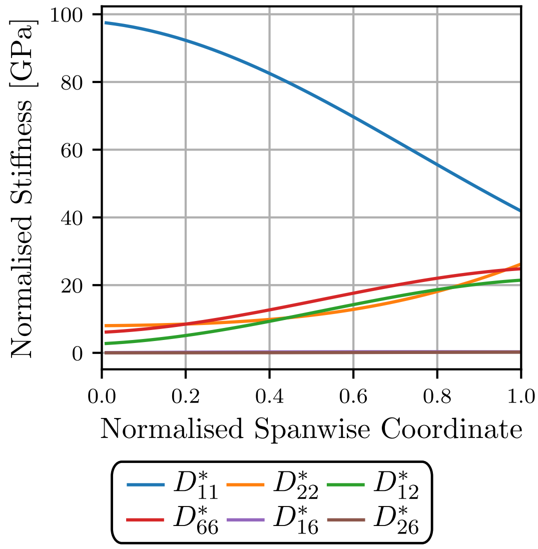

(b) $[D^*]$

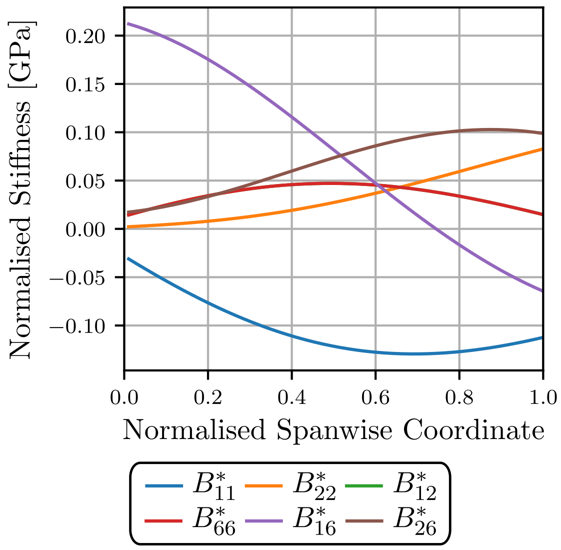

(c) $[B^*]$

Figure 4.15: Normalised stiffness terms for optimal tow steered Double-Double for static aeroelastic condition

4.3.2. Critical Aeroelastic Velocity

Table 4.5 shows the results of the optimisation study seeking to maximise the critical aeroelastic velocity. There are no significant differences between the critical velocities for the three laminate types considered. The critical velocity of the unidirectional Double-Double laminate is 2.35% higher than that of the 6-ply laminate. The change in Double-Double angles in the tow steered laminate is smaller when compared to the steered laminate of the static aeroelastic condition optimisation. The introduction of steering only increased the critical velocity of the Double-Double laminate marginally by 0.51%. Figure 4.16 shows the spanwise evolution of the normalised stiffness terms of the tow steered Double-Double.

Table 4.5: Critical aeroelastic velocity optimisation results

	Optimal Laminate	Critical Aeroelastic Velocity $(\mathrm{m/s})$
6-ply symmetric:	$[36.6/-41.2/-37.7]_S$	45.60
Double-Double:	$\Phi = 25\ \Psi = 35$	46.68
Double-Double Tow Steering:	Root: $\Phi = 32.3\ \Psi = 33.5$ Tip: $\Phi = 45.8\ \Psi = 9.7$	46.92

The eigenvalue migration of all three laminates is shown in Figure 4.17. The critical mode for all laminates is the second one and the instability is flutter. While for the 6-ply laminate the 3rd mode is a hump mode, that is it goes unstable but eventually restabilises, this mode is always stable for the Double-Double laminates, although it gets very close to being unstable. In all laminates, there is a clear approach of the frequencies of the 2nd and 3rd modes, which indicates that these modes mix and are responsible for flutter. There is a significant difference in the divergence behaviour between the unbalanced 6-ply laminate and the Double-Double laminates. While the first one diverges only near $84\,\mathrm{m/s}$, the Double-Double laminates diverge shortly after flutter near 53-54$\mathrm{m/s}$. The behaviour of eigenvalue of the tow steered Double-Double laminate is similar to that of the unidirectional Double-Double.

The natural vibration modes of the optimal unidirectional Double-Double laminate are shown in Figure 4.18. The 3rd mode is a torsion mode while the remaining modes are of bending. As mentioned in the previous paragraph, flutter is caused by the unfavourable coupling of the 2nd and 3rd modes. Therefore, the flutter instability is a classical binary flutter of the bending-torsion type. The resulting flutter mode shape is shown in Figure 4.19 and the corresponding frequency is of $33.91\,\mathrm{Hz}$.

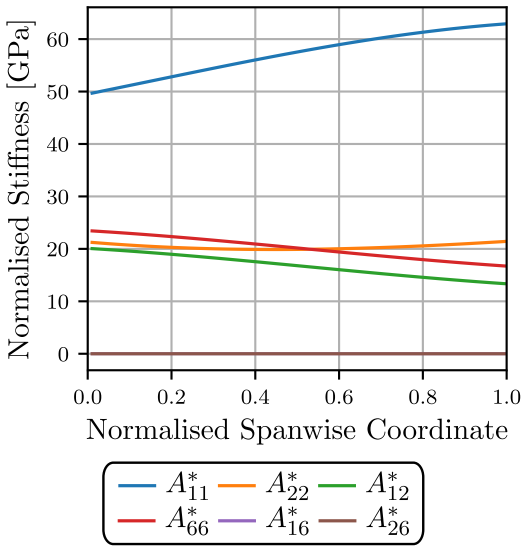

(a) $[A^*]$

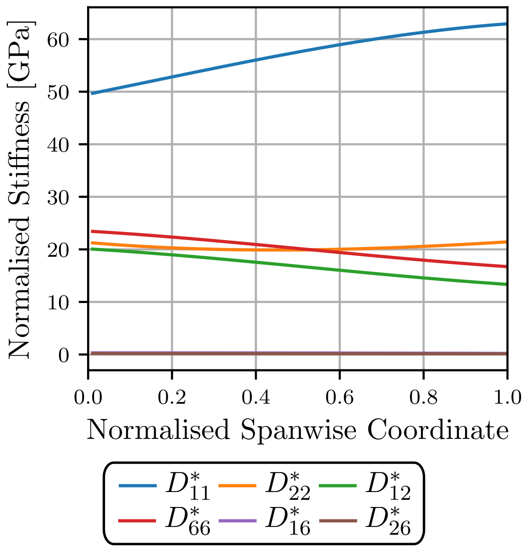

(b) $[D^*]$

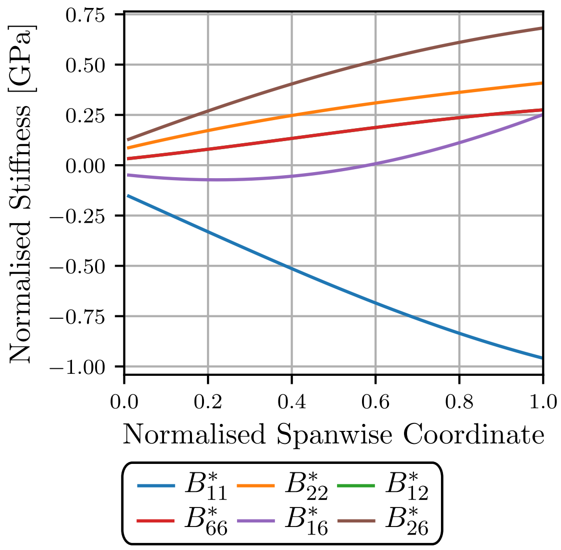

(c) $[B^*]$

Figure 4.16: Normalised stiffness terms for optimal tow steered Double-Double for critical aeroelastic velocity

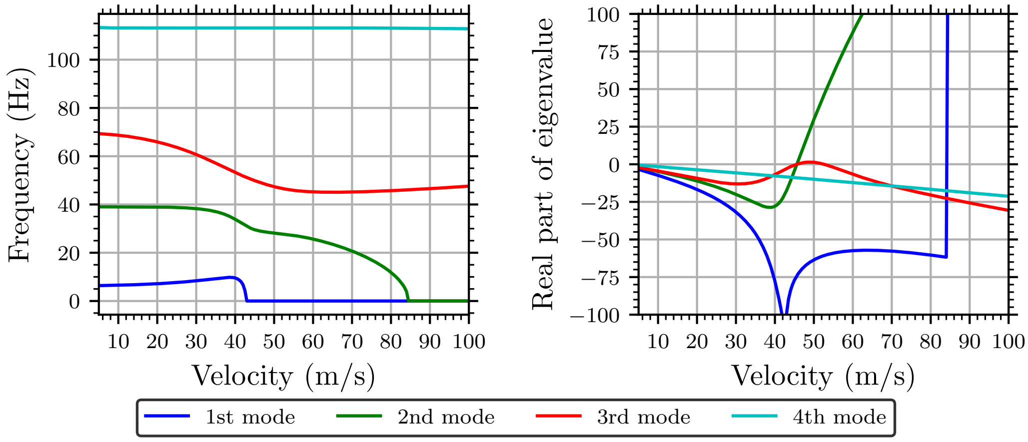

(a) 6-ply symmetric

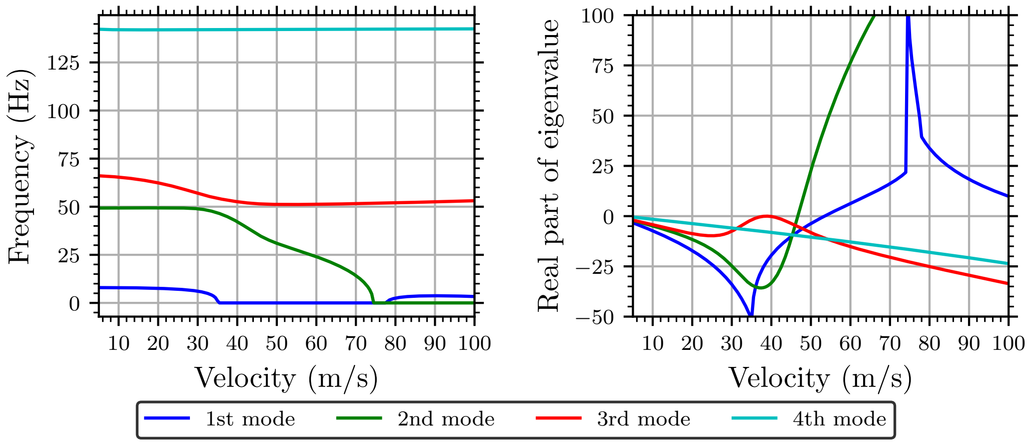

(b) Double-Double

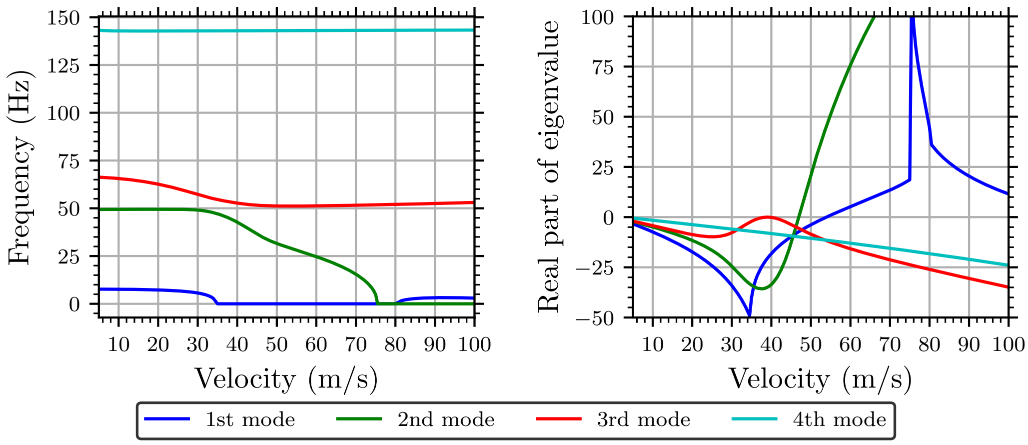

(c) Double-Double Tow Steered

Figure 4.17: Eigenvalue migration of optimal laminates for critical aeroelastic velocity

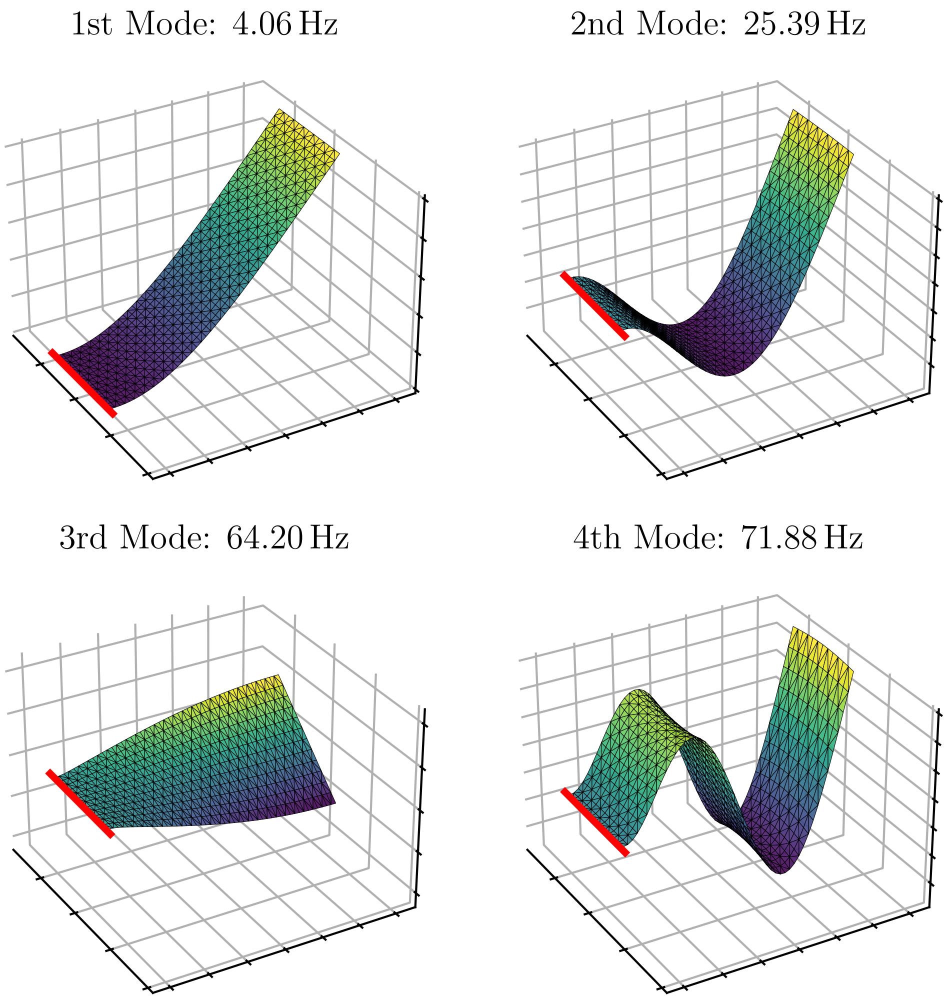

Figure 4.18: Natural vibration modes of optimal Double-Double for critical aeroelastic velocity: $\Phi = 25$ $\Psi = 35$

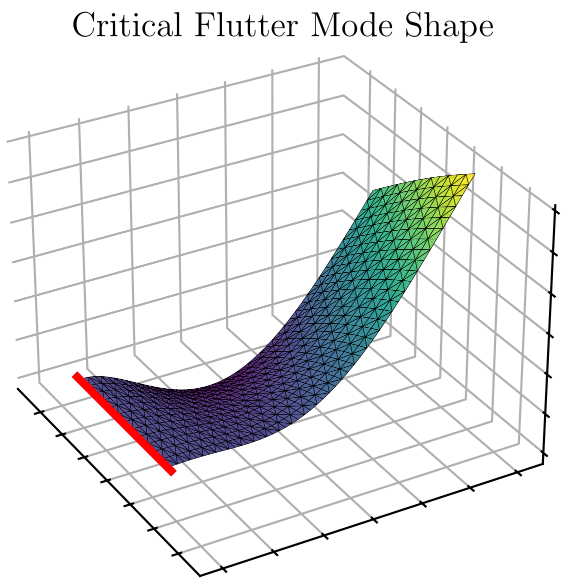

Figure 4.19: Flutter mode shape of optimal Double-Double for critical aeroelastic velocity: $\Phi = 25$ $\Psi = 35$

4.3.3. Multi-Objective optimisation

The Pareto fronts obtained from the multi-objective optimisation are shown in Figure 4.20. The front of the Double-Double laminates is dominated almost in its entirety by the front of the 6-ply symmetric laminates. This lack of improvement of the Double-Double front is related to the Tsai-Wu failure index, where Double-Double laminates have higher values. While introducing tow steering in Double-Double laminates does not allow to obtain the same lowest Tsai-Wu failure index as the 6-ply laminates, as seen in Section 4.3.1, it still allows for a reduction of the failure index in Double-Double laminates. In fact, it can be seen even improving compared to the unbalanced 6-ply laminates. Additionally, the lowest critical velocity found in the pareto front of the tow steered Double-Double laminates is higher than the corresponding lowest velocity of the other fronts.

4.4. Discussion

Overall, Double-Double laminates are adequate for use in aeroelastic tailoring. When it comes to critical aeroelastic velocity, the improvements offered by Double-Double laminates (both unidirectional and tow steered) are small when compared to the unbalanced 6-ply laminates. However, a significant advantage might come when production is considered. With homogenised laminates (Double-Double) the warping caused by the thermal steps in the manufacturing process is greatly reduced. The biggest drawback in the application of unidirectional Double-Double laminates lies in the static aeroelastic condition. At high aerodynamic loading conditions, *i.e.* high dynamic pressure, the lack of bending-twist coupling in unidirectional Double-Double laminates means they cannot create a sufficient wash-out behaviour that counters and reduces the aerodynamic loads and, therefore they require higher thickness not to fail, when compared to unbalanced symmetric laminates. This introduces additional structural weight, which is not wanted in aircraft structures. Using tow-steering with linear fibre angle variation along one direction, allows for a great reduction of this penalty, although it still cannot achieve the lowest failure index values obtained by the 6-ply symmetric laminates. In fact, tow steered Double-Double laminates are

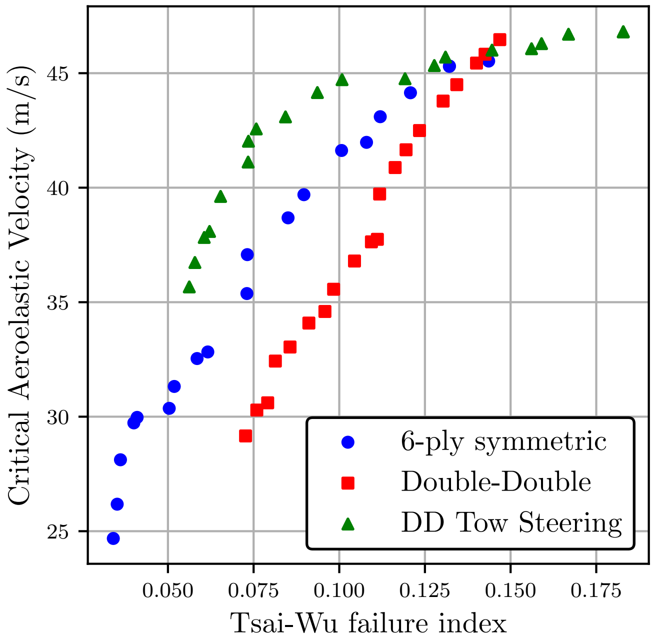

Figure 4.20: Pareto fronts of aeroelastic optimisation

preferable to both unidirectional Double-Double and 6-ply unbalanced laminates in a significant portion of the objective space (Figure 4.20). These results indicate that for aeroelastic tailoring applications, tow steered Double-Double laminates can be beneficial. If the results from the sensitivity analysis with tapered plates are considered, it is likely that the ideal Double-Double laminates for aeroelastic tailoring are tow steered Double-Double with thickness tapering.

5

Baseline Model for Aeroelastic Tailoring of Representative Wingbox

The study of a cantilevered composite plated allowed for a better understanding of the aeroelastic behaviour of Double-Double laminates and to identify the potential for use in aeroelastic tailoring. However, aircraft structures have far more complex stiffness and mass distributions that a simple plate and are not made of one single component. Therefore, to fully understand Double-Double in the context of aeroelastic tailoring it is necessary to explore its application to more realistic structures. To that end, in this chapter a model of a wingbox structure representative of current commercial aircraft configurations that can be used for the study of aeroelastic tailoring is developed. Recommendations are made for the potential future use of this model to better understand the applicability of Double-Double to aeroelastic tailoring.

5.1. Wingbox Aeroelastic Model

The wingbox model used in this study is based on the NASA Common Research Model (CRM) configuration, developed as a benchmark model for computational aerodynamic studies [55]. The transonic CRM wing is representative of modern commercial long range aircraft and is designed for cruise level flight at Mach number $M = 0.85$.

The wing planform has an aspect ratio of 9, a wingspan of $58.76\,\mathrm{m}$, a taper ratio of 0.275, a quarter chord sweep angle of $35°$ and a Mean Aerodynamic Chord (MAC) of $7.01\,\mathrm{m}$. The trailing edge has a kink, known as yehudi break, at the 37% semi-span station. The fuselage intercepts the wing at the 10% semi-span position: the wing root. The wing can be dividied in three main sections: the centre wing section, *i.e.* the portion of the wing inside the fuselage, the inner wing section, from the fuselage interception up to the yehudi break, and the remaining wing is the outer wing section. The surface files of the undeflected Common Research Model (uCRM) outer mold line and wingbox, available at Ref. [56], were used for the geometry definition, and additional information was extracted for the readily available finite element input files. The structural model was built in the MSC Nastran software, while the aerodynamic and aeroelastic components were developed with pyNastran [45] and the Femap software.

The wingbox follows a conventional structural layout with two straight spars, ribs and stiffened skins. The front spar is placed at the 10% local chord position in the root and tapers to the 35% local chord at the tip, while the rear spar remains constantly at the 60% local chord position through the wingspan. A total of 49 evenly spaced ribs are used, with the first 5 ribs at the centre wingbox being parallel to the airflow and the remaining ribs perpendicular to the trailing edge spar. The upper and lower skins are stiffened with 6 T-shape stringers, which were placed so that they are equally spaced both at wing root and wing tip. To include the stringers, the wingbox surface files were edited, removing all the ribs except for the ones at the wingbox extremities. The stringer curves were then added in MSC Patran and the internal ribs rebuilt. It should be noted that while the number of stringers used is consistent with other work done in the CRM model [32, 33], typical reference aircraft designs have a higher number of stringers, which means the skins of the model carry more loads when compared to more realistic designs. This could result in excessively low buckling loads [32].

As the CRM was developed for validation of computational aerodynamics, its geometry represents a 1-g cruise condition deformed flying shape. Due to these built in deflections, the original CRM is not adequate for aeroelastic analysis. To address this issue Kenway *et al.* [35] defined an undeflected Common Research Model (uCRM) which deflects to the original CRM flying shape at the cruise condition. The jig shape, *i.e.* wing twist distribution, found by Kenway *et al.* [35] was used for the development of the model and the corresponding wingbox configuration was adapted.

The structural components were made of aluminium with the properties listed in Table 5.1 and their dimensions adapted from available literature [23, 32–35]. The current model was intended for optimisation of the skins only, therefore both spars and the ribs were kept with a constant thickness of $5\,\mathrm{mm}$. The T stringers were considered with equal height and width that decreased linearly from $140\,\mathrm{mm}$ at the wing root to $60\,\mathrm{mm}$ at the wing tip and a constant thickness of $5\,\mathrm{mm}$. The stringer dimensions at the centre wingbox are constant and equal to the dimensions at the wing root. To allow for thickness variation, each skin was divided into 12 patches made of 4 bays limited by spars and ribs that have independent thickness. Given that this model is intended as a starting point for optimisation, all skin patches were considered with $15\,\mathrm{mm}$ thickness. The structure was modelled with 6 degree-of-freedom shell elements (`CTRIAR` and `CQUADR`) for the spars, skins and ribs and with beam elements (`CBEAM`) for the stringers in a total of 49937 elements.

Table 5.1: Material properties for baseline wingbox model

Property	Value
Young's modulus, E	$71.7\,\mathrm{GPa}$
Density, ρ	$2830\,\mathrm{kg/m^3}$
Poisson's ratio, ν	0.33

Concentrated point masses rigidly connected (`RBE3`) to spar and rib nodes were added to represent aircraft weight due to leading ang trailing edge control surfaces ($1200\,\mathrm{kg}$ and $2500\,\mathrm{kg}$ respectively), fuel (both maximum fuel capacity of $55\,000\,\mathrm{kg}$ in half aircraft and 20% fuel) and engine/nacelle/pylon structure ($7500\,\mathrm{kg}$), as shown in Figure 5.1. To allow for the calculation of trimmed manoeuvres a rigid (`RBE2`) fuselage and trimmable Horizontal Tailplane (HTP), with the characteristics of the horizontal tail in Ref. [55], were added and are displayed in Figure 5.2. The model boundary conditions are specified at a single control point at the aircraft centre of gravity. The centre of gravity position was considered at 25% fuselage height in the aircraft symmetry plane and at the 28% MAC position, since in Ref. [55] it was found that for cruise condition with this centre of gravity position the tail incidence was of $0°$. The rib at the aircraft symmetry plane is rigidly connected to this point in all degrees of freedom and to simulate a fuselage connection with some small flexibility the remaining ribs at the centre wingbox sections are rigidly connected in the longitudinal and vertical degrees of freedom.

For the aerodynamics the Doublet-Lattice Method (DLM) was used. As the DLM is based on linearised potential flow it cannot accurately capture transonic aerodynamics so care must be taken with the results. However, significant work on aeroelastic tailoring of the CRM with DLM has been done and this method is still considered industry standard for flutter predictions. Furthermore, it is less computationally expensive that more advanced computational fluid dynamics, making it ideal for optimisation studies [23, 32, 33]. The aerodynamic panels are divided into two main surfaces: the wing and the tail. For the wing a chordwise cosine distribution with 25 boxes was considered to more accurately predict the pressure variation near the leading and trailing edges. The wing aerodynamic panel has a total of 2925 boxes. The tail surface has a mesh of 30 by 15 boxes in the spanwise and chordwise directions, respectively, and is hinged about the 25% chord point at the root. The DLM mesh of the wing and tail is shown in Figure 5.3.

To account for camber and twist, *i.e.* local angle of attack, aerodynamic downwash corrections were input as `W2GJ` entries. For the horizontal tail plane there is no camber, but the twist increases linearly by 3° from root to tip. On the wing however, both airfoil camber and twist are present. Using a Python script, airfoils were extracted from the outer mold line of the uCRM at the centre spanwise coordinate of the columns of boxes of the mesh. A spline for the airfoil camber line, as the half thickness line in the airfoil were created. Then for each control point of the aerodynamic boxes, as defined in appendix A.1, was projected onto the unrotated airfoil taking into account the local wing twist, and the local angle of attack due to camber was calculated as the derivative of the camber spline at the control point projection. This local angle of attack of each box was then added to the corresponding wing jig twist at its span position and input into the downwash correction entries. Figure 5.4 shows some of the airfoil sections and respective camber lines obtained.

Three-dimensional surface splines (`SPLINE6`) were used for the load and displacement transfer between the structural and aerodynamic meshes.

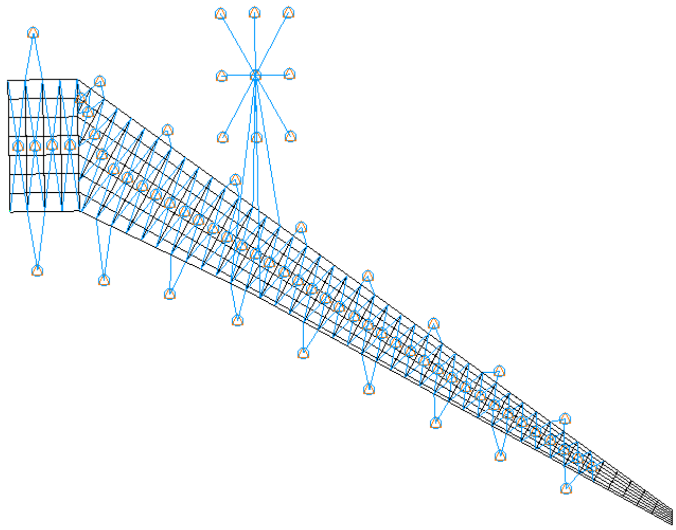

Figure 5.1: uCRM wingbox (with stringers and rib positions outline) including concentrated point masses of control surfaces, fuel and engine

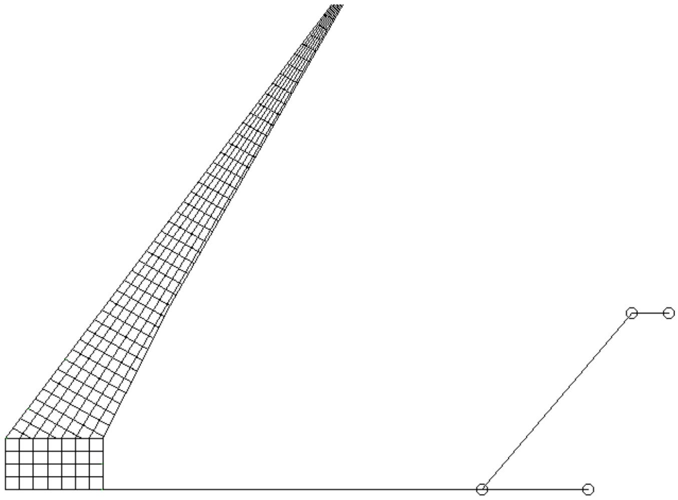

Figure 5.2: uCRM wingbox outline integrated with rigid elements for fuselage and HTP

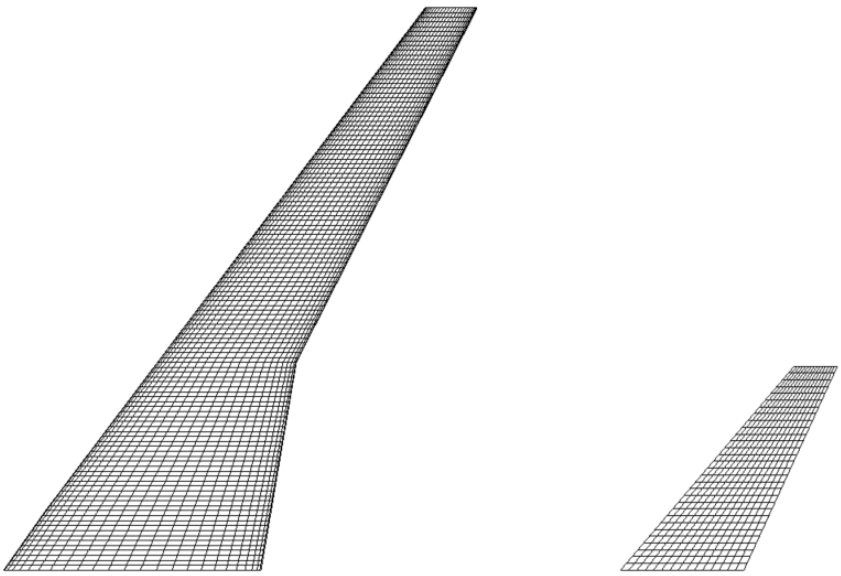

Figure 5.3: uCRM wing and tail DLM mesh

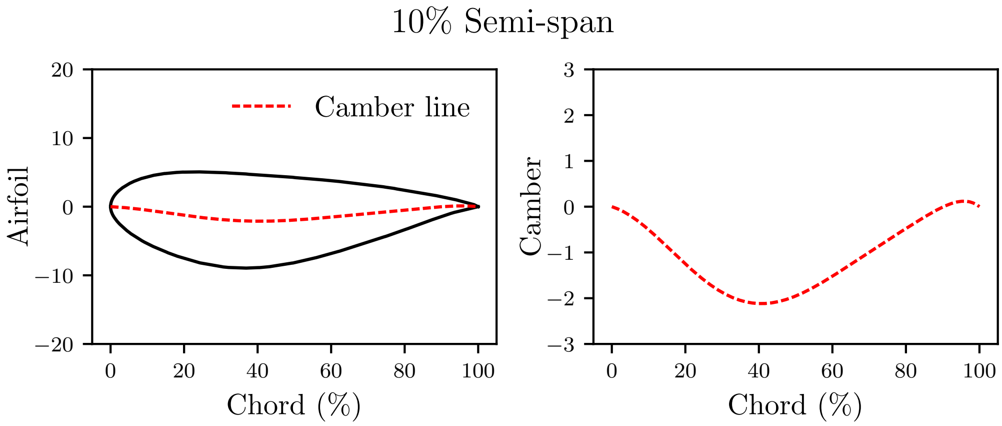

(a) 10% Semi-span position (root)

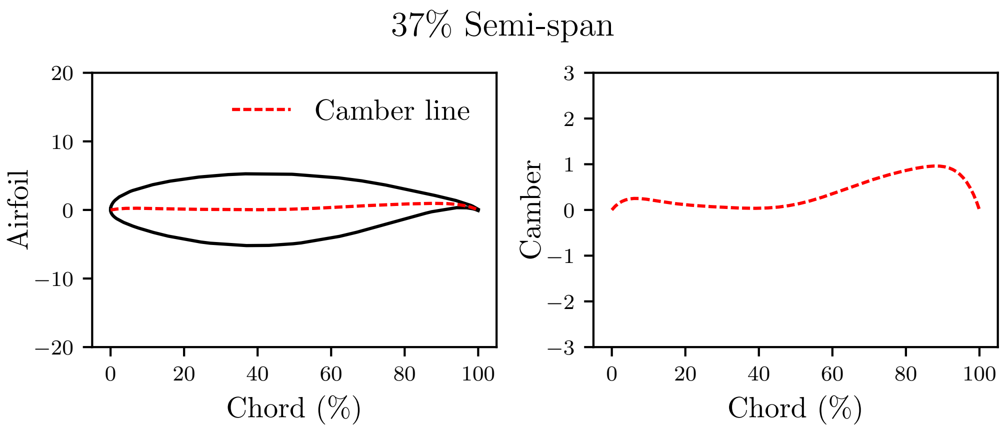

(b) 37% Semi-span position (yehudi break)

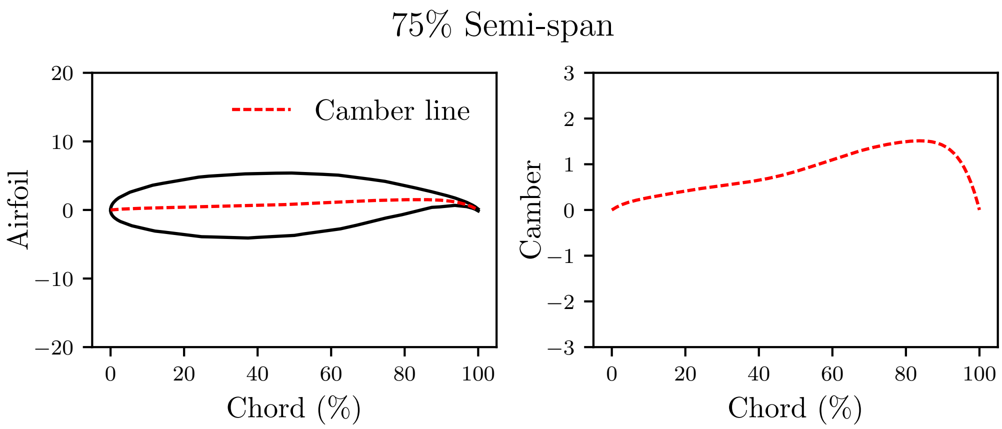

(c) 75% Semi-span position

Figure 5.4: Airfoils and corresponding camber line of uCRM wing sections

5.2. An Approach to Aeroelastic Tailoring of the Wingbox Structure

The previous model was developed with the intention of performing aeroelastic tailoring studies on the wingbox structure to evaluate the potential benefits of Double-Double laminates for this purpose. With this in mind, the model was implemented so that aeroelastic tailoring could be achieved by optimising the thickness distribution of the skins, seeking to minimise the structural weight, subjected to several aeroelastic constraints. As previously mentioned, the skins were each divided into 12 independent patches of 4 bays delimited by spars and ribs, for a total of 24 tailorable zones in terms of material and thickness. In an ideal scenario the following optimisation studies can be performed:

1. Optimisation of all metallic wingbox to have a benchmark for comparison;
2. Optimisation of the wingbox with composite skins following the design guidelines for traditional aerospace composites;
3. Optimisation of the wingbox with Double-Double skins, where the Double-Double angles are constant throughout the skins;
4. Optimisation of the wingbox with Double-Double skins, where the Double-Double angles can change throughout the skins in a tow-steered design.

These analyses would allow for a high level exploration of the thickness tapering opportunities brought on by Double-Double. It would also be possible to understand how they compare with typical composite laminates used in aircraft structures, by evaluating the final optimal weight and the aerodynamic load distribution of the optimal configurations.

6
Conclusions and Future Work

6.1. Conclusions

The work of this thesis has been driven by the need to understand the impact of Double-Double (DD) laminates on the aeroelastic behaviour of composite structures. While the use of composites in aircraft structures has evolved, how they are designed has not changed significantly. New approaches to composite design, like Double-Double, need to be studied and evaluated before they can be certified and implemented in aircraft structures. In modern commercial aircraft, aeroelasticity plays a significant role in aircraft design and certification. Therefore, Double-Double laminates need to be evaluated in this context.

An aeroelastic model of a composite plate based on a commercial finite element code was implemented and integrated in a multi-objective optimisation framework. Double-Double laminates were studied considering two aeroelastic conditions: a static aeroelastic load case and aeroelastic instability of divergence or flutter.

Through the evaluation of unidirectional laminates, it was found that, when in a homogenised condition, the aeroelastic behaviour of Double-Double laminates was independent of the number of building block repeats. The aeroelastic instability of Double-Double laminates was found to be flutter in the entire domain, as these laminates do not have unfavourable bending-twist coupling that can lead to early torsional divergence failure. By modifying the thickness distribution of the laminate, it was possible to positively influence the aeroelastic behaviour, by decreasing the failure condition under the static case and delaying the instability velocity.

The aeroelastic optimisation of both unbalanced and Double-Double laminates further clarified the aeroelastic behaviour of DD. The homogenised condition of Double-Double layups implied low bending-twist coupling unable to achieve significant load reduction under the static aeroelastic condition. Compared with the optimal unbalanced configuration, DD highlighted a higher failure index. In terms of aeroelastic instability, unidirectional Double-Double laminates showed small improvements of the critical aeroelastic velocity when compared to laminates that present higher couplings. The introduction of tow-steering in DD brought promising results in terms of load reduction: the failure index of Double-Double laminates was reduced by 20%. Despite still not being able to achieve as low a failure index as unbalanced laminates, when considered in a multi-objective optimisation with both aeroelastic metrics (static aeroelastic condition and aeroelastic instability), tow steered Double-Double laminates are a better solution in a significant part of the objective space. With only a small penalty in the static aeroelastic failure index, the critical velocity was increased considerably.

This work showed that, while the lack of bending-twist coupling in Double-Double laminates can be severely penalising in some conditions, this drawback can be easily surpassed. Both thickness tapering and a simple tow steering approach with linear fibre angle variation were able to significantly improve their aeroelastic behaviour. These results place a combination of these two approaches: laminate tapering and tow steering as the ideal Double-Double laminates for aeroelastic applications.

Finally, in an effort to extend these studies to built-up aircraft structures intended for aeroelastic tailoring, an aeroelastic model of a wingbox structure representative of a modern, long range commercial aircraft was developed.

6.2. Future Work

The current work allowed for a greater understanding of the aeroelastic behaviour of DD laminates and their potential for aeroelastic tailoring applications considering both static aeroelastic conditions and aeroelastic instability. However, a significant aeroelastic condition still requires study: gusts. Gust encounters are critical for aircraft sizing and certification. Therefore, the response of Double-Double laminates under gusts should be explored to identify any potential advantages or shortcomings of these laminates. Additionally, different steering strategies that allow for more aggressive stiffness variation can be explored to see if they further open the objective space.

An important evolution, would be to expand this work to realistic aircraft structures. Aircraft structures have significantly more complex stiffness and mass distributions that can be influenced by a high number of factors. The design and manufacture of these structures with typical aerospace composite laminates is extremely complex. Double-Double laminates offer a possibility for a significant reduction of this level of complexity. The application of Double-Double in aircraft structures is dependent on a comprehensive understanding of how these laminates can be used to influence the aeroelastic response of these structures.

A
Aeroelastic Modelling

A.1. Doublet-Lattice Method

The Doublet-Lattice Method (DLM) was presented by Albano and Rodden [57], Giesing *et al.* [58] and Kalman *et al.* [59]. It is based on linearised potential flow aerodynamics and is an extension of the steady Vortex-Lattice method to unsteady flow. The theory considers that the undisturbed flow is uniform and is either steady or varying harmonically.

In DLM, the lifting surfaces are divided into trapezoidal 'boxes' or panels, in a way that the boxes are aligned in columns parallel to the airflow. The 25% line of each box contains a distribution of potential doublets of unknown uniform strength. The normal wash boundary condition is enforced at a control point at the mid-span of the 75% line of each box [57–59]. The normal velocity at the surface and the pressure difference across the surface are related by Equation A.1 [57, 60]:

$$w(x,s) = \iint K(x,\xi;s,\sigma)\overline{p}(\xi,\sigma)d\xi d\sigma \tag{A.1}$$

where

- w is the normal velocity
- (x,s) are orthogonal coordinates on the lifting surface as shown in Figure A.1
- K is the Kernel function, explicitly defined in Refs. [57, 58, 60]
- $\overline{p}$ is the complex amplitude of the lifting pressure coefficient

The numerical form of Equation A.1 in matrix notation is given by [60]:

$$\{\boldsymbol{w}\} = [\boldsymbol{D}]\{\boldsymbol{p}\} \tag{A.2}$$

where the elements of the normalwash factor matrix, $\boldsymbol{D}$, are given by:

$$D_{rs} = \frac{\Delta x_s}{8\pi}\int_{-e}^{e} K d\overline{\eta} \tag{A.3}$$

where

- Δx_s – chord at box mid-span
- e – panel semiwidth (semispan)

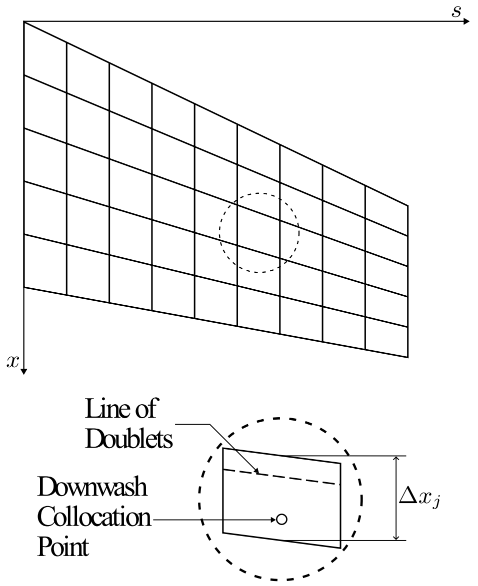

Figure A.1: Doublet-Lattice Method discretisation of lifting surface with trapezoidal boxes (adapted from [58])

In MSC Nastran, the downwash is obtained from the deflections, using the substantial differentiation matrix, by Equation A.4 [40, 61]:

$$\{w_j\} = \left[D^1_{jk} + ikD^2_{jk}\right]\{u_k\} + \left\{w^g_j\right\} \tag{A.4}$$

The lifting pressures are related to the downwash, *i.e.* the dimensionless normal velocity induced by the inclination of the surface relative to the airflow, by implementing Equation A.2 as:

$$\{w_j\} = [A_{jj}]\{f_j/\overline{q}\} \tag{A.5}$$

The lifting pressures are then integrated over the lifting surface to obtain forces and moments as:

$$\{P_k\} = [S_{kj}]\{f_j\} \tag{A.6}$$

where:

- w_j is the downwash
- w^g_j is the static aeroelastic downwash. It includes, primarily, the static incidence distribution that may arise from an initial angle of attack, camber, or twist
- f_j is the pressure on lifting element j
- $\overline{q}$ is the flight dynamic pressure
- k is the reduced frequency
- $A_{jj}(m,k)$ is the aerodynamic influence coefficient matrix, function of Mach number (m) and reduced frequency (k)

- u_k, P_k are the displacements and forces at aerodynamic grid points, respectively
- D^1_{jk}, D^1_{jk} are the real and imaginary parts of substantial differentiation matrix, respectively
- S_{kj} is the integration matrix

The aerodynamic influence coefficient matrix, Q_{kk}, is obtained using the previously defined matrices as:

$$[Q_{kk}] = [S_{kj}] \, [A_{jj}]^{-1} \left[D^1_{jk} + ikD^2_{jk}\right] \tag{A.7}$$

A.1.1. Aerodynamic Corrections

The theoretical aerodynamic pressures are obtained from Equation A.5 as:

$$\{f_j\} = \overline{q}[A_{jj}]^{-1} \{w_j\} \tag{A.8}$$

It is possible to introduce two experimental corrections so that the force distribution of Equation A.6 becomes:

$$\{P_k\} = [W_{kk}] \, [S_{kj}] \, \{f_j\} + \overline{q} \, [S_{kj}] \left\{f^e_j / \overline{q}\right\} \tag{A.9}$$

where

- $[W_{kk}]$ is a matrix of empirical correction factors to adjust each theoretical aerodynamic box lift and moment to agree with experimental data for incidence changes
- $\left\{f^e_j / \overline{q}\right\}$ is a vector of experimental pressure coefficients at a reference incidence for each aerodynamic element

A.2. Finite Plate Spline

Splines give an interpolation capability to couple the structural and aerodynamic meshes in aeroelastic analysis. Splines are used for force interpolation, calculating a structurally equivalent force distribution on the structure given a force distribution on the aerodynamic mesh, and for displacement interpolation by calculating aerodynamic displacements from structural displacements. The force and deformation interpolation are given respectively by [40]:

$$[F_s] = [G_{sa}] \, [F_a] \tag{A.10}$$

$$[U_a] = [G_{as}] \, [U_s] \tag{A.11}$$

where G is the spline matrix, F and U are the forces and displacements, respectively, and the s and a subscripts refer to structure and aerodynamics, respectively. Via the virtual works principals it can be shown that: $[G_{sa}] = [G_{as}]^T$. The spline $[G_{as}]$ is obtained depending on the spline method used. In MSC Nastran splines can be used to interpolate forces and displacements simultaneously or just for displacements or force.

The Finite Plate Spline (FPS) uses a virtual mesh of quadrilateral or triangular plate elements to calculate the interpolation. The interpolation is based on structural behaviour and compared to the Infinite Plate Spline has the advantage of approximating the boundaries of the interpolation region more accurately [40]. The theory of FPS was presented by Appa [62].

Figure A.2 shows a generic discretisation of a planar surface into finite elements. This mesh is used to perform the interpolation between n structural points and m aerodynamic points which don't need to have

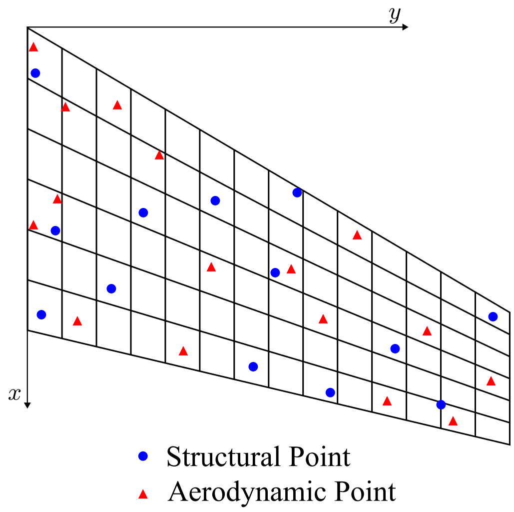

Figure A.2: Finite Plate Spline mesh with arbitrary structural and aerodynamic points (adapted from [62])

a regular arrangement or coincide with the virtual mesh points. The normal displacements $w = w(x, y)$ and the rotations, $\theta = \theta(x, y)$ about the x axis and $\phi = \phi(x, y)$ about the y axis, in an element are given by [40, 62]:

$$\{r\} = [\Omega] \{u^e\} \tag{A.12}$$

$$\{r\} = \begin{Bmatrix} w \\ \theta \\ \phi \end{Bmatrix} \qquad [\Omega] = \begin{Bmatrix} \lfloor \omega \rfloor \\ \lfloor \omega_{,x} \rfloor \\ \lfloor \omega_{,y} \rfloor \end{Bmatrix} \qquad \{u^e\} = \lfloor w_1 \;\, \theta_1 \;\, \phi_1 \ldots w_4 \;\, \theta_4 \;\, \phi_4 \rfloor^T \tag{A.13}$$

where

$$\theta = \frac{dw}{dy} \qquad \phi = \frac{dw}{dx} \tag{A.14}$$

and $\lfloor \omega \rfloor$ is a 1x12 row matrix of shape functions used to interpolate the displacement field in a four node quadrilateral element in terms of the nodal displacements. A boolean connectivity matrix, $[B]$, is defined for each element of the virtual mesh to relate nodal displacements to the overall finite element mesh displacements:

$$\{u^e\}_i = [B]_i \{u\} \tag{A.15}$$

Introducing Equation A.15 into Equation A.12, the displacement of the structural points and aerodynamic points is related to the virtual mesh displacements, respectively, by the matrices:

$$[\Psi_s] = \begin{bmatrix} [\Phi]^s{}_1 [B]_1 \\ \vdots \\ [\Phi]^s{}_n [B]_n \end{bmatrix} \tag{A.16}$$

$$[\Psi_a] = \begin{bmatrix} [\Phi]^a{}_1 [B]_1 \\ \vdots \\ [\Phi]^a{}_m [B]_m \end{bmatrix} \tag{A.17}$$

The structural points deflections and aerodynamic points deflection are then expressed as a function of the virtual mesh displacements:

$$\{u_s\} = [\Psi_s]\{u\} \tag{A.18}$$

$$\{u_a\} = [\Psi_a]\{u\} \tag{A.19}$$

The virtual surface define by the virtual finite element mesh is required to pass through the structural points, which are the independent ones. Therefore, a penalty method is used to express the equilibrium of the virtual mesh:

$$[K]\{u\} + [\alpha][\Psi_s]^T([\Psi_s]\{u\} - \{u_s\}) = 0 \tag{A.20}$$

where $[\alpha]$ is an invertible diagonal weighting matrix and $[K]$ is the stiffness of the plate. This equation can be solved for the virtual mesh displacements, resulting in:

$$\{u\} = \left\{[\alpha]^{-1}[K] - [\Psi_s]^T[\Psi_s]\right\}^{-1}[\Psi_s]\{u_s\} = [A]^{-1}[\Psi_s]\{u_s\} \tag{A.21}$$

Replacing into Equation A.19, the spline matrix $[G_{as}]$ is obtained:

$$[G_{as}] = [\Psi_a]\left\{[\alpha]^{-1}[K] - [\Psi_s]^T[\Psi_s]\right\}^{-1}[\Psi_s]^T \tag{A.22}$$

References

[1] C. Kassapoglou, *Design and Analysis of Composite Structures: With Applications to Aerospace Structures*. John Wiley & Sons, 2013.

[2] R. M. Jones, *Mechanics of Composite Materials*. Taylor & Francis, 1999.

[3] L. P. Kollár and G. S. Springer, *Mechanics of Composite Structures*. Cambridge University Press, 2003.

[4] S. W. Tsai and N. J. Pagano, "Invariant Properties of Composite Materials", Air Force Materials Lab Wright-Patterson AFB Ohio, Tech. Rep., 1968.

[5] S. W. Tsai and J. D. D. Melo, "An invariant-based theory of composites", *Composites Science and Technology*, vol. 100, pp. 237–243, 2014, ISSN: 0266-3538. DOI: https://doi.org/10.1016/j.compscitech.2014.06.017. [Online]. Available: https://www.sciencedirect.com/science/article/pii/S0266353814002188.

[6] A. Arteiro *et al.*, "A case for tsai's modulus, an invariant-based approach to stiffness", *Composite Structures*, vol. 252, p. 112 683, 2020, ISSN: 0263-8223. DOI: https://doi.org/10.1016/j.compstruct.2020.112683. [Online]. Available: https://www.sciencedirect.com/science/article/pii/S026382232032609X.

[7] J. A. Bailie, R. P. Ley, and A. Pasricha, "A Summary and Review of Composite Laminate Design Guidelines", NASA and Northrop Grumman, NASA Contract NAS1-19347, 1997.

[8] S. W. Tsai, "Double-double: New family of composite laminates", *AIAA Journal*, vol. 59, no. 11, pp. 4293–4305, 2021. DOI: 10.2514/1.J060659. [Online]. Available: https://doi.org/10.2514/1.J060659.

[9] S. W. Tsai *et al.*, *Double-Double: A New Perpective in the Manufacture and Design of Composites*. 2022.

[10] K. Zhao, D. Kennedy, A. Miravete, S. W. Tsai, C. A. Featherston, and X. Liu, "Defining the Design Space for Double-Double Laminates by Considering Homogenization Criterion", *AIAA Journal*, vol. 61, no. 7, pp. 3190–3203, 2023. DOI: 10.2514/1.J062639. [Online]. Available: https://doi.org/10.2514/1.J062639.

[11] H. Ghiasi, D. Pasini, and L. Lessard, "Optimum stacking sequence design of composite materials Part I: Constant stiffness design", *Composite Structures*, vol. 90, no. 1, pp. 1–11, 2009, ISSN: 0263-8223. DOI: https://doi.org/10.1016/j.compstruct.2009.01.006. [Online]. Available: https://www.sciencedirect.com/science/article/pii/S026382230900018X.

[12] H. Ghiasi, K. Fayazbakhsh, D. Pasini, and L. Lessard, "Optimum stacking sequence design of composite materials part ii: Variable stiffness design", *Composite Structures*, vol. 93, no. 1, pp. 1–13, 2010, ISSN: 0263-8223. DOI: https://doi.org/10.1016/j.compstruct.2010.06.001. [Online]. Available: https://www.sciencedirect.com/science/article/pii/S0263822310001947.

[13] G. Ntourmas, “Detailed Sizing Optimisation of Industrial-Scale Composite Aeronautical Structures”, Ph.D. dissertation, University of Nottingham, 2022.

[14] J. Grenestedt and P. Gudmundson, “Layup optimization of composite material structures”, in *Optimal Design with Advanced Materials*, P. PEDERSEN, Ed., Oxford: Elsevier, 1993, pp. 311–336, ISBN: 978-0-444-89869-2. DOI: https://doi.org/10.1016/B978-0-444-89869-2.50027-5. [Online]. Available: https://www.sciencedirect.com/science/article/pii/B9780444898692500275.

[15] J. R. Wright and J. E. Cooper, *Introduction to Aircraft Aeroelasticity and Loads*, 2nd ed. Wiley, 2015.

[16] R. L. Bisplinghoff, H. Ashley, and R. L. Halfman, *Aeroelasticity*. Dover Publications, 1996.

[17] A. Collar, “The first fifty years of aeroelasticity”, *Aerospace*, 1978.

[18] European Union Aviation Safety Agency, *Certification Specifications for Large Aeroplanes (CS-25)*.

[19] Federal Aviation Administration, *14 CFR part 25-AIRWORTHINESS STANDARDS: TRANSPORT CATEGORY AIRPLANES*.

[20] M. H. Shirk, T. J. Hertz, and T. A. Weisshaar, “Aeroelastic tailoring - Theory, practice, and promise”, *Journal of Aircraft*, vol. 23, no. 1, pp. 6–18, 1986. DOI: 10.2514/3.45260.

[21] T. Weisshaar, C. Nam, and A. Batista-Rodriguez, “Aeroelastic tailoring for improved UAV performance”, in *39th AIAA/ASME/ASCE/AHS/ASC Structures, Structural Dynamics, and Materials Conference and Exhibit*. DOI: 10.2514/6.1998-1757.

[22] C. V. Jutte and B. K. Stanford, “Aeroelastic Tailoring of Transport Aircraft Wings: State-of-the-Art and Potential Enabling Technologies”, NASA, Technical Memorandum NASA/TM-2014-218252, 2014.

[23] E. P. Krupa, “Aeroelastic Tailoring of a Composite Wing with Adaptive Control Surfaces for Optimal Aircraft Performance”, Ph.D. thesis, University of Bristol, 2019.

[24] T. A. Weisshaar and R. J. Ryan, “Control of aeroelastic instabilities through stiffness cross-coupling”, *Journal of Aircraft*, vol. 23, no. 2, pp. 148–155, 1986. DOI: 10.2514/3.45282.

[25] T. Weisshaar, “Aeroelastic tailoring of forward swept composite wings”, in *21st Structures, Structural Dynamics, and Materials Conference*. DOI: 10.2514/6.1980-795.

[26] T. Weisshaar, “Aeroelastic tailoring - Creative uses of unusual materials”, in *28th Structures, Structural Dynamics and Materials Conference*. DOI: 10.2514/6.1987-976.

[27] S. J. Hollowell and J. Dugundji, “Aeroelastic flutter and divergence of stiffness coupled, graphite/epoxy cantilevered plates”, *Journal of Aircraft*, vol. 21, no. 1, pp. 69–76, 1984. DOI: 10.2514/3.48224.

[28] M. Kameyama and H. Fukunaga, “Optimum design of composite plate wings for aeroelastic characteristics using lamination parameters”, *Computers & Structures*, vol. 85, no. 3, pp. 213–224, 2007, ISSN: 0045-7949. DOI: https://doi.org/10.1016/j.compstruc.2006.08.051. [Online]. Available: https://www.sciencedirect.com/science/article/pii/S0045794906003002.

[29] O. Stodieck, J. E. Cooper, P. M. Weaver, and P. Kealy, “Improved aeroelastic tailoring using tow-steered composites”, *Composite Structures*, vol. 106, pp. 703–715, 2013, ISSN: 0263-8223. DOI: https://doi.org/10.1016/j.compstruct.2013.07.023. [Online]. Available: https://www.sciencedirect.com/science/article/pii/S0263822313003462.

[30] O. Stodieck, J. E. Cooper, P. M. Weaver, and P. Kealy, "Optimization of tow-steered composite wing laminates for aeroelastic tailoring", *AIAA Journal*, vol. 53, no. 8, pp. 2203–2215, 2015. DOI: 10.2514/1.J053599.

[31] B. K. Stanford, C. V. Jutte, and K. Chauncey Wu, "Aeroelastic benefits of tow steering for composite plates", *Composite Structures*, vol. 118, pp. 416–422, 2014, ISSN: 0263-8223. DOI: https://doi.org/10.1016/j.compstruct.2014.08.007. [Online]. Available: https://www.sciencedirect.com/science/article/pii/S0263822314003973.

[32] O. Stodieck, J. E. Cooper, P. M. Weaver, and P. Kealy, "Aeroelastic Tailoring of a Representative Wing Box Using Tow-Steered Composites", *AIAA Journal*, vol. 55, no. 4, pp. 1425–1439, 2017. DOI: 10.2514/1.J055364.

[33] B. Stanford, C. D. Wieseman, and C. Jutte, "Aeroelastic Tailoring of Transport Wings Including Transonic Flutter Constraints", in *56th AIAA/ASCE/AHS/ASC Structures, Structural Dynamics, and Materials Conference*. DOI: 10.2514/6.2015-1127.

[34] C. V. Jutte, B. Stanford, C. D. Wieseman, and J. B. Moore, "Aeroelastic Tailoring of the NASA Common Research Model via Novel Material and Structural Configurations", in *52nd Aerospace Sciences Meeting*. DOI: 10.2514/6.2014-0598.

[35] G. Kenway, G. Kennedy, and J. R. R. A. Martins, "Aerostructural optimization of the Common Research Model configuration", in *15th AIAA/ISSMO Multidisciplinary Analysis and Optimization Conference*. DOI: 10.2514/6.2014-3274.

[36] T. R. Brooks, G. Kennedy, and J. R. R. A. Martins, "High-fidelity Multipoint Aerostructural Optimization of a High Aspect Ratio Tow-steered Composite Wing", in *58th AIAA/ASCE/AHS/ASC Structures, Structural Dynamics, and Materials Conference*. DOI: 10.2514/6.2017-1350.

[37] P. D. Dunning, B. K. Stanford, H. A. Kim, and C. V. Jutte, "Aeroelastic tailoring of a plate wing with functionally graded materials", *Journal of Fluids and Structures*, vol. 51, pp. 292–312, 2014, ISSN: 0889-9746. DOI: https://doi.org/10.1016/j.jfluidstructs.2014.09.008. [Online]. Available: https://www.sciencedirect.com/science/article/pii/S0889974614002096.

[38] S. W. Tsai and E. M. Wu, "A general theory of strength for anisotropic materials", *Journal of composite materials*, vol. 5, no. 1, pp. 58–80, 1971.

[39] S. Tsai, J. Melo, S. Sihn, A. Arteiro, and R. Rainsberger, *Composite Laminates: Theory and Practice of Analysis, Design and Automated Layup*. Stanford Aeronautics & Astronautics, 2017, ISBN: 978-0-9860845-2-2.

[40] HEXAGON, *MSC Nastran 2023.1 Aeroelastic Analysis User's Guide*.

[41] A. J. Lawrence and P. Jackson, "Comparison of different methods of assessing the free oscillatory characteristics of aeroelastic systems", 1968, British Aeronautical Research Council Current Paper No. 1084. [Online]. Available: https://reports.aerade.cranfield.ac.uk/handle/1826.2/1097.

[42] J. Blank and K. Deb, "Pymoo: Multi-objective optimization in python", *IEEE Access*, vol. 8, pp. 89 497–89 509, 2020.

[43] K. Deb, A. Pratap, S. Agarwal, and T. Meyarivan, "A fast and elitist multiobjective genetic algorithm: Nsga-ii", *IEEE Transactions on Evolutionary Computation*, vol. 6, no. 2, pp. 182–197, 2002. DOI: 10.1109/4235.996017.

[44] C. C. António, *Otimização de Sistemas em Engenharia - Fundamentos e algoritmos para o projeto ótimo*, Engebook, Ed. 2020.

[45] S. Doyle, *PyNastran: A Python-based interface tool for Nastran's file formats*. [Online]. Available: `https://github.com/SteveDoyle2/pyNastran`.

[46] K. Deb and R. B. Agrawal, "Simulated binary crossover for continuous search space", *Complex Syst.*, vol. 9, 1995.

[47] K. Deb, K. Sindhya, and T. Okabe, "Self-adaptive simulated binary crossover for real-parameter optimization", in *Proceedings of the 9th Annual Conference on Genetic and Evolutionary Computation*, 2007, pp. 1187–1194. DOI: `10.1145/1276958.1277190`. [Online]. Available: `https://doi.org/10.1145/1276958.1277190`.

[48] K. Deb and D. Deb, "Analyzing mutation schemes for real-parameter genetic algorithms", KanGAL, Tech. Rep. 2012016.

[49] J. Blank and K. Deb, "A running performance metric and termination criterion for evaluating evolutionary multi- and many-objective optimization algorithms", in *2020 IEEE Congress on Evolutionary Computation (CEC)*, 2020, pp. 1–8. DOI: `10.1109/CEC48606.2020.9185546`.

[50] A. Miravete and S. W. Tsai, *Quad to DD Direct Conversion Tool*, Composite Design Workshop XXV, 2023.

[51] A. Miravete, "Lamination parameter plots", in *Composite Design Workshop XXV*, Stanford University, Jun. 2023.

[52] A. Arteiro, C. Furtado, G. Catalanotti, P. Linde, and P. Camanho, "Thin-ply polymer composite materials: A review", *Composites Part A: Applied Science and Manufacturing*, vol. 132, p. 105 777, 2020, ISSN: 1359-835X. DOI: `https://doi.org/10.1016/j.compositesa.2020.105777`. [Online]. Available: `https://www.sciencedirect.com/science/article/pii/S1359835X20300154`.

[53] Z. Gurdal and R. Olmedo, "In-plane response of laminates with spatially varying fiber orientations - Variable stiffness concept", *AIAA Journal*, vol. 31, no. 4, pp. 751–758, 1993. DOI: `10.2514/3.11613`.

[54] A. Alhajahmad, M. M. Abdalla, and Z. Gürdal, "Optimal Design of Tow-Placed Fuselage Panels for Maximum Strength with Buckling Considerations", *Journal of Aircraft*, vol. 47, no. 3, pp. 775–782, 2010. DOI: `10.2514/1.40357`.

[55] J. Vassberg, M. Dehaan, M. Rivers, and R. Wahls, "Development of a Common Research Model for Applied CFD Validation Studies", in *26th AIAA Applied Aerodynamics Conference*. DOI: `10.2514/6.2008-6919`.

[56] T. R. Brooks, G. G. Kenway, and J. R. Martins, *uCRM: undeflected Common Research Model*, Mendeley Data, 2019. DOI: `10.17632/gpk4zn73xn.1`.

[57] E. Albano and W. P. Rodden, "A doublet-lattice method for calculating lift distributions on oscillating surfaces in subsonic flows.", *AIAA Journal*, vol. 7, no. 2, pp. 279–285, 1969. DOI: `10.2514/3.5086`.

[58] J. P. Giesing, T. P. Kalman, and W. P. Rodden, "Subsonic unsteady aerodynamics for general configurations", Air Force Flight Dynamics Laboratory, Tech. Rep. AFFDL-TR-71-5, Part I, Vol I, 1971.

[59] T. P. Kalman, W. P. Rodden, and J. P. Giesing, "Application of the doublet-lattice method to nonplanar configurations in subsonic flow", *Journal of Aircraft*, vol. 8, no. 6, pp. 406–413, 1971. DOI: 10.2514/3.59117.

[60] W. P. Rodden, P. F. Taylor, and S. C. McIntosh, "Further refinement of the subsonic doublet-lattice method", *Journal of Aircraft*, vol. 35, no. 5, pp. 720–727, 1998. DOI: 10.2514/2.2382.

[61] W. P. Rodden and J. D. Revell, "The Status of Unsteady Aerodynamic Influence Coefficients", Tech. Rep., 1961.

[62] K. Appa, "Finite-surface spline", *Journal of Aircraft*, vol. 26, no. 5, pp. 495–496, 1989. DOI: 10.2514/3.45792.